STUDY OF PURE AND GADOLINIUM DOPED SINGLE CRYSTALS OF EUROPIUM MONOXIDE BY NUCLEAR MAGNETIC RESONANCE

THÈSE N^{O} 2882 (2003)

PRÉSENTÉE À LA FACULTÉ SCIENCES DE BASE

Institut de physique des nanostructures

SECTION DE PHYSIQUE

ÉCOLE POLYTECHNIQUE FÉDÉRALE DE LAUSANNE

POUR L'OBTENTION DU GRADE DE DOCTEUR ÈS SCIENCES

PAR

Arnaud COMMENT

ingénieur physicien diplômé EPF
de nationalité suisse et originaire de Courgenay (JU)

acceptée sur proposition du jury:

Prof. J.-Ph. Ansermet, Prof. C.P. Slichter, directeurs de thèse
Dr J. Cibert, rapporteur
Dr J. Gavilano, rapporteur
Prof. F. Mila, rapporteur

Lausanne, EPFL
2003

Version abrégée

Nous avons étudié l'EuO et l'EuO dopé au Gd par RMN des noyaux ^{153}Eu et ^{151}Eu en utilisant un spectromètre fait maison nous permettant de mesurer des signaux avec des temps de relaxation spin-spin très courts. Nous avons déterminé et décrit les mécanismes d'élargissement donnant lieu à la structure de la raie spectrale de l'EuO pur. La description complète de la raie spectrale de l'EuO pur nous a permis de mettre en évidence l'influence du dopage au Gd sur la raie spectrale. En étudiant la dépendance en température des raies spectrales, nous avons démontré la présence d'une inhomogénéité magnétique statique dépendante de la température dans l'EuO dopé au Gd. Nos résultats ont suggéré que l'inhomogénéité dans l'EuO dopé avec 0.6% de Gd était lié à la magnétorésistance colossale. Nous avons aussi déterminé et décrit l'origine de la dépendance en température des mécanismes de relaxation spin-spin et spin-réseau. La mesure des temps de relaxation spin-réseau en fonction de la température ont conduit à la détermination de la valeur de l'intégrale d'échange en fonction du niveau de dopage au Gd.

Abstract

We performed an Eu^{153} and Eu^{151} NMR study of EuO and Gd doped EuO using a home-made spectrometer designed to measure signals with fast spin-spin relaxation times. We determined and described the broadening mechanisms giving rise to the structure in the lineshape of pure EuO. The complete description of the lineshape of pure EuO allowed us to highlight the influence of doping EuO with Gd impurities on the lineshape. We demonstrated the presence of a temperature dependent static magnetic inhomogeneity in Gd doped EuO by studying the temperature dependence of the lineshapes. Our results suggested that the inhomogeneity in 0.6% Gd doped EuO was linked to colossal magnetoresistance. We also determined and described the origin and the temperature dependence of both the spin-spin and the spin-lattice relaxation mechanisms. The measurement of the spin-lattice relaxation times as a function of temperature led to the determination of the value of the exchange integral as a function of Gd doping.

Remerciements

J'aimerais tout d'abord remercier Charlie Slichter pour m'avoir accueilli dans son groupe de recherche. Il a toujours été très enthousiaste au sujet des expériences que j'ai effectuées et sa fabuleuse expérience en physique et en RMN en particulier a été un inestimable atout pour la réalisation de ce travail. L'opportunité de travailler dans le département de physique de l'Université de l'Illinois ne se serait pas présentée sans la fantastique créativité de Jean-Philippe Ansermet. Il a donné naissance à ce projet de recherche et m'a donné la possibilité de travailler sur un sujet excitant dans un environnement stimulant. Il m'a aussi soutenu et encouragé à poursuivre ce travail à l'Université de l'Illinois.

L'environnement stimulant et amical du laboratoire de recherche de Charlie Slichter était en grande partie due à la présence de Dylan Smith. Il a toujours été un collaborateur scientifique très rigoureux sur lequel j'ai toujours pu compter. Notre amitié a très fortement contribué au plaisir que j'ai eu à travailler dans le labo. Je voudrais aussi remercier Craig Milling dont l'expertise en instrumentation RMN et en électronique ont été d'une grande aide. J'aimerais aussi remercier Lance Cooper pour les discussions enrichissantes que j'ai eues avec lui. J'ai eu beaucoup de plaisir à participer aux repas de groupe du vendredi midi, et je remercie aussi certains des anciens membres de son groupe, Heesuk Rho, Clark Snow et Seokhyun Yoon. Je remercie aussi Mattenberger pour avoir fourni les échantillons de EuO et de EuO dopé au Gd et Mike Abrecht pour avoir fourni les films minces de EuO. Finalement, je suis reconnaissant envers le département de physique de l'Université de l'Illinois à Urbana-Champaign pour m'avoir autorisé à rester pendant presque quatre années en tant qu'étudiant en échange. Je remercie aussi les membres de la faculté et le personnel de cette université qui m'ont aidé et ont fourni l'équipement nécessaire au bon déroulement de ma recherche.

Maintenant, d'un point de vue plus personnel, je suis profondément reconnaissant à ma future femme Sarah Clark, que j'ai rencontré dans le département de physique de l'Université de l'Illinois, pour son grand soutien durant l'achèvement de ce travail. Elle a été très présente pour m'aider durant certains moments difficiles de ma vie à Urbana et je me réjouis de construire une nouvelle vie avec elle. Je suis aussi extrêmement reconnaissant envers ma soeur Ariane, ma mère Marie-Claire et mon père Gérard qui m'ont tous soutenu dans ma décision de passer quatre années de ma vie à Urbana-Champaign. Et finalement, j'aimerais sincèrement remercier la famille de Sarah, Arlene et David, Mike et Susan, Katie et Andrew qui m'ont toujours chaleureusement accueilli dans leurs maisons respectives de Chicago et Evanston. D'une manière générale, passer environ quatre années sur le campus de l'Université de l'Illinois à Urbana-Champaign fut une très belle expérience personnelle.

Ce travail a été financé par le Département Américain de l'Energie, division des sciences des matériaux, au travers du Laboratoire Frederick Seitz de recherche en matériaux de l'Université de l'Illinois Urbana-Champaign sous le contrat No. DEFG02-91ER45439.

Acknowledgements

I would first like to thank Charlie Slichter for welcoming me in his research group. He has always been very enthusiastic about the experiments I performed and his fabulous experience in physics and NMR in particular was of invaluable help. The opportunity of working in the Physics Department of the University of Illinois would not have been possible without the fantastic scientific creativity of Jean-Philippe Ansermet. He initiated this research and gave me the opportunity to work on this exciting subject in a stimulating environment. He also supported and encouraged me to pursue this work at the the University of Illinois.

The stimulating and friendly environment of the research lab of Charlie Slichter was in great part due to the presence of Dylan Smith. He has always been a very reliable and rigorous scientific collaborator. Our friendship made my life in the lab very enjoyable. I also want to thank Craig Milling whose expertise in NMR hardware and electronics were of great help.

I would also like to thank Lance Cooper for the enriching discussions I had with him. I had fun at the "Friday group lunches", and I also thank some of the former members of his group, Heesuk Rho, Clark Snow and Seokhyun Yoon. I also thank Mattenberger for the EuO and Gd doped EuO samples and Mike Abrecht for the thin films of EuO.

Finally, I am grateful to the Physics Department of the University of Illinois at Urbana-Champaign for letting me stay almost four years as a non-degree graduate student. I also thank all the faculty and staff members who helped me and provided the equipment needed for my research.

Now, from a more personal point of view, I am deeply thankful for the support of my future wife Sarah Clark who I met in the Physics department of the University of Illinois. She was very dedicated to me during the challenging times of my life in Urbana and I look forward to building a new life with her. I am also extremely grateful to my sister Ariane, my mother Marie-Claire and my father Gérard who supported me in my decision to spend four years of my life in Urbana-Champaign. And finally, I would like to sincerely thank Sarah's family, Arlene and David, Mike and Susan, and Katie and Andrew who always warmly welcomed me in their homes in Chicago and Evanston. Overall, it has been a wonderful experience for me to spend about four years on the campus of the University of Illinois at Urbana-Champaign.

This work was supported by the U.S. Department of Energy, Division of Materials Sciences, through the Frederick Seitz Materials Research Laboratory at the University of Illinois at Urbana-Champaign under Award No. DEFG02-91ER45439.

Contents

List of Tables

List of Figures

Chapter 1

Introduction

It might appear to the reader who first looks at the title of this work and sees the date of its publication that there is something anachronistic: europium oxide, nuclear magnetic resonance, 2003! Do we not already know everything about this material? Was this system not already studied by NMR in the late 60's and early 70's? The aim of this introduction is to show that europium monoxide and gadolinium doped europium monoxide are intimately related to current research topics. In this work, we will uncover new discoveries related to the physical phenomena involved in these systems. Our results will show that NMR is an invaluable technique for clarifying some of the issues related to the magnetic and electric properties of gadolinium doped and pure europium oxide.

The original aim of this study was to contribute to the understanding of the unconventional magnetic and electric behavior of manganites. In particular, searching for the origin of the so-called colossal magnetoresistance (CMR) is currently very popular due to the potential applications of such a dramatic effect in the computer industry. The existence of quasi-particles called ferrons or magnetic polarons, which can be described as ferromagnetic clusters created by polarized conduction electron spins, is thought to play an important role in this phenomenon [1]. NMR is a local probe for magnetic structure and magnetic fluctuations, so it was clearly an appropriate technique for this study. This was further demonstrated by Kapusta *et al.* who showed, using NMR, the existence of a residual electronic magnetization above the transition temperature in various ferromagnetic manganites [2]. We performed the same kind of NMR measurements on another ferromagnetic manganite and obtained similar results. However, it appeared that it would be difficult to go further in the study for several reasons: first, the homogeneity and the type of magnetic phases in these materials do not seem to be well defined (see for example [3]). Second, the order of the magnetic phase transition in ferromagnetic manganites seems to be dependent on the doping level, adding complexity to the problem [4]. Third, the numerous exotic phenomena taking place in these systems, such as phase separation, charge and orbital ordering, intrinsically inhomogeneous ground states, fluctuating electric field gradients or Jahn-Teller distortions would certainly not simplify the task of highlighting the mechanisms of CMR. Let us mention finally that the crystal structure of manganites is rather complex.

However, CMR has not been observed only in manganites. Europium chalcogenides also exhibit a magnetoresistive effect, and in fact the amplitude of the effect can be much larger in these systems than in manganites. The CMR observed in Eu-rich EuO is among the largest ever measured [5–7]. The change in resistivity ρ is of the order of $(\rho(H)-\rho(H=0))/\rho(H=0) \cong 10^7$ for a magnetic field of

amplitude $H = 14$ T [5]. One of the numerous advantages of europium chalcogenides over manganites is that the former have a cubic crystal structure, which simplifies the analysis of NMR measurements. A very attractive system exhibiting CMR is Gd doped EuO in which gadolinium atoms play the role of electron donors. The advantage of studying the magnetic and electric properties as a function of doping level in Gd doped EuO rather than in Eu-rich EuO is that the concentration of the dopant can be measured and thus checked more easily. We therefore chose to focus on the study of pure EuO and Gd doped EuO.

Apart from the issues related to the causes of CMR, there are other characteristics of EuO systems that make them attractive. First of all, EuO is one of the only natural ferromagnetic semiconductors and there is currently a great deal of attention on ferromagnetic semiconductors. A new field called spintronics has been developed around the possibilities of using the spin degree of freedom of the electron in solid-state electronics [8]. Of course, EuO is not going to be implemented in any of the next generations of cellular phones or laptops with its Curie temperature of about 70 K, but it is certainly a suitable system to study the physics involved in ferromagnetic semiconductors like GaMnAs, InMnAs or GaMnN.

EuO is also an ideal system for testing new theories in magnetism, in particular the recent developments made on the Kondo-lattice model. The localized magnetic moments of the half-filled $4f$-shell of the Eu atoms and the existence of a conduction band makes EuO an appropriate system to apply the Kondo-lattice model [9, 10]. In addition, the low magnetic anisotropy of the material along with the localized $J = S = 7/2$ spins of the Eu^{2+} ions makes europium monoxide a nearly ideal Heisenberg ferromagnet. It is therefore a very good candidate for applying spin-wave theory and related theoretical developments. Europium chalcogenides are also still among the most suitable materials to study the problem of phase transitions (see for example the neutron scattering experiment on EuS in [11]). Finally, it is worth noting that several experimental research projects have been conducted very recently on EuO [12, 13]. This system is thus still of interest for the scientific community and the aim of the present work is to contribute to the understanding of the properties of EuO and Gd doped EuO.

Chapter 2

Studying unconventional electric and magnetic behavior in $Eu_{1-x}Gd_xO$

Europium monoxide (EuO) was first identified as a ferromagnetic semiconductor by Matthias *et al.* [14]. It crystalizes in an NaCl structure with a lattice constant of 5.14 Å[15]. Pure EuO has a Curie temperature of about 69 K. Certainly one of the most important reasons for the interest towards EuO and europium chalcogenides in general is the fact that europium forms a strong ionic bond with oxygen, sulfur, selenium or tellurium. Consequently, these materials are insulators and can be seen as 3 dimensional arrays of Eu^{2+} ions, the distance between the ions depending on the atomic radius of oxygen, sulfur, selenium or tellurium. From Hund's rules we deduce $L = 0$ and $S = \frac{7}{2}$ for the Eu^{2+} ion. The electron spin has the maximum possible value for an ion and the orbital angular momentum of the ion is zero. These properties are ideal for applying standard theories of ferromagnetism such as the Heisenberg model.

Let us first start by describing the electronic structure of stoichiometric EuO as determined using augmented-plane-wave (APW) method by S. J. Cho [16]. The valence band is formed with the p orbitals of O^{2-} and it is full ($2p^6$). The conduction band is built up with the $6s$ and the $5d$ orbitals of Eu^{2+} and is empty. In between these two bands lies a narrow half-filled $4f$-band. The energy gap between the f band and the conduction band is about 1.1 eV [17]. The consequences of the replacement of a part of the Eu atoms by Gd atoms on the population of these bands will be addressed in this chapter. We will discuss the influence of the presence of Gd in the EuO matrix on the electric and magnetic properties of $Eu_{1-x}Gd_xO$. Then, we will present the characteristics of the samples we studied in this work.

2.1 The influence of doping

Pure stoichiometric EuO is an insulator, but the physical properties of the material can vary dramatically when the stoichiometry is not perfect or when it is doped. Shafer *et al.* grouped the various samples $Eu_{1+x}O$ as a function of x in 5 groups labelled with the roman numbers I to V [18]. Two of them (I and II) describe O-rich samples, which have a high resistivity and do not presently

Table 2.1: Classification of samples in groups as a function of the doping level. The doping level values are from [20].

Group	Doping level in $Eu_{1+x}O$ (%)	Doping level in $Eu_{1-x}Gd_xO$ (%)
I,II	$x < 0$	-
III	$x \cong 0$	$x \cong 0$
IV	$0 < x \leq 0.1$	$0 < x \leq 1.5$
V	$x > 0.1$	$x > 1.5$

interest us. Group III consists of stoichiometric samples and therefore contain insulating materials (n-type semiconductors). The last two groups describe Eu-rich and are of particular interest when studying CMR behavior. Group IV contains the samples with low values of x and group V those with higher values of x (c.f. Table 2.1). The materials of group IV exhibit metallic conduction at low temperature and present a metal-insulator transition (MIT) at a temperature of about 50 K. The resistivity around 50 K may change by a factor as large as 10^{13} [6, 7]. The value of x for these samples is small (c.f. Table 2.1). Finally, the conductivity of the samples belonging to group V is metallic at high temperature as well as at low temperature. Let us note here that the density of Eu-doped EuO is very similar to pure EuO and consequently the excess Eu atoms do not occupy interstitial sites but rather take the place of oxygen vacancies. Along with the changes in conductivity, Shafer *et al.* observed an x-dependent variation of T_C in $Eu_{1+x}O$, ranging from 69 K to about 79 K [19]. We shall discuss the reason for this x-dependence in the following sections.

The highest concentration of Eu atoms in $Eu_{1+x}O$ that was obtained experimentally is $x = 0.5\%$ [21]. The study of the effect of adding electrons in the EuO matrix is therefore limited to a small doping range for this system. However, EuO can also be doped by substitution of Eu^{2+} ions by other rare earth ions or divalent ions. Of course, since the radius of the dopant is different than the radius of Eu^{2+}, the overlap between orbitals on neighboring sites is modified and so are the magnetic exchange interactions. For example, doping EuO with Ca increases T_C since the radius of a Ca^{2+} ion is smaller than an Eu^{2+} ion, and thus the exchange interactions are increased. A case of particular interest is EuO doped with Gd^{3+} leading to $Eu_{1-x}Gd_xO$. Gd has one more electron than Eu that is in a $5d$ orbital. We expect that a given Gd atom in the EuO matrix can be in two different states: either the extra d-electron is delocalized in the conduction band of $Eu_{1-x}Gd_xO$ and the atom becomes a Gd^{3+} ion or the d-electron stays localized and the atom is a Gd^{2+} ion. For a given Gd concentration, we will have a number N_{2+} of Gd^{2+} ions and a number N_{3+} of Gd^{3+}ions in the EuO matrix. The ratio N_{3+}/N_{2+} is expected to change with the concentration of Gd. Typically, this ratio should be zero at very low concentrations and large at high concentrations. This will most likely affect the magnetic interactions between Gd and Eu electron spins since Gd^{2+} is not in a ${}^8S_{\frac{7}{2}}$ configuration. However, the fact that $S = 7/2$ for Gd^{3+} indicates that Gd is a good substitution for Eu to minimize spin disorder effects. Gd^{3+} has a smaller radius than Eu^{2+} and doping EuO with Gd^{3+} will therefore lead to an increase of ferromagnetic interactions. But the extra d-electron may increase the electrical conductivity of the material.

Following the general results of N. F. Mott [22] on the metal-insulator transition, we know that for low concentrations of dopants, the two excess electrons coming from a Eu^{2+} ion or the excess electron from a Gd^{3+} ion stay localized respectively on the O vacancy or on the Gd site due to

the fact that the thermal energy of the electrons are lower than the donor binding energy.[1] When the concentration becomes higher than a critical concentration x_c, the potential is screened by the excess electrons and the additional electrons are excited into the conduction band and the material becomes metallic. The critical electron concentration n_c at which the transition occurs is usually given by the Mott criterion

$$n_c^{1/3} a_H^* = K, \tag{2.1}$$

where a_H^* is the experimental value of the effective Bohr radius of the isolated donor center in the nonmetallic regime far from the transition (low-electron-density regime) and K is a constant close to 0.25 [23, 24]. In the case of EuO with excess Eu, this expression gives approximately $n_c = 8 \cdot 10^{18}\,\mathrm{cm}^{-3}$ [25] (this value corresponds to $x_c \cong 0.05\%$).[2] However, (2.1) is no longer valid in the case of magnetic semiconductors since magnetic interactions modify electron-electron interactions. Leroux-Hugon [26] has shown that taking into account the exchange interaction leads to a new value of $n_c = 4.8 \cdot 10^{19}$ cm^{-3} ($x_c \cong 0.3\%$)[2] that is consistent with the experimental results of Oliver *et al.* [27]. There is another peculiarity in the carrier density of these materials: the carrier density n is a function of temperature. If $x > 0$, n is larger below about 50 K and sharply decreases at higher temperatures. If x is greater than a value x_0, then n is larger than n_c at low temperature and therefore a temperature change drives a MIT. For concentrations above the critical concentration x_c, n is larger than n_c for all temperatures and there is no MIT in these samples. A schematic representation of these different regimes is presented in Fig. 2.1. Note that the curves shown in this figure do not correspond to real measurements. The values of n are approximate values taken from the results on $Eu_{1+x}O$ of Oliver *et al.* [27]. Experimentally, the value of x_c is approximatively 0.1% for $Eu_{1+x}O$ and about 1.5% for $Eu_{1-x}Gd_xO$ according to Samokhvalov *et al.* [20] (c.f. Table 2.1). The value of x_0 is not well defined but is clearly very close to zero for both systems.

We can summarize the electrical properties of $Eu_{1+x}O$ and $Eu_{1-x}Gd_xO$ by emphasizing that there are three different regimes: if $0 \leq x < x_0$, the material is semiconducting at all temperatures; if $x_0 \leq x < x_c$, the material has a metallic behavior at low temperature and an insulating behavior at high temperature; finally, if $x_c \leq x$, the material is metallic at all temperatures. That means that a temperature change as well as a change in the doping can drive a MIT. These two types of MIT were independently observed in $Eu_{1-x}Gd_xO$ by Godart *et al.* [28] and by Samokhvalov *et al.* [20]. However, it is important to note that Schoenes and Wachter did not observe a temperature-induced MIT in Gd doped EuO and they claimed that if a MIT is observed it is only due to the presence of oxygen vacancies [29]. It is therefore not entirely clear that the presence of Gd atoms in EuO has the same effect as Eu excess.

Let us examine the magnetic properties of samples belonging to each of the three groups III, IV and V. It was observed experimentally that the bulk magnetic properties go through a dramatic change when the doping level reaches x_c. Indeed, the Curie temperature jumps from about 69 K up to 120 K over a very short range of x. Moreover, for $x < x_c$ the temperature dependence of the bulk magnetization $|\boldsymbol{M}(T)|$ follows quite well a Brillouin law, whereas for $x \geq x_c$ there is a notable

[1] The donor binding energy is equal to the Couloumb potential of the donor.

[2] We calculated x_c from n_c assuming that all the electrons from the excess Eu atoms (2 electrons per atom) become conduction electrons at the Mott transition. Since EuO is a cubic crystal, $N/V = 1/a^3$, where N is the number of sites, V is the volume of the sample and $a = 5.14$ Å is the lattice constant. We then obtained $x_c = (n_c/2)/(N/V) = \frac{1}{2}\, n_c a^3$.

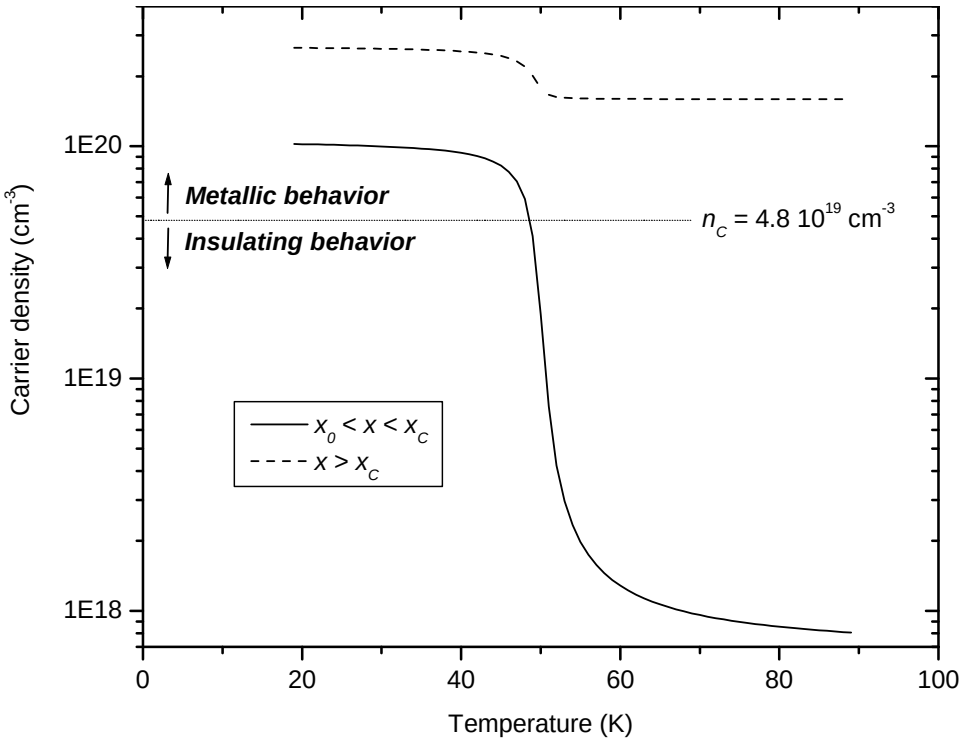

Figure 2.1: Carrier density vs. temperature for two different doping regimes: $x_0 < x < x_c$ and $x > x_c$. The shapes of the curves are deduced from the experimental results on $Eu_{1+x}O$ presented in [27].

departure from a Brillouin law. Therefore, in terms of macroscopic magnetic properties, only two regimes were observed: if $0 \leq x < x_c$, the Curie temperature is close to 69 K (69-79 K) and the temperature behavior of the bulk magnetization follows rather well a Brillouin law; if $x \geq x_c$, the Curie temperature is approximately in the range 120-140 K and $|\boldsymbol{M}(T)|$ does not behave according to a Brillouin law. One of the challenges of this NMR study of the materials was to detect the microscopic magnetic differences between samples with $0 \leq x < x_0$ and samples with $x_0 \leq x < x_c$ that could explain the difference in electrical properties.

Now let us examine the correlation between the temperature dependence of the carrier density $n(T)$ and $|\boldsymbol{M}(T)|$, i.e., we would like to determine the contribution of the conduction electrons on the magnetic properties of the material. This discussion leads to an examination of the exchange interactions present in these systems.

2.2 Exchange interactions

As we discussed previously, the Eu atoms in EuO can be considered as Eu^{2+} ions. Since $L = 0$ for these ions, the ground state of these ions does not couple to any excited state and therefore the exchange interactions are isotropic. For this reason, the effective Hamiltonian of this system is very well approximated by the Heisenberg model:[3]

[3]Note that we will denote vectors with bold face, e.g., $\boldsymbol{r}_{ij}$. Also, operators will be denoted with a hat, e.g., $\hat{S}_i^z$, and the thermal expectation value of an operator will be enclosed between brackets, e.g., $< \hat{S}_i^z >$.

$$\hat{\mathcal{H}}_{Heisenberg} = -\frac{1}{2}\sum_{i,j} J(\boldsymbol{r_{ij}})\hat{\boldsymbol{S}}_i \cdot \hat{\boldsymbol{S}}_j. \tag{2.2}$$

It is usually sufficient to calculate the exchange integral $J(\boldsymbol{r_{ij}})$ between the two electron spins $\hat{\boldsymbol{S}}_i$ and $\hat{\boldsymbol{S}}_j$ over the nearest neighbors (nn) and the next nearest neighbors (nnn) and we therefore have for the exchange constants:

$$J(\boldsymbol{r_{ij}}) = \begin{cases} J_1 & \text{if i and j nn} \\ J_2 & \text{if i and j nnn} \\ 0 & \text{otherwise.} \end{cases} \tag{2.3}$$

The exchange mechanisms that are responsible for J_1 and J_2 in EuO were described in detail by Kasuya [30]. His model shows that J_1 is generated by an indirect exchange process calculated in a third-order perturbation analysis and that J_2 arises from three different superexchange mechanisms corresponding to calculations performed in a fourth-order perturbation analysis. Kasuya obtained $J_1/k_B = 0.406\,\mathrm{K}$ and found a positive value of J_2 with $J_2/k_B = 0.014\,\mathrm{K}$. Neutron scattering experiments on powdered EuO led to the following experimental values: $J_1/k_B = 0.606 \pm 0.008\,\mathrm{K}$ and $J_2/k_B = 0.119 \pm 0.015\,\mathrm{K}$ [31]. We see that the theoretical value of J_1 is very close to the experimental value, but the value of J_2 is underestimated in the calculations of Kasuya. However, the model does give the correct sign for J_2, which suggests that it is adapted for the description of the exchange interactions taking place in pure EuO.

Let us examine how adding free carriers in a EuO matrix affects the exchange interactions. As we noted in Sect. 2.1, free carriers can be added either by adding Eu^{2+} (departure from stoichiometry) or by doping EuO with rare earth ions, in particular Gd^{3+}. Also, we saw that for a concentration of donors higher than x_c, the Curie temperature increases dramatically and the temperature behavior of the magnetization changes. Several models were developed to relate the variation of the ordering temperature with the exchange interactions. The analysis is always split in two parts: on one hand, the study of the case $x < x_c$ and on the other hand the case $x > x_c$. We will start by discussing the latter case and treat the former case in Sect. 2.3.

The most successful model treating the case $x > x_c$ seems to be the one developed by A. Mauger based on the Ruderman-Kittel-Kasuya-Yosida (RKKY) theory [32, 33].[4] In this theory, three major modifications were made to adapt the RKKY theory for metals to the case of magnetic semiconductors like EuO. First, to take into account the narrow conduction band, Mauger defined a dispersion relation that is not parabolic. Second, the model assumes that the conduction band is split into spin up and spin down subbands. Finally, Mauger noted that the exchange interactions between the localized electron spin and the conduction electron spin are not negligible and he therefore took into account the polarization of the electron gas. The effective spin Hamiltonian between the $4f$ spins is then written

$$\hat{\mathcal{H}}_{eff} = -\frac{1}{2}\sum_{i,j} J_{eff}(\boldsymbol{r}_{ij})\hat{S}_i^z \hat{S}_j^z, \tag{2.4}$$

with

$$J_{eff}(\boldsymbol{r}_{ij}) = J_{eff}(\boldsymbol{r}_{ij}, \sigma, T, E_F), \tag{2.5}$$

[4] Note that Holtzberg *et al.* had already invoked the RKKY theory to explain the dependence on n of the paramagnetic Curie temperature in rare earth chalcogenides in 1964 [34].

where $\boldsymbol{r_{ij}}$ is the radius vector between the sites i and j, $\sigma =< \hat{S}^z > /S$ represents the polarization of the localized spins and E_F is the Fermi energy of the crystal. Mauger *et al.* used the molecular field approximation to determine σ:

$$\sigma = B_S \left(\frac{\sigma S^2 (I(\boldsymbol{k}=0) + J_{eff}(\boldsymbol{k}=0, \sigma, T, E_F)) + g\mu_B H_{ext}}{k_B T} \right), \tag{2.6}$$

where B_S is the Brillouin function, $I(\boldsymbol{k})$ and $J_{eff}(\boldsymbol{k}, \sigma, T, E_F)$ are the Fourier transforms of the direct exchange constant and of the indirect exchange constant $J_{eff}(\boldsymbol{R}_{ij}, \sigma, T, E_F)$ respectively.

Since EuO has a NaCl structure, we take $I(\boldsymbol{k}=0) = 12J_1 + 6J_2$. The dependence on x of J_{eff} comes through the dependence on x of the Fermi energy. In the model, the authors took $E_F = E_F(x)|_{T=0}$ and $E_F(x)$ is calculated from the density of states derived from the dispersion law. By solving the system of two equations given by (2.5) and (2.6), we get $J_{eff}(\boldsymbol{k}=0, T, x)$ and $\sigma(T, x)$. From these two equations, it is easy to deduce the two variables that interest us:

$$T_{\mathrm{C}}(x) = \frac{S(S+1)}{3k_B}[I(\boldsymbol{k}=0) + J_{eff}(\boldsymbol{k}=0, T=T_{\mathrm{C}}, x)] \tag{2.7}$$

$$M(T, x) = \frac{N}{V} S\sigma(T, x) \tag{2.8}$$

The function $T_{\mathrm{C}}(x)$ obtained is a growing function of x that increases up to about 155 K over a very small range of x (approximatively 0-0.05) [32]. For larger x, T_{C} decreases to reach 90 K around $x = 20\%$. The temperature behavior of the magnetization is shown in Fig. 2.2 for $x = 2\%$ along with experimental data obtained by Mauger *et al.*. The model developed by Mauger *et al.* reproduces the striking experimental behavior: the sharp increase of T_{C} with the doping together with the non-Brillouin behavior of the magnetization. We therefore take this model as the starting point for our discussions.

Let us mention that Nolting and Oleś developed a different theory to explain the increase in T_{C} of Gd doped EuO [35]. The dependence of T_{C} on the carrier density n is derived from magnon scattering processes due the presence of conduction electrons. More recently, Santos and Nolting have presented a theory based on the Kondo-lattice model [10].

2.3 Magnetic polarons

For $x < x_c$, the model of Mauger *et al.* is not valid anymore. As mentioned previously, in this range a variation of the doping level has a tremendous effect on the transport properties of the samples but the Curie temperature is almost not affected. The dramatic change of resistivity associated with a sharp decrease in carrier density n is very often explained by the formation of bound magnetic polarons (BMP) [1, 36]. A magnetic polaron is a quasi particle formed by a conduction electron and its neighboring localized electron spins. The existence of such a quasi particle can be demonstrated by minimizing the energy of the system formed of an electron and a certain number of localized spins, that is

$$E = E_{kin} + E_{Coulomb} + E_{s-f} \tag{2.9}$$

where E_{kin} is the kinetic energy of the conduction electron, $E_{Coulomb}$ is the Coulomb interaction between the donor center and the conduction electron, and E_{s-f} is the exchange energy coming from

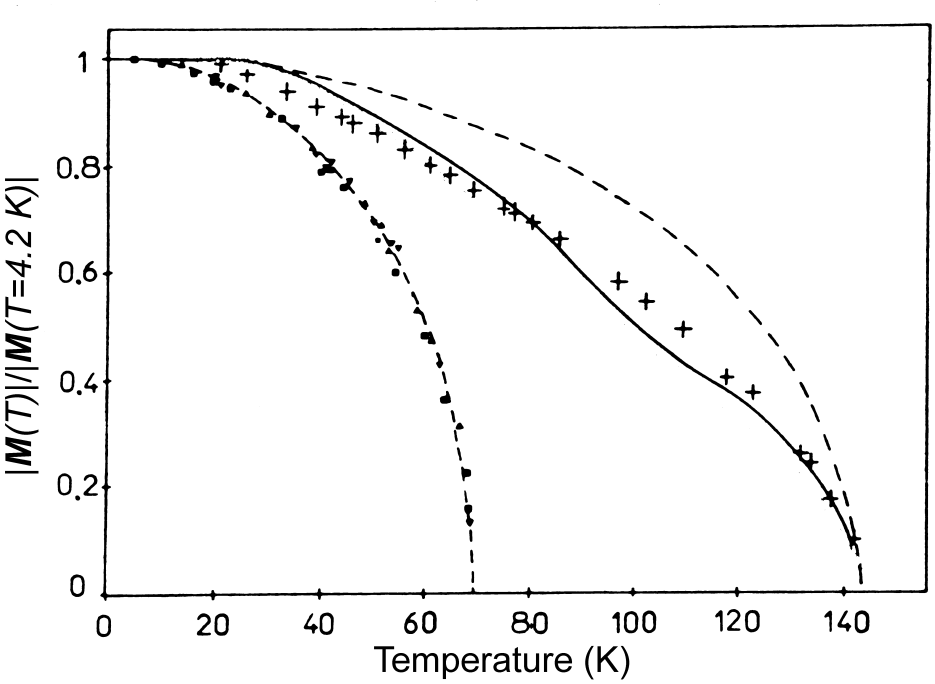

Figure 2.2: Reduced magnetization vs. temperature. The squares represent data taken on stoichiometric EuO, the triangles data taken on Eu-rich EuO, and the crosses data taken on 2% Gd doped EuO. The two dashed lines are Brillouin curves for $T_C = 69.5\,\mathrm{K}$ and $T_C = 148\,\mathrm{K}$. The solid line represents the result of Mauger's model for $n = 5 \cdot 10^{20}\,\mathrm{cm}^3$ (The figure is from [33]).

the magnetic $s - f$ interaction between the conduction electron spin and the localized spins [1]. The net moment of a BMP is calculated to be of the order of 25 Bohr magnetons [37]. It is important to distinguish a bound magnetic polaron from a free magnetic polaron (FMP). The conduction electron of the latter is unbound whereas the electron of the former is trapped at a donor site by electrostatic forces. In Gd doped EuO as well as in Eu-rich EuO, we expect to observe mainly BMPs trapped around the donors.

While the role of magnetic polarons in CMR material is widely recognized, the observation of magnetic polarons in systems such as EuO and Gd doped EuO has only been suggested by transport and magnetization measurements. As P.A. Wolff noted in 1988, "None of these experiments, however, unambiguously determines microscopic parameters-such as binding energy, moment, or size-of the BMP." Note that the existence of magnetic polarons in $Eu_{1-x}Gd_xO$ has recently been inferred from Raman scattering data [13, 38, 39].

2.4 Our samples and their magnetic characterization

The samples that we measured in this study belong to the family $Eu_{1-x}Gd_xO$. They are single crystals. We studied samples with four different doping levels: pure EuO, $x = 0.6\%$, $x = 2\%$ and $x = 4.3\%$. These crystals were grown in Zürich at ETHZ by Mattenberger. According to the description given in Sect. 2.1, pure EuO belongs to group III, 0.6% Gd doped EuO to group IV and the two other doping levels to group V (c.f. Table 2.1).

A way to verify that these single crystals indeed belong to the categories mentioned above, is to

Table 2.2: Paramagnetic Curie temperature of the four samples we studied (measurements performed by Heesuk Rho).

Doping level x (%)	Paramagnetic Curie temperature θ_C (K)
0	69.55
0.6	73.05
2	123.45
4.3	132.5

measure their Curie temperature T_C. Determining the Curie temperature of a bulk ferromagnet by measuring the temperature dependence of its zero-field magnetization is not an easy task because of the presence of magnetic domains leading to a small net magnetization. It is however straightforward to determine the so-called paramagnetic Curie temperature θ_C. While T_C is the temperature below which there is spontaneous local magnetization in the absence of an applied magnetic field, θ_C is deduced by fitting the measured temperature dependence of the magnetic susceptibility χ in the paramagnetic regime with a Curie-Weiss law of the form $\chi = C/(T - \theta_\mathrm{C})$. Using a SQUID magnetometer, our collaborator Heesuk Rho determined the values presented in Table 2.2.

The saturation magnetic moment of each sample has also been measured using a SQUID magnetometer. The curves obtained in a field of 7 T are shown on Fig. 2.3. Gd having the same electron spin $S = 7/2$ as Eu, the extra electrons that the Gd^{3+} ions bring to the EuO matrix should most likely be the cause of the differences in low temperature magnetic moments between samples. However, the difference in magnetic moment between pure EuO and 0.6% Gd doped EuO shown on Fig. 2.3 is clearly too large to be only due to the presence of additional electrons coming from Gd ions. We think that there was a problem during the measurement of the pure sample although we are not sure of its origin. Samokhvalov *et al.* found that the magnetic moment at 4.2 K of pure EuO is about 198 emu/g, which is substantially larger than the value shown on Fig. 2.3 [40]. Note also that the magnetic moment of the 2% and 4.3% samples at the lowest temperature are almost identical. The reason for this last fact is not clear. It might be due to an imperfect alignment of the field along the easy axis of the sample. In any case, we observe that an increase in Gd concentration leads to an increase of the magnetic moment. This suggests that the Gd spins are aligned parallel to the Eu spins. This is in disagreement with Schoenes and Wachter who observed that "The Gd spin has a tendency to enter the material antiparallel to the Eu spins" [29].

Another crucial point about the magnetic properties of $Eu_{1-x}Gd_xO$ is that the paramagnetic Curie temperature is rather different than the Curie temperature for all doping levels $x > 0$. This difference has been measured by Samokhvalov *et al.* [41]. Their results, presented in Fig. 2.4, show that for doping below about 0.8% the Curie temperature of $Eu_{1-x}Gd_xO$ is almost exactly the same as for pure EuO. However, the paramagnetic Curie temperature increases as soon as the Gd concentration increases and reaches a maximum. Note that the model of Mauger does not explain the difference between the Curie paramagnetic temperature and the Curie temperature.

It is possible to determine the Curie temperature T_C of a sample without directly measuring its magnetization as a function of temperature. A straightforward method is to place the sample in the coil of a resonant LC circuit and to measure the shift of the resonance frequency as a function of temperature. Indeed, the resonance frequency of the circuit is, to a good approximation, given by $\omega = 1/\sqrt{LC}$ where L is related to the complex susceptibility $\chi(\omega) = \chi'(\omega) - i\chi''(\omega)$ through the expression

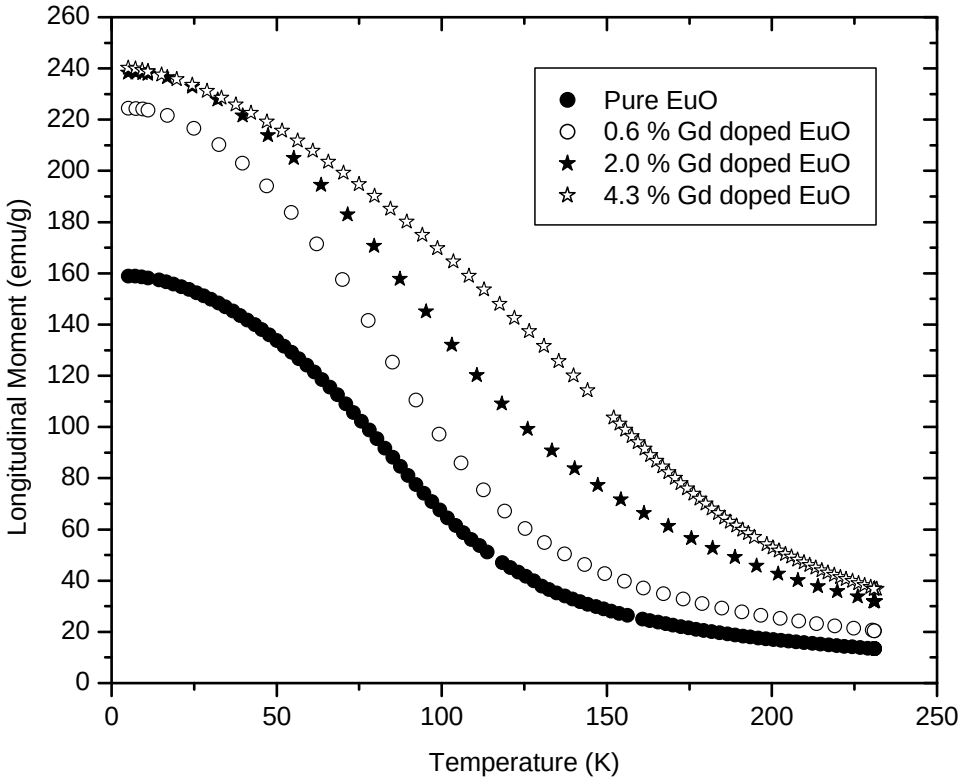

Figure 2.3: Longitudinal magnetic moment vs. temperature of pure and Gd doped EuO samples in a magnetic field of 7T (Measurement performed by Heesuk Rho).

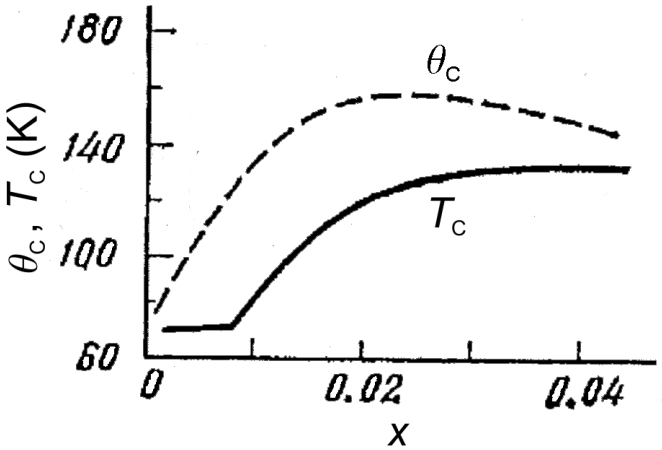

Figure 2.4: Paramagnetic Curie temperature θ_C and Curie temperature T_C as a function of Gd doping x (from [42]).

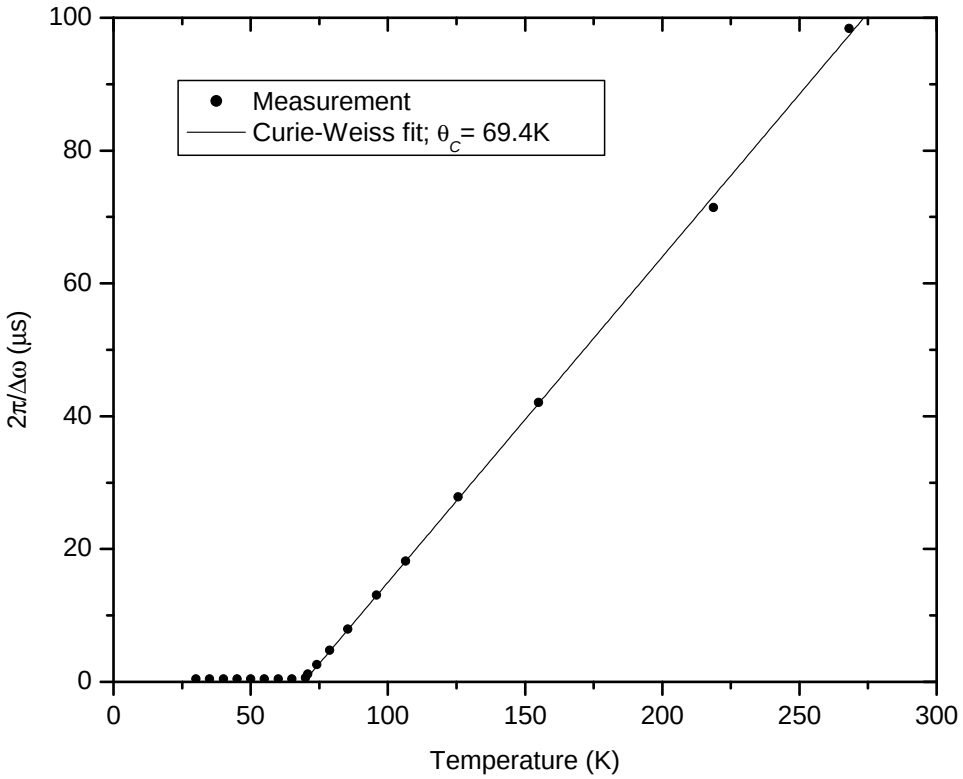

Figure 2.5: Inverse zero-field frequency shift vs. temperature in 0.6% Gd doped EuO. The zero value of the shift is defined as the value of the shift at 300K. The straight line is a fit of the data with a Curie-Weiss law.

$$L = L_0[1 + 4\pi\chi(\omega)], \tag{2.10}$$

where L_0 is the inductance of the empty coil (c.f. e.g. [43]). Therefore, a dramatic change in the magnetic susceptibility, such as that expected at the ferromagnetic-paramagnetic phase transition, will induce a dramatic change $\Delta\omega$ in the resonance frequency ω.

The measurement performed on 0.6% Gd doped EuO is presented in Fig. 2.5. The temperature behavior of the inverse shift above the transition temperature follows well a Curie-Weiss law. From the Curie-Weiss fit, we determined the paramagnetic Curie temperature to be about 69.4 K which is clearly lower than the value of 73.05 K presented in Table 2.2 but is very close to the paramagnetic Curie temperature of pure EuO (c.f. Table 2.2). We see that it is therefore important to specify what measurement technique is used to determine the transition temperature since the value of the transition temperature may vary from one technique to another.

The values of θ_C and T_C we have measured clearly show that the 0.6% Gd-doped sample belongs to group IV whereas the 2% and 4.3% samples belong to group V. Also, the fact that the paramagnetic Curie temperature of the pure sample is very close to the expected Curie temperature $T_C = 69.5$ K determined in previous studies (see e.g. [27]) shows that the chemical composition of this sample is close to the perfect stoichiometry.

2.4.1 NMR frequency vs. T

The NMR frequency of a nucleus in a magnetic field $\boldsymbol{H}$ corresponds to the Larmor frequency

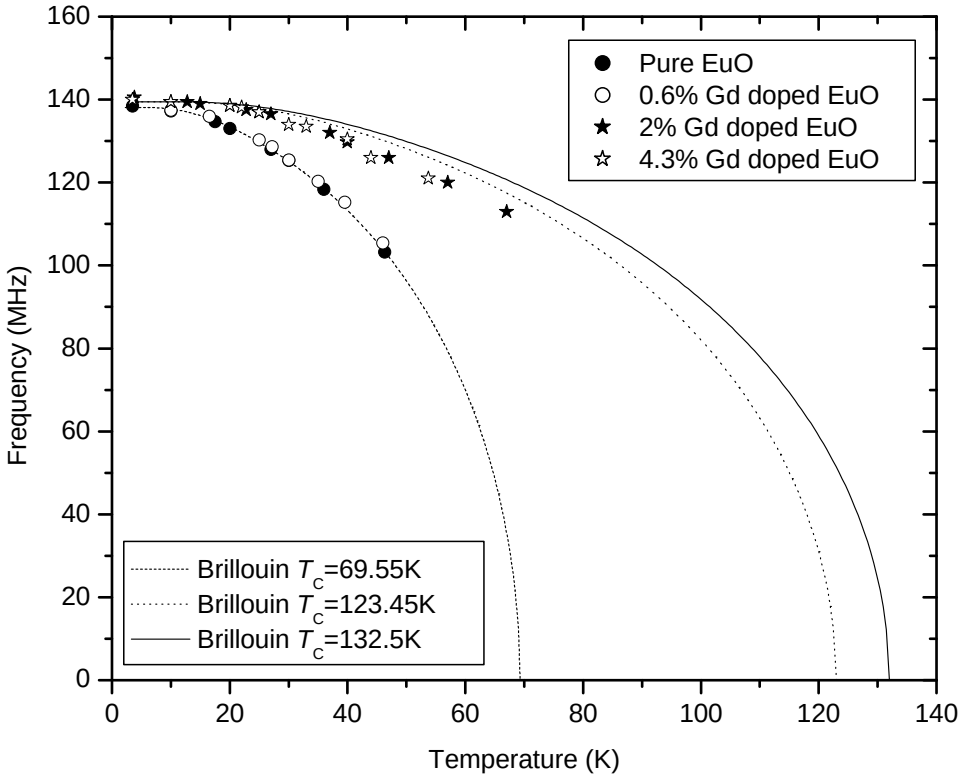

Figure 2.6: Zero-field NMR frequency of the center of the NMR line of pure and Gd doped EuO vs. temperature. Brillouin functions are plotted along with the data. Note that we took $T_{\mathrm{C}} = \theta_{\mathrm{C}}$, which is not exact in the case of 2% and 4.3% Gd doped EuO. However, even with a value of T_{C} smaller than θ_{C} a Brillouin curve does not accurately fit the data of 2% and 4.3% Gd doped EuO.

$$\nu_0 = \frac{\gamma_n}{2\pi}|\boldsymbol{H}|, \tag{2.11}$$

where γ_n is the gyromagnetic ratio of the nucleus. As will be shown in Sect. 3.1, in ferromagnetic material, when no external field is applied, the field acting on the nuclei is, too a very good approximation, proportional to the magnetization of the sample. Therefore, the temperature dependence of the zero-field NMR frequency follows the temperature dependence of the magnetization.[5] We measured the ^{153}Eu resonance frequency in EuO and Gd doped EuO as a function of temperature. In Fig. 2.6, we plotted the frequency of the center of the NMR line of each type of sample as a function of temperature. We observed that the temperature dependence of the frequency of pure EuO and 0.6% Gd doped EuO is accurately described by a Brillouin function with $T_{\mathrm{C}} = 69.55\,\mathrm{K}$. However, in the case of 2% and 4.3% Gd doped EuO, the frequency is not well described by a Brillouin function: for temperature above about 30 K, the frequency has a lower value than the frequency predicted by the theoretical curve. These results confirm the magnetometric measurements performed by Mauger (c.f. Fig. 2.2).

[5] By looking at the temperature dependence of the ^{153}Eu NMR frequency in the vicinity of the magnetic transition of the ferromagnet EuS, Heller and Benedek determined very accurately the critical exponent β through the relation $\nu_0(T) \propto |\boldsymbol{M}(T)| \propto (T_{\mathrm{C}} - T)^{\beta}$ [44].

Chapter 3

NMR in ferromagnets

Nuclear spins are highly sensitive to electronic spins and their fluctuations. On the other hand, electronic spins are negligibly affected by nuclear spins. Nuclear spins can therefore be thought of as "invisible" probes of the electronic structure and its dynamics. For this reason, NMR is an attractive tool to study ferromagnetism and more specifically the dynamics of electronic spins. There are several reasons why NMR in ferromagnets is slightly more complex than in non-magnetic materials, especially when the studied nucleus belongs to the ion carrying the magnetic moment. One of the important characteristics is that the unpaired spins of the inner shell responsible for the magnetism of the ion, namely the $3d$-shell electron spins in the iron group elements and the $4f$-shell electron spins for rare earth elements, are the source of an effective magnetic field that strongly perturbs the nuclear system. The presence of this effective field leads to shifts and broadening of the resonance lines. It also affects the dynamics of the nuclear spins.

The purpose of this chapter is to address the experimental issues related to the presence of a strong electronic magnetization in the $Eu_{1-x}Gd_xO$ systems. We will start by listing the interactions taking place between the measured nuclei and their environment. Then, we will discuss these interactions and examine how to extract information about the nuclear environment from NMR measurements performed on magnetic ions such as Eu^{2+}.

3.1 NMR Hamiltonian

NMR experiments consist of exciting and detecting transitions between nuclear spin states. In this study, we will deal with ^{151}Eu and ^{153}Eu nuclei which are both spin $I = \frac{5}{2}$. The degeneracy of the five nuclear spins states can be lifted by the application of an external magnetic field, $\boldsymbol{H}_0$. However, since internal magnetic and electric fields participate in the splitting of the levels, even in the absence of external field the degeneracy may be lifted. The resonance frequencies measured in NMR experiments correspond to the transition frequencies between eigenstates of the nuclear Hamiltonian

$$\hat{\mathcal{H}}_{nuclear} = \hat{\mathcal{H}}_{Zeeman} + \hat{\mathcal{H}}_{quadrupole} + \hat{\mathcal{H}}_{electron-nucleus} + \hat{\mathcal{H}}_{internuclear} \tag{3.1}$$

These four terms are developed and explained below.

Zeeman Hamiltonian

The Zeeman part represents the interaction of the nucleus with an applied external field $\boldsymbol{H}_0$. It is given by

$$\hat{\mathcal{H}}_{Zeeman} = -\gamma_n \hbar \boldsymbol{H}_0 \cdot \hat{\boldsymbol{I}} \tag{3.2}$$

where γ_n is the nuclear gyromagnetic ratio and $\hat{\boldsymbol{I}}$ is the nuclear spin operator. In most of the experiments done in this study, we did not apply any external field to measure the ^{151}Eu and ^{153}Eu spin systems. We performed what is commonly called zero-field NMR experiments. This type of experiment is possible in $Eu_{1-x}Gd_xO$ systems because of the presence of a strong local magnetic field created by the unpaired electron spins of Eu and Gd atoms.[1]

Quadrupole Hamiltonian

Nuclei with spin I larger than $\frac{1}{2}$, such as ^{151}Eu and ^{153}Eu, have a nuclear electric quadrupole moment that interacts with electric field gradients (EFGs) created by the surrounding crystal structure. The Hamiltonian representing this interaction has the form

$$\hat{\mathcal{H}}_{quadrupole} = \frac{e^2qQ}{4I(2I-1)}(3\hat{I}_z^2 - I^2 + \beta(\hat{I}_x^2 - \hat{I}_y^2)), \tag{3.3}$$

where Q is the electric quadrupole moment of the studied nucleus, q is the electric field gradient (EFG) and β is a factor describing the asymmetry of the EFG [43]. If the measured nuclei are located at lattice sites of perfect cubic symmetry, the EFGs acting on those nuclei cancel. Thus, since EuO has the fcc symmetry, we do not expect a quadrupolar splitting of the spin levels of ^{151}Eu and ^{153}Eu. However, defaults such as vacancies and deformations of the lattice can lower the symmetry of the Eu sites, and in that case we would observe five transitions in the frequency spectrum.

Electron-nucleus Hamiltonian

Nuclear spins couple to both the orbital angular momentum $\hat{\boldsymbol{L}}$ and the spin $\hat{\boldsymbol{S}}$ of the surrounding electrons. It is common to make the distinction between the coupling of a nuclear spin to its own electron shells and the coupling of the nuclear spin to the outside electron shells. The former is usually called the (on-site) hyperfine interaction. The latter can be decomposed in two types of interactions: the so-called transferred hyperfine interaction describing the coupling of the nuclear spin to the total angular momentum (orbital and spin) of the neighboring magnetic ions through electronic excitations [45],[2] and the dipole-dipole interaction between the nuclear spin and total angular momentum of the neighboring magnetic ions [46, 47]. In $Eu_{1-x}Gd_xO$, the magnetic neighbors of Eu^{2+} ions are Eu^{2+}, Gd^{2+} and Gd^{3+} ions.[3] In addition, the conduction electrons also interact with the nuclei.

[1] Zero-field experiments are also possible in non-magnetic materials, for nuclear spins $I > \frac{1}{2}$, in the presence of electric field gradients (EFGs) that lift the degeneracy of the nuclear spins states. This type of experiment is called nuclear quadrupole resonance (NQR).

[2] Ueno *et al.* showed that mechanisms similar to those explaining the exchange interaction (used by Kasuya to determine J_1 and J_2 (c.f. Sect. 2.2)) can explained the transferred hyperfine interaction in europium chalcogenides.

[3] As we have seen in Sect. 2.1, not all the extra electrons brought by Gd^{2+} will participate in the conduction. We will make the distinction between Gd^{2+} and Gd^{3+} ions, the latter bringing a conduction electron in the conduction band.

This last interaction is sometimes called the contact interaction and is described by a Fermi contact term (see, e.g., [43] for a description of the Fermi contact term).[4]

The hyperfine interaction is generally composed of an orbital term, a dipolar term and a Fermi contact term.[5,6] Since the resulting orbital angular momentum of the ground state of Eu^{2+} ions is equal to zero (configuration ${}^8S_{\frac{7}{2}}$), the orbital part of the hyperfine interaction is zero. The electron-nucleus Hamiltonian of a crystal containing N magnetic atoms and n conduction electrons can therefore be written as

$$\hat{\mathcal{H}}_{electron-nucleus} = \hat{\boldsymbol{I}} \cdot \mathbf{A} \cdot \hat{\boldsymbol{S}} + \sum_{i=1}^{N-1} \hat{\boldsymbol{I}} \cdot \widetilde{\mathbf{A}}^{i} \cdot \hat{\boldsymbol{J}}_i - \gamma_n \hbar \sum_{j=1}^{N-1} \boldsymbol{H}^{j}_{dipolar} \cdot \hat{\boldsymbol{I}} + \sum_{k=1}^{n} C \hat{\boldsymbol{I}} \cdot \hat{\boldsymbol{s}}_k \delta(\boldsymbol{r}_k), \qquad (3.4)$$

where the tensor $\mathbf{A}$ is the hyperfine tensor describing the hyperfine interaction between the reference nuclear spin $\hat{\boldsymbol{I}}$ and the electron spin $\hat{\boldsymbol{S}}$ of its own electron shell, the tensor $\widetilde{\mathbf{A}}^{i}$ is the transferred hyperfine tensor describing the transferred hyperfine interaction between the reference nuclear spin $\hat{\boldsymbol{I}}$ and the total angular momentum $\hat{\boldsymbol{J}}_i$ of the ith neighboring magnetic ion, $\boldsymbol{H}^{j}_{dipolar}$ is the dipolar field created by the jth neighboring magnetic ion, C is a constant taking into account the mixing of the s- and d-orbitals forming the conduction band [51], $\hat{\boldsymbol{s}}_k$ is the spin operator of the kth conduction electron, and $\boldsymbol{r}_k$ is the radius vector between the reference nuclear spin $\hat{\boldsymbol{I}}$ and the kth conduction electron.

Let us distinguish between the different type of neighbors surrounding the reference nuclear spin. Since the spin ground state of Gd^{3+} and Eu^{2+} is the same, both will couple to the reference spin through a similar magnetic interaction. This is not the case for Gd^{2+}. Also, as a consequence of the resulting zero orbital angular momentum of the state ${}^8S_{\frac{7}{2}}$, the orbital part of the dipolar field created by Eu^{2+} and Gd^{3+} is zero. Following the treatment of Yasuoka *et al.* [47], we can rewrite the dipolar coupling between the reference spin and the electron spin of the ith Eu^{2+} or Gd^{3+} neighbor as a tensor. Equation (3.4) then becomes

$$\hat{\mathcal{H}}_{electron-nucleus} = \hat{\boldsymbol{I}} \cdot \mathbf{A} \cdot \hat{\boldsymbol{S}} + \sum_{i=1}^{n'} \hat{\boldsymbol{I}} \cdot \mathbf{B}^{i} \cdot \hat{\boldsymbol{S}}_i + \sum_{j=1}^{n''} \hat{\boldsymbol{I}} \cdot \mathbf{D}^{j} \cdot \hat{\boldsymbol{J}}_j + C \sum_{k=1}^{n} \hat{\boldsymbol{I}} \cdot \hat{\boldsymbol{s}}_k \delta(\boldsymbol{r}_k), \qquad (3.5)$$

where n' is the number of Eu^{2+} and Gd^{3+} neighboring ions, n'' is the number of Gd^{2+} neighboring ions, the tensor $\mathbf{B}^{i}$ describes the sum of the transferred hyperfine interaction and dipolar interaction between the reference nuclear spin $\hat{\boldsymbol{I}}$ and the electron spin $\hat{\boldsymbol{S}}_i$ of its ith Eu^{2+} or Gd^{3+} neighbor, and the tensor $\mathbf{D}^{j}$ describes the sum of the transferred hyperfine interaction and dipolar interaction between the reference nuclear spin $\hat{\boldsymbol{I}}$ and the total angular momentum $\hat{\boldsymbol{J}}_j$ of its jth Gd^{2+} neighbor. The couplings represented by the tensors $\mathbf{B}^{i}$ and $\mathbf{D}^{j}$ are much smaller than the hyperfine coupling represented by $\mathbf{A}$. Clearly, we can neglect the effect of the far neighbors on the reference spin. Taking into account only the nearest neighbors and the next nearest neighbors is usually appropriate in magnetic systems. If we define the z axis to be the direction of the anisotropy field, [7] and if we

[4] The conduction electrons in $Eu_{1-x}Gd_xO$ are not pure s-electrons. The conduction band is formed by 6s and 5d orbitals. This fact needs to be taken into account in the calculation of the Fermi contact term.

[5] In the case of Eu^{2+}, Gd^{2+}, and Gd^{3+} ions, the Fermi contact is due to the core polarization of the s-electrons located in the inner shells (see [48–50] for more details).

[6] In the presence of Gd in the system, the $4f$-electrons of Gd^{2+} and Gd^{3+} ions also participate in the polarization of the unpaired electrons of Eu^{2+} and consequently contribute to the hyperfine field.

[7] If an external magnetic field is applied, we assume that it is applied along the direction of the anisotropy field, i.e. along [111] in the case of EuO.

assume that the axis of quantization of $\hat{\boldsymbol{I}}$ coincides with the axis of quantization of $\hat{\boldsymbol{S}}$, [8] we obtain, from (3.5),

$$\hat{\mathcal{H}}_{electron-nucleus} = [(A_{zz} + \sum_{i=1}^{n'} B_{zz}^i) < \hat{S}^z >_T + \sum_{j=1}^{n''} D_{zz}^j < \hat{J}^z >_T + C \sum_{k=1}^{n} < \hat{s}_k >_T \delta(\boldsymbol{r}_k)]\hat{I}_z, \quad (3.6)$$

where n' and n'' now only count the next and next nearest neighbors, $< \hat{S}^z >_T$ is the thermal average at temperature T of the electron spin moment of Eu^{2+} and Gd^{3+} ions, $< \hat{J}^z >_T$ is the thermal averaging of the total angular momentum of the neighboring Gd^{2+} ions, and $< \hat{s}_k >_T$ is the thermal average at temperature T of the kth conduction electron spin. Note that we have assumed that the terms B_{lm}^i and D_{lm}^j with $l \neq z, m \neq z$ are negligible. This is motivated by the fact that the strong exchange interaction between neighboring angular momentum forces them to be aligned. In the case of pure EuO, the last two terms of (3.6) are zero and the the second term is a sum over all 12 first and 6 second Eu^{2+} neighbors ($n' = 18$). For low doping levels, typically $x < 1.5\%$, there is no contribution from the last term of (3.6) (c.f. Sect. 2.1).

From (3.6), we define two quantities that will often be mentioned in this work: the hyperfine field

$$\boldsymbol{H}_{hf} = \frac{A_{zz}}{\gamma_n \hbar} < \hat{S}^z >_T \boldsymbol{e}_z, \quad (3.7)$$

used to describe the hyperfine coupling in Eu atoms, and the local field

$$\boldsymbol{H}_{loc} = \frac{1}{\gamma_n \hbar}[(A_{zz} + \sum_{i=1}^{n'} B_{zz}^i) < \hat{S}^z >_T + \sum_{j=1}^{n''} D_{zz}^j < \hat{J}^z >_T + C \sum_{k=1}^{n} < \hat{s}_k >_T \delta(\boldsymbol{r}_k)]\boldsymbol{e}_z, \quad (3.8)$$

used to describe the total effective field felt by the reference Eu nuclear spin in the absence of an external field. In most cases, the hyperfine field is found to be antiparallel to $< \hat{S}^z >_T$ and consequently $A_{zz} < 0$. This is the case for Eu^{2+} ions. However, we do not know a priori the sign of B_{zz}^i, D_{zz}^j and C. Note that usually B_{zz}^i, D_{zz}^j, $C \ll A_{zz}$ and it is often a good approximation to take $\boldsymbol{H}_{loc} \cong \boldsymbol{H}_{hf}$.

Internuclear Hamiltonian

Nuclear spins can couple to each other either directly through dipole-dipole interactions, or indirectly via the electron spins. The dipole-dipole interaction has the well-known form

$$\hat{\mathcal{H}}_{dipole} = \frac{\gamma_{n_i} \gamma_{n_j} \hbar^2}{r_{ij}^3} \left[\hat{\boldsymbol{I}}_{\boldsymbol{i}} \cdot \hat{\boldsymbol{I}}_{\boldsymbol{j}} - 3 \frac{(\hat{\boldsymbol{I}}_{\boldsymbol{i}} \cdot \boldsymbol{r}_{\boldsymbol{ij}})(\hat{\boldsymbol{I}}_{\boldsymbol{j}} \cdot \boldsymbol{r}_{\boldsymbol{ij}})}{r_{ij}^2} \right] \quad (3.9)$$

where $\boldsymbol{r}_{ij}$ is the radius vector between spin I_i and spin I_j. Indirect interactions are second-order effects and the energy levels are calculated using second-order perturbation theory. In metals, the indirect interaction via the electron spin of the conduction electron is called the RKKY interaction [52]. In magnetic materials, the nuclei also interact through excitations of virtual magnons. This indirect interaction is called the Suhl-Nakamura interaction and will be discussed in more detail in Sect. 3.6.

[8] Since the hyperfine field created by the electron spin is by far larger than any other local field, we indeed expect the two axes of quantization to be parallel.

3.2 The nature of NMR in ferromagnets

In this study, we focused on the ferromagnetic phase of $Eu_{1-x}Gd_xO$, i.e., we mostly performed measurements at temperatures below the Curie temperature. At such temperatures, europium nuclei are influenced by a large local magnetic field due to the strong electronic magnetization present in the sample. Even in the case of pure EuO we can expect a rather large magnetic broadening due to spatial inhomogeneities in the magnetic structure of the material. The presence of Gd in the EuO matrix will further increase the inhomogeneity of the local field, giving rise to an additional broadening of the NMR lines. Therefore, we expect to have to deal with rather broad lines. Another consequence of the presence of a large local field in the $Eu_{1-x}Gd_xO$ systems is the strong temperature dependence of the resonance frequency (c.f. Sect. 2.4.1). Indeed, we saw in Sect. 3.1 that the local field is, to a good approximation, proportional to $< \hat{S}^z >_T$, the thermal average at temperature T of the electron spin moment of Eu^{2+} and Gd^{3+}. The resonance frequency is therefore strongly temperature dependent. As a consequence, NMR measurements in the magnetic phase of ferromagnetic systems require a very stable temperature control. In this study, we used two different cryogenic methods. For measurements at temperatures below 20 K as well as for all measurements performed with an external magnetic field, we used liquid helium and a standard continuous flow cryostat (Oxford model CF 1200). For zero-field measurements at temperature above 20 K, we used a closed-cycle helium refrigerator (CTI-Cryogenics model 21SC Cryodyne cryocooler).

A peculiarity of NMR in ferromagnets is the fact that the unpaired electron spins of the magnetic ions amplify by a rather large factor the RF field acting on the observed nuclei. Also, the measured NMR signal detected in the coil of the tank circuit is amplified by the same factor. This factor is called the amplification factor and will be discussed in Sect. 3.4.1. A very important consequence of the presence of such a factor is that the amplitude of the signals is very large. Also, the power needed to flip the nuclear spins is rather low. The excitation pulses can therefore be short allowing the excitation of a large portion of the frequency spectrum. This is very important since, as we mentioned above, the lines are expected to be broad.

The single crystals we studied were bulk samples. In an external magnetic field weaker than the coercive field, the microscopic magnetic structure of the crystals is composed of domains and domain walls. In the case of zero-field NMR measurements, the microscopic magnetic structure of the samples is clearly multidomain. Due to this structure, we do not expect the same physical mechanisms to influence the behavior of the electron spins both in domains and in domain walls. It is therefore important to differentiate between the signal coming from nuclei located in domains and the signal coming from nuclei located in domain walls. Usually, the amplification factor for the nuclei in domain walls is larger by at least an order of magnitude. This is therefore a potential way to distinguish the signals. This issue will be further discussed in Sect. 3.4.1.

Finally, since the lines are broadened by magnetic interactions, we can expect to observe short spin-spin relaxation times. As will be shown in Chap. 5, we did indeed observe short T_2's in $Eu_{1-x}Gd_xO$. We also observed very short spin-lattice relaxation times under certain conditions of field and temperature.

3.3 Modified commercial spectrometer to measure NMR signals with very short T_2

The spectrometer used for this study is based on a TecMag Apollo HF-1 commercial spectrometer. This instrument is controlled by computer using the NTNMR software delivered with the commercial spectrometer. Due to the fact that T_2 can be unusually short in the studied systems, we had to add several components to improve the performance of the spectrometer. Most importantly, the recovery time had to be reduced in order to perform measurements using short delays between the excitation pulses. The nominal recovery time of the Apollo HF-1 is about 2 μs, while spin-spin relaxation times as short as 0.5 μs have been observed in $Eu_{1-x}Gd_xO$. Also, the receiver sampling rate had to be greatly increased to detect the fast echoes observed in these materials. The minimum dwell time of the receiver of the Apollo HF-1 is 0.3 μs. Since in certain cases the echo lasts for only about 0.4 μs, only a single point in the echo could be recorded with the commercial receiver. Finally, we developed the transmitter in order to be able to reduce the length of the excitation pulses. This has been done in order to further decrease the delay between the excitation pulses. However, most of the data we will present in this work were taken without modifying the transmitter.

A block diagram of the modified spectrometer is presented on Fig. 3.1. The RF pulses are provided at the output *F1* of the commercial TecMag spectrometer. A 16-phase CYCLOPS pulse sequence was programmed to cancel the ringdown coming from the pulses [53]. The RF output is amplified and split (using a power splitter Mini-Circuits ZFSC 2-1W) into two channels,[9] one that will be used to excite the sample, the other that will be used to demodulate the detected signal. A sketch of the RF output *F1* for a particular phase of a spin-echo experiment is shown in Fig. 3.2. It has two parts: the excitation part, composed of two short square pulses of time length t_1 and t_2 separated by a time denoted as *delay*, and the detection part consisting of a long pulse whose length is named *acquisition time*. In the following, we will refer to this last pulse as the demodulation pulse. The two parts are separated by a time called $offset$. Each phase of the sequence is followed by a waiting time denoted *repetition time*.

Let us start by describing the transmitter part of the modified spectrometer (c.f. Fig. 3.1). The output of the power splitter is connected to a fast RF gate that truncates the demodulation pulse of the RF signal. The gate (Watkins-Johnson model S1) has a switching time of 1 ns and an on-off ratio of about 70 dB for RF frequencies between 100 MHz and 200 MHz. The TTL signal sent to the driver piloting the gate is coming out of the *F1 UNBLANK* output of the Apollo HF-1. A sketch of the TTL signal is shown in the second line of the diagram of Fig. 3.1. Then the RF signal is amplified by a power amplifier (Kalmus model LP1000) and filtered by crossed diodes before being sent to the probe.

3.3.1 Short recovery time receiver

The receiver of the spectrometer is protected during the excitation sequence by a $\lambda/4$ cable followed by crossed diodes connected to the ground. In addition, a gate (Watkins-Johnson model S1) has been incorporated between the two preamplifiers (Doty model LN-2H) used to amplify the NMR signal coming from the probe. This gate is preceded by a 6 dB attenuator to reduce the noise going back in the first preamplifier. The TTL signal driving the gate is coming out of the *SCOPE TRIGGER*

[9] All the power splitter used in this spectrometer are Mini-Circuits model ZFSC 2-1W.

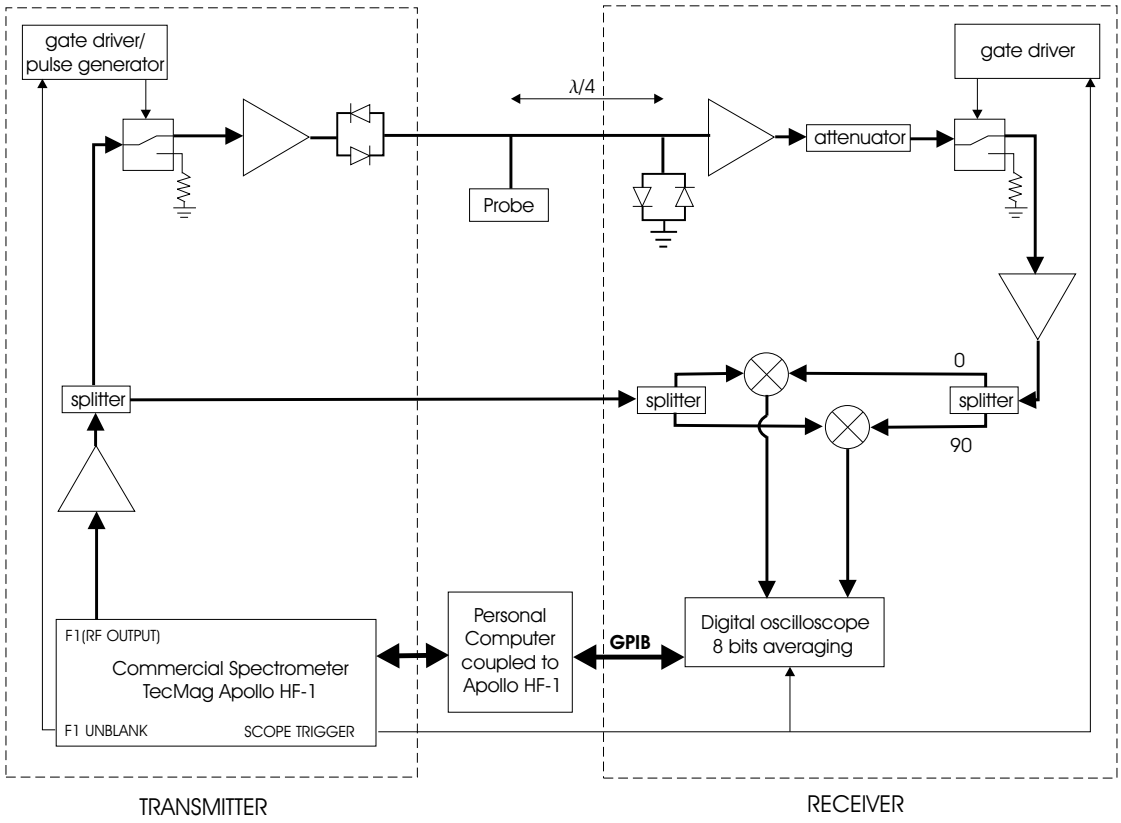

Figure 3.1: Block diagram of the spectrometer. A circle containing a cross symbolizes a frequency mixer.

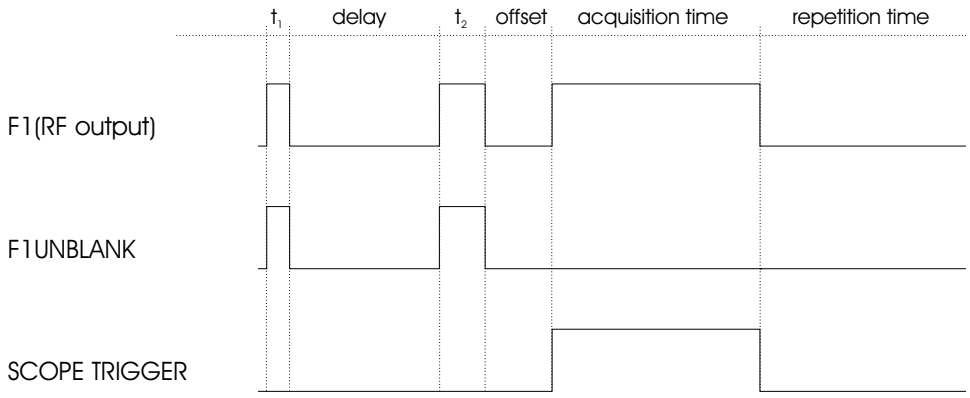

Figure 3.2: RF output, *F1 UNBLANK* output and *SCOPE TRIGGER* output for one of the 16 phases of the CYCLOPS sequence.

output of the Apollo. A sketch of the TTL signal is shown in Fig. 3.2. At the output of the second amplifier, the signal is split into two channels, one of them which is phase shifted by 90° to perform what is called commonly quadrature detection. Both channels are demodulated by two frequency mixers (Mini-Circuits model ZAD-1W) connected to the amplified *F1* output. The resulting signals are sent to a digital oscilloscope (Tektronix model TDS 224) triggered by the TTL signal coming from the *SCOPE TRIGGER* output. This oscilloscope also plays the role of averager. It has a sampling rate of 1 gigasample per second which means a maximum time resolution of 1 nanosecond. However, its digitizer is only 8-bit resolution. To increase the resolution of the signal, the averaging process is made in two steps: first, 64 curves (4 times the 16 echoes produced by the 16 phases pulse sequence) are acquired and averaged in the memory of the oscilloscope. Then, the resulting curve is transferred through a GPIB connection to the computer where it is stored in an array. Once the required number of arrays has been acquired, this number being defined by the user, a Visual Basic script process them to obtain the averaged curve. The resulting curve is then exported to the graphics environment of the NTNMR software that controls the pulse sequences.

In order to have a short recovery-time receiver, every component must be broadband. The Doty LN-2H preamplifiers have a recovery time of 0.3 μs. Since the gates have a switching time of 1ns, they will not alter the recovery time. The maximum bandwidth of the oscilloscope is 100 MHz but we limited it to 20 MHz in order to remove the high-frequency noise. The bandwidth of the receiver is determined by the minimum bandwidth of all the components, and therefore it is equal to the bandwidth of the preamplifiers. The recovery time of the receiver described above is thus 0.3 μs.

It is important to mention that the Apollo HF-1 does not have the capability to produce pulses with different phases if the delay between the pulses is shorter than 0.3 μs. Since a 16-phase pulse sequence requires pulses with different phases, the minimum delay between the two excitation pulses was limited to 0.3 μs. Also, the time $offset$ described in Fig. 3.2 will always be set to this minimum value 0.3 μs because the demodulation pulse also needs to have a different phase than the excitation pulses. Therefore, even if the recovery time of the receiver were faster than 0.3 μs, the performance of the Apollo HF-1 would limit the spectrometer to the same value of $delay$.

3.3.2 The need for low Q tank circuit

The recovery time of the receiver is the technical limitation that needed to be improved, but in order to be able to use short delays between the excitation pulses, the ringdown of the tank circuit has to be at least as short as the recovery time of the receiver. That means that the quality factor Q of the tank circuit has to be small. Let us approximate the maximum Q value corresponding to a recovery time of 0.3 μs. Typically, the recovery time needs to be equal to about 20 times the time constant of the tank circuit in order to measure a NMR signal after sending a excitation RF pulse in the tank circuit [54]. The straightforward relationship between the time constant τ and the quality factor of a tank circuit resonating at ω_0, $Q = \omega_0\tau$, gives us the value of Q (at 100 MHz):

$$Q = \omega_0 \frac{T_{recovery}}{20} \cong 10. \tag{3.10}$$

With this value of Q, the bandwidth of the tank circuit is about 10 MHz, which allows us to cover a broad frequency range in excitation. A simple way to obtain a tank circuit matched at 50 ohms with a low value of Q is to use a serial circuit composed by a resistor of about 50 ohms, a low Q coil

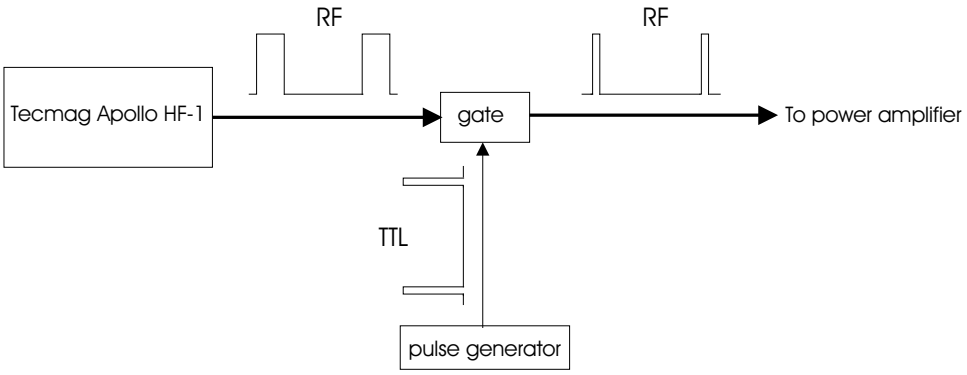

Figure 3.3: Block diagram of the modified transmitter.

and a capacitor. Typically, we used a coil of inductance $L = 1\,\mu$H and a capacitor of capacitance $C = 10\,$pF.

3.3.3 Modification of the transmitter: how to create very short RF pulses

The TecMag Apollo HF-1 commercial spectrometer is not capable of producing pulses shorter than $0.1\,\mu$s. In most cases this is short enough, but if T_2 is very short, it is necessary to use spin-echo sequences with very short delays (typically, we used delays of the order of $0.5\,\mu$s). By reducing the length of the excitation pulses, we reduce the time between the end of the second pulse and the echo. That means that for a given recovery time, it is possible to detect echoes using shorter delays.

To reduce the pulse length, we replace the gate driver connected to the output *F1 UNBLANK* by a pulse generator (Hewlett-Packard Model 8015A) that can produces pulses as short as 10 ns (c.f Fig. 3.1).[10] The RF pulses coming out of the *F1* output of the Apollo HF-1 can be truncated by adjusting the length of the pulses generated by the HP 8015A. This is diagrammatically represented in Fig. 3.3. A sketch of the outputs of the Apollo HF-1 along with a sketch of the output of the HP pulse generator is presented in Fig. 3.4. The nomenclature of the time events is the same as in Fig. 3.2.

Note that the pulse generator model 8015A is only able to produce a sequence consisting of two pulses of same length. As an example of the kind of measurements that are possible with this modified spectrometer, we show in Fig. 3.5 a spin-echo measured in $Eu_{0.957}Gd_{0.043}O$. This zero-field measurement was performed at 20 K and the frequency of the excitation pulses was 120 MHz. The pulses have a length of about 20 ns and are separated by a delay of about 500ns. The fact that we can flip the nuclear spins of this system with such short pulses is due to the existence of an amplification factor that amplifies the RF field acting on the nuclear spins. This will be treated in the next Section.

3.4 Amplification factor

In ferromagnetic materials, the unpaired electron spins are also susceptible to the applied RF magnetic field $\boldsymbol{H}_1$. However, since the gyromagnetic ratio γ_e of the electron is about 10^4 times larger than γ_n, RF frequencies are almost static from the point of view of the electron spins and therefore

[10] In fact, the pulse generator Hewlett-Packard 8015A can produce pulses even shorter than 10 ns, but we never used pulses shorter than that value.

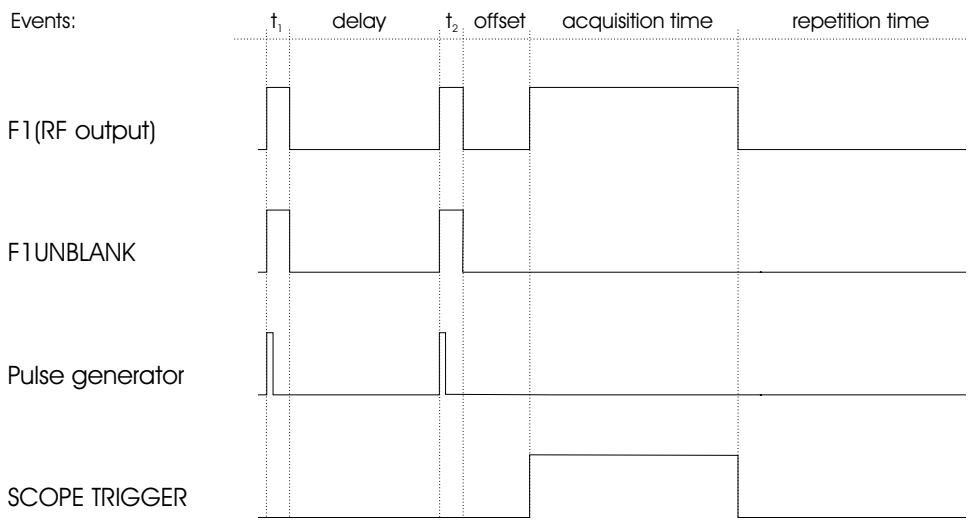

Figure 3.4: RF output, *F1 UNBLANK* output and *SCOPE TRIGGER* output along with the output of the HP pulse generator driving the gate

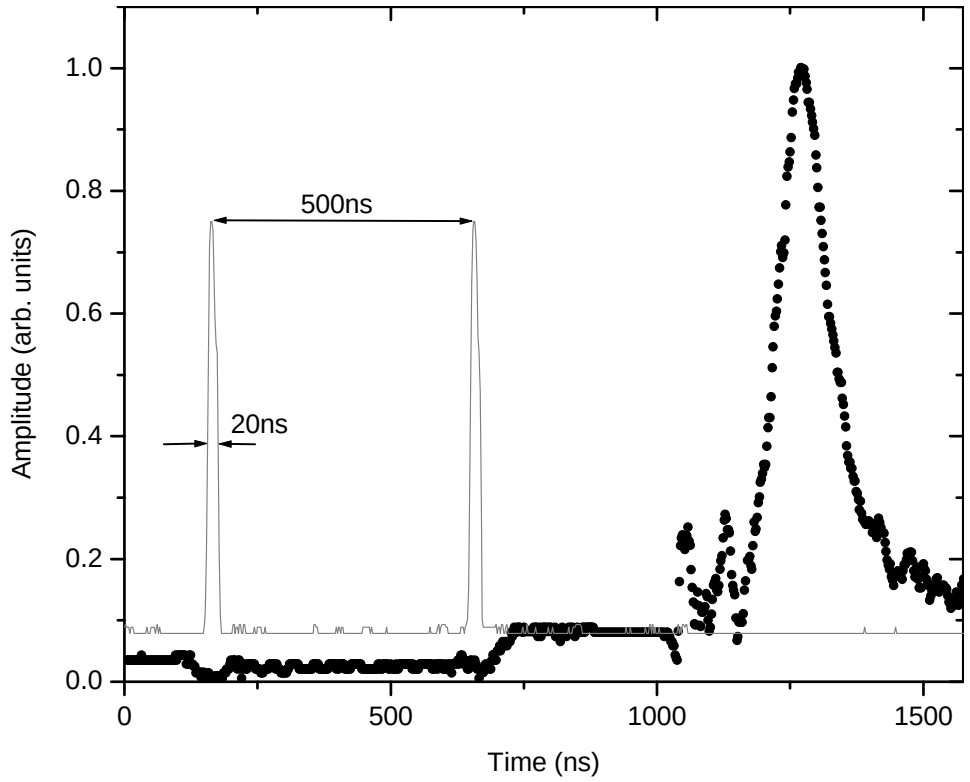

Figure 3.5: Echo in 4.3% Gd doped EuO after 20ns pulses. Screenshot of the oscilloscope set on Average 64.

the electron magnetization adiabatically follows $\boldsymbol{H}_1$. For the nuclei, the motion of the electron spins along $\boldsymbol{H}_1$ represents an additional RF field that adds to the direct $\boldsymbol{H}_1$ (the nuclei being sensitive to the unpaired electron spins through the hyperfine coupling). The resulting RF field acting on the nuclei can be written $\boldsymbol{H}_1 + \eta\boldsymbol{H}_1$, where η is a factor depending on the strength of the hyperfine coupling and is called the amplification factor (or amplification factor). Since usually $\eta \gg 1$, it is the custom to make the approximation $(1+\eta)\boldsymbol{H}_1 \cong \eta\boldsymbol{H}_1$.

After the RF excitation, the nuclear spins precess in the plane perpendicular to the effective static field.[11] This precession acts on the electron spins. Again, since $\gamma_e \gg \gamma_n$, the electron spins adiabatically follow the nuclear spins. Therefore, the e.m.f created in the receiver coil is caused by the motion of the nuclear spins and the motion of the electron spins. It can be easily shown that the e.m.f. created by the motion of the electron spins is η times larger than the e.m.f. created by the motion of the nuclear spins [55]. Consequently, the measured current at the output of the tank circuit is enhanced by the same factor $\eta + 1 \cong \eta$. This phenomena is often referred to as "amplification in detection".

In the presence of magnetic domain walls, this amplification process is not uniform throughout the sample.[12] In particular, the amplification factor for nuclei located in domain walls or in the vicinity of domain walls is different than for those located in the center of magnetic domains. Domain walls undergo reversible displacements under the action of $\boldsymbol{H}_1$ as a consequence of the reconfiguration of the microscopic magnetic structure. The electron spins located in domain walls experience a large rotation during the domain wall motions. The thinner the walls, the larger the rotation. The microscopic magnetic structure, and in particular the thickness of the domains walls, is determined by the exchange interactions and the magnetic anisotropy. The electron spins located in the domains that are not influenced by domain walls motions are more rigid, the rigidity being determined by the magnetic anisotropy, and they will experience a smaller rotation under the influence of $\boldsymbol{H}_1$. Therefore, while a strong magnetic anisotropy results in a large amplitude of rotation of the electron spins in domain walls, it causes the amplitude of rotation for electron spins in domains to be small.

It is possible to calculate the amplitude of the amplification. The amplification in domains is simply given by

$$\eta_{Domain} = \frac{|\boldsymbol{H}_{hf}|}{|\boldsymbol{H}_{an} + \boldsymbol{H}_{int}|}, \tag{3.11}$$

where $\boldsymbol{H}_{an}$ is the anisotropy field and $\boldsymbol{H}_{int}$ is the internal field defined as the sum of the external field $\boldsymbol{H}_0$, the demagnetization field $\boldsymbol{H}_{dm}$ and the Lorentz field $\boldsymbol{H}_L$ [56]. As implied in the discussion above, the stronger the hyperfine coupling, the stronger the amplification. Also, the larger the anisotropy (or the external field), the weaker the amplification.

The amplification for nuclei in a domain wall contained in a spherical particle has been first calculated by Portis and Gossard and is given by

$$\eta_{DW} = \frac{\pi}{N}\frac{D}{\delta}\frac{|\boldsymbol{H}_{hf}|}{|\boldsymbol{M}(T)|}, \tag{3.12}$$

where N is the demagnetization factor of a domain, D is the domain size, δ is the width of the domain wall and $\boldsymbol{M}(T)$ is the magnetization in domains at temperature T [57].

[11] The effective static field is equal to the local field when no external field is applied. In the presence of an external magnetic field, it is the sum of the local field, the external field, the demagnetization field and the Lorentz field.

[12] Note that even in a single domain particule, the amplification factor is not expected to be completely uniform due to surface effects or other constraints on the rigidity of certain spins in the domain.

3.4.1 Amplification in domain walls vs. amplification in domains

The problem associated with NMR in bulk ferromagnetic materials is related to the presence of domain walls. Since the broadening mechanisms, as well as the relaxation mechanisms, might be different for nuclei in domain and in domain walls, it is therefore desirable to be able to distinguish between the signals coming from the two sources. The fact that the amplification factor is different is a way to distinguish them. Usually the amplification in domain walls is at least an order of magnitude larger than the amplification in domains, but as we will show below, it is probably not true in the case of $Eu_{1-x}Gd_xO$.

Let us determine the value of the ratio η_{Domain}/η_{DW} in the case of zero-field Eu NMR in EuO. From (3.11) and (3.12), we obtain:

$$\frac{\eta_{Domain}}{\eta_{DW}} = \frac{N}{\pi}\frac{\delta}{D}\frac{|\boldsymbol{M}(T)|}{|\boldsymbol{H}_{an}|}. \tag{3.13}$$

From the study of the dynamic susceptibility on an EuO sphere, Flosdorff *et al.* [58] have determined that

$$\frac{D}{\delta} \cong \frac{|\boldsymbol{M}(T)|}{0.08|\boldsymbol{M}(T=0)|}. \tag{3.14}$$

Then, by taking $N = \frac{4\pi}{3}$, assuming a spherical domain, we have

$$\frac{\eta_{Domain}}{\eta_{DW}} = \frac{4 \cdot 0.08|\boldsymbol{M}(T=0)|}{3}\frac{1}{|\boldsymbol{H}_{an}|}. \tag{3.15}$$

Using $|\boldsymbol{M}(T = 4.2\,\mathrm{K})| = 1623\,\mathrm{emu/cm^3}$ [40] and $|\boldsymbol{H}_{an}(T = 4.2\,\mathrm{K})| = 247.5 \pm 2.5\,\mathrm{Oe}$ [59], we obtain $\eta_{Domain}/\eta_{DW} \cong 0.7$. Therefore, at 4.2 K the amplification for nuclei in domains is only slightly weaker than the amplification for nuclei in domain walls. This is due to the fact that the magnetic anisotropy in EuO is rather weak.[13] When the temperature is increased, we see from (3.15) that η_{Domain}/η_{DW} follows the temperature dependence of the inverse of the anisotropy field. Since the anisotropy field also decreases when the temperature increases, that means that the amplification for the nuclei in domains starts surpassing the amplification in domain walls.[14]

From the above calculation, it appears that we cannot a priori decide if the NMR signal will be dominated by nuclei in domains or nuclei in domain walls. However, there are two arguments suggesting that we actually measured the nuclei in domains.

The first argument is that not all the electron spins in domain walls or in the vicinity of domain walls will experience the same rotation as the domain walls move. Consequently, we can expect a distribution of amplification factors for the nuclei in domain walls. Conversely, the electron spins in domains will all experience the same rotation. Therefore, if H_1 is large, the distribution of flip angles for the nuclei in domain walls will be broad and the signal will be strongly reduced due to the fact that only a part of the nuclei will flip by an angle close to $\pi/2$. And since the amplitude of the amplification factor for nuclei in domains is very similar to the one for nuclei in domain walls, we can expect the signal from nuclei in domains to be dominant. This argument has been already invoked in several studies (see, e.g., [63]).

[13] For comparison, the anisotropy field in cobalt is $|\boldsymbol{H}_{an}(T = 300\,\mathrm{K})| \cong 5500\,\mathrm{Oe}$ [60] and $|\boldsymbol{M}(T = 300\,\mathrm{K})| = 1430\,\mathrm{emu/cm^3}$ [61], and consequently, $\eta_{Domain}/\eta_{DW} \cong 0.03$.

[14] Kasuya and Tachiki have calculated the temperature dependence of the anisotropy field. They have found $|\boldsymbol{H}_{an}(T)| \propto (|\boldsymbol{M}(T)|/|\boldsymbol{M}(T=0)|)^5$, which is in very good agreement with experimental results [62].

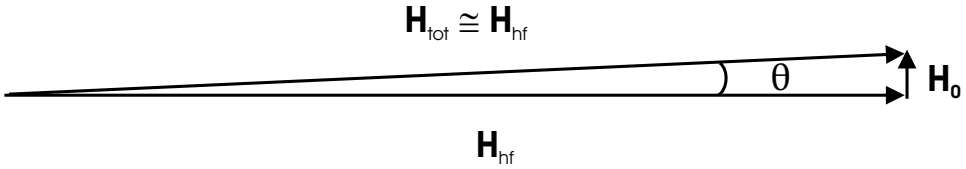

Figure 3.6: Hyperfine field and applied field at the center of a domain wall.

The second argument is related to the spin-lattice relaxation times we have measured. In most NMR studies performed on nuclei in domain walls, the spin-lattice relaxation curves have been reported to be non-exponential (see [55] for a general review). Moreover, it has been observed that the spin-lattice relaxation times were dependent on the amplitude of the RF field $\boldsymbol{H}_1$ [57, 64]. As will be shown in Chap. 5, the relaxation curves of Eu nuclei we have measured in $Eu_{1-x}Gd_xO$ were all well fitted by single exponentials and the relaxation times were independent of the amplitude of $\boldsymbol{H}_1$.

In fact, there is a third argument that will be presented below. The effect of an external static magnetic field $\boldsymbol{H}_0$ weaker than the coercive field on a multidomain sample is to rearrange the domains by moving the domain walls in order to minimize the total magnetic energy. If the external field is applied along the easy axis of the crystal, the magnetization in the domains, and therefore the hyperfine field acting on the nuclei in the domains, will be parallel to the field. Consequently, the hyperfine field acting on the nuclei located at the center of the domain walls will be perpendicular to the applied field, as shown in Fig. 3.6. Moreover, since the hyperfine field is considerably larger than the coercive field, it will be only very weakly affected by the external field. As a consequence, the resonance frequency of the nuclei located in domain walls is essentially independent of the applied field. Therefore, by studying the resonance frequency as a function of the amplitude of the external magnetic applied field, we should be able to distinguish if we are looking at domain walls or domains. We did not have the opportunity to perform this measurement before writing this report.

3.5 Relaxation in magnetic insulators

The interactions between the nucleus and the electrons described in Sect. 3.1 give rise to relaxation mechanisms. Typically, the hyperfine interaction is by far the largest of these interactions, and consequently it is the main cause of relaxation for the nuclei. If the hyperfine interaction is isotropic and the axes of quantization of the electron and the nuclei are collinear, the first term of (3.4) can be written as

$$\hat{\mathcal{H}}_{hf} = A\hat{\boldsymbol{I}} \cdot \hat{\boldsymbol{S}} = \frac{1}{2}A(\hat{I}^+\hat{S}^- + \hat{I}^-\hat{S}^+ + 2\hat{I}^z\hat{S}^z), \tag{3.16}$$

where A is the isotropic hyperfine constant, $\hat{I}^\pm = \hat{I}_x \pm \hat{I}_y$ and $\hat{S}^\pm = \hat{S}_x \pm \hat{S}_y$ are the raising and lowering operators for the nuclear spin and the electron spin, respectively. The first and second terms of (3.16) represent an interaction that can be described as a mutual flip between the nuclear spin and the electron spin. To calculate the relaxation processes deriving from these terms, it is useful to use spin-wave theory. Since EuO is a Heisenberg-type ferromagnet, spin-wave theory is particularly well adapted to the description of the magnetic interaction taking place in this material. By developing the operator $\hat{S}^+$ using the Holstein-Primakoff transformation [65], we can write the first term of (3.16) in terms of magnon creation and annihilation operators. The development of $\hat{S}^+$

yields terms involving products of odd numbers of operators. Therefore, the relaxation processes can involve only odd numbers of magnons: one magnon, three magnons, etc. The one-magnon process is not allowed because of energy conservation; indeed, the energy of a nuclear spin-flip is much smaller than the energy of a electron spin-flip. The first allowed process is therefore the three-magnon process. Calculated to the first-order in perturbation theory, the three-magnon processes lead to a spin-lattice relaxation rate given by

$$\frac{1}{T_1} = \frac{11.29}{16(2\pi)^5} \frac{A^2}{2JS \cdot \hbar S} \left(\frac{k_B T}{2JS} \right)^{7/2}, \tag{3.17}$$

where $J = J_1 + J_2$ is the exchange integral and k_B is the Boltzmann constant. This expression was first derived by Oguchi and Keffer [66]. Pincus showed that a second-order process may enhance the first-order process given in (3.17) [67]. This second-order process arises from the four-magnon exchange interaction and can be described as the scattering process of a virtual magnon by thermal magnons via the exchange interaction. Beeman and Pincus calculated this factor to be about 8 in the case $k_B T \gg g\mu_B H$ [68]. Note that the factor 11.29 in (3.17) is the result of our own calculations. We have indeed recalculated (3.17) and have found that the factor 7.6 given by Beeman and Pincus in [68] should be replace by the factor 11.29. We present this calculation in Appendix A along with a discussion on the accuracy of the enhancement factor of 8. As we will see in Chap. 5, the factor 11.29 is in better agreement with our measurements.

Now, if the hyperfine interaction is anisotropic, there will be terms of the form $A_{xz}\hat{I}_x\hat{S}_z$ and $A_{yz}\hat{I}_y\hat{S}_z$. Also, if there is a non-zero angle between the axes of quantization of the electron and the nuclei, then there will be terms of the form $\frac{1}{2}A\hat{I}^+\hat{S}_z sin\theta$, where θ is the angle between the two axis of quantization. In other words, some terms involving the operator $\hat{S}^z$ will participate at the relaxation of the nuclei. Since the development of $\hat{S}^z$ using the Holstein-Primakoff transformation gives terms involving even numbers of magnon creation and annihilation operators, this implies that in these cases, two-magnon relaxation processes are allowed. These processes are often called Raman relaxation processes and were first calculated by Mitchell in the case of ferromagnets [69].

3.6 Suhl-Nakamura interaction

When the temperature is lowered, the number of magnons decreases. Therefore, the contribution of direct spin-wave scattering processes to the relaxation becomes very small. Scattering processes deduced from higher order in perturbation theory have then to be considered. The Suhl-Nakamura interaction describes an effective nuclear spin-spin interaction via emission and absorption of virtual spin waves [70, 71]. It is obtained from a second-order perturbation treatment of the hyperfine interaction. It is actually the equivalent of the RKKY interaction (valid for free electron gases) for permanent magnetic materials. In the Suhl-Nakamura interaction, the spin-waves play the role played by the conduction electrons in the RKKY interaction. However, whereas the RKKY indirect coupling is isotropic,[15] the Suhl-Nakamura coupling is not, due to the fact that it depends on the direction of the electronic magnetization. The Suhl-Nakamura interaction is of the form

$$\hat{\mathcal{H}}_{S-N} = \sum_{i \neq j} V_{ij} \hat{I}_i^+ \hat{I}_j^-, \tag{3.18}$$

[15] This is in fact only true for s electrons.

with

$$V_{ij} = \frac{A^2}{2Jz} f(|\boldsymbol{r}|), \tag{3.19}$$

and $f(|\boldsymbol{r}|)$ a decaying sinusoidal function of the distance $\mathbf{r}$ between the two nuclei i and j. Note that, contrary to the dipolar Hamiltonian, the Hamiltonian describing the Suhl-Nakamura interaction does not contain terms involving the z component of the nuclear spin operators. An interaction such as (3.18) is expected to produce a lineshape similar to a Gaussian. Then T_2 can be determined by using the Van Vleck theory of moments: $T_2 = \sqrt{2}/\sqrt{M_2}$ where the second moment M_2 is given by

$$M_2 = \frac{1}{3} I(I+1) \sum_j V_{ij}^2. \tag{3.20}$$

Suhl assumed that the range of the interaction is long enough to replace the sum in (3.20) by an integral. He obtained the following expression for the second moment:

$$\sigma = \sqrt{M_2} = \left[\frac{I(I+1)}{24\pi S^2}\right]^{1/2} \frac{\omega_0^2}{\gamma_e |\boldsymbol{H}_{ex}|^{3/4} \boldsymbol{H}^{1/4}}, \tag{3.21}$$

where ω_0 is the Larmor frequency, $\boldsymbol{H}_{ex}$ is an effective exchange field between electronic spins and $\boldsymbol{H}$ is the sum of the static fields acting on the electron spins, that is $\boldsymbol{H} = \boldsymbol{H}_{an} + \boldsymbol{H}_0 + \boldsymbol{H}_{dm}$. The exchange field can be approximated by the expression

$$g\mu_B |\boldsymbol{H}_{ex}| = 2J_1 z_1 S, \tag{3.22}$$

where g is the g-factor, μ_B is the Bohr magneton, and z_1 is the number of first neighbors.

For a specific transition $m \leftrightarrow m+1$, the factor $\frac{1}{3}I(I+1)$ in (3.20) needs to be replaced by the factor

$$F(I,m) = \frac{2(I-m)^2(I+m+1)^2 + (I+m)^2(I-m+1)^2 + (I-m-1)^2(I+m+2)^2}{8(2I+1)}, \tag{3.23}$$

as shown in [47]. Also, when there is more than one isotope, (3.20) has to be multiplied by the abundance c of the measured isotope.

The interaction described by (3.20) only applies to homogeneous lineshapes. In real magnetic materials, the microscopic inhomogeneities give rise to spatially dependent local fields that broaden the spectra and change the local Zeeman energy levels. Therefore, the number of allowed mutual spin-flips between nuclei within the range of the S-N interaction is reduced and as a consequence the relaxation times are expected to be longer. Hone, Jaccarino, Ngwe and Pincus were the first to describe this adaptation of the Suhl-Nakamura interaction (it will be referred to as the HJNP theory in the following) [72]. The line is a Lorentzian $g(\omega)$ and T_2 is therefore given by:

$$\frac{1}{T_2} = \frac{1}{2}\Gamma = \frac{1}{6}\pi\sqrt{3}\left(\frac{M_2^2}{M_4}\right)^{1/2} M_2^{1/2}, \tag{3.24}$$

where the second moment is now given by

$$M_2 = \frac{1}{3} I(I+1) g(\omega) \sum_j V_{ij}^2 \frac{|V_{ij}|}{\hbar}, \tag{3.25}$$

and the fourth moment is a more complex function of I, V_{ij}, and $g(\omega)$. Note that $g(\omega)$ is a normalized shape function, i.e., $\int g(\omega)d\omega = 0$. The result is that T_2 is now of the form

$$\frac{1}{T_2} = \frac{1}{6}\pi\sqrt{3}g(\omega)\left(\frac{A^2}{2Jz_1}\right)^2 R(I, f(|\mathbf{r}|)), \tag{3.26}$$

where $R(I, f(|\mathbf{r}|))$ is a function of I and $f(|\mathbf{r}|)$(c.f. formula (3.12) of [72]). Therefore, T_2 is frequency dependent and can therefore be noticeably different at different part of the line.

Equation (3.26) needs to be further modified for a specific transition $m \leftrightarrow m+1$. As shown by Fekete *et al.* [73], (3.26) is multiplied by a factor $\left[\frac{1}{3}F(I,m)\right]^{1/2}$, with $F(I,m)$ given in (3.23), and $g(\omega)$ needs to be replaced by a m dependent function $g_m(\omega)$. Finally, as for the homogeneous case, we need to take into account the abundance c of the studied nuclei.

3.7 NMR in CMR materials: overview of what has been observed

Numerous ^{139}La NMR studies in the magnetically ordered state of various $La_{1-y}A_yMnO_3$ (A=alkaline-earth metal such as Ca or Sr) compounds have been published (see e.g. [74–78]). Results in the paramagnetic phase have also been reported by Sakaie *et al.* [79]. Also, several groups have measured the nuclei of the ion that is the source of the magnetism, namely ^{55}Mn. The first ^{55}Mn NMR measurements on manganites were published in 1970 by Matsumoto [80]. All the measurements were done in the magnetic phase (due to fast T_2). More recently, after the discovery of the unconventionally large magnetoresistance (CMR) of these materials, Allodi *et al.* performed ^{55}Mn NMR on $La_{1-y}Ca_yMnO_3$ systems [81]. They showed that an antiferromagnetic phase and a ferromagnetic phase coexist (phase separated) in these materials. Following this work, numerous ^{55}Mn NMR studies on various manganites were performed, and it has been shown that the spectrum is composed of several lines, the lowest of which is usually assigned to the signal from Mn^{4+} (see e.g. [82, 83] and the references therein for the most recent developments).

According to several theories, CMR is associated with the formation of magnetic polarons (c.f. 2.3). If magnetic polarons were present in a material and were static on the NMR timescale, it would be reasonable to expect a non-zero static hyperfine field around the electron donors, namely Mn in manganites and Eu or Gd in $Eu_{1-x}Gd_xO$. That is the assumption of Kapusta *et al.* [2, 84]. As already mentioned in the introduction, they have detected an NMR signal above T_C in various manganites. They show that the NMR frequency does not drop to zero at $T = T_C$. We have performed the same experiment on $Y_{0.09}La_{0.5}Ca_{0.41}MnO_3$ and have observed a similar result as shown in Fig. 3.7. This is in disagreement with the results of Novák *et al.* who observed that the hyperfine field follows the bulk magnetization, as measured with a SQUID magnetometer [4, 85]. The homogeneity of the magnetization of the samples might be the cause of this disagreement. Indeed, a given sample might contain more than one phase and therefore the value of T_C as measured by magnetometry might not apply to the entire sample. In any case, as underlined by Novák *et al.*, the order of the magnetic phase transition in manganites varies from one sample to another. Therefore, the magnetic properties of these systems in the vicinity of T_C are difficult to study.

We also measured the temperature dependence of the hyperfine field on ^{153}Eu nuclei in the $Eu_{1-x}Gd_xO$ systems. As will be shown in 2.4.1, the frequency of the resonance follows closely the

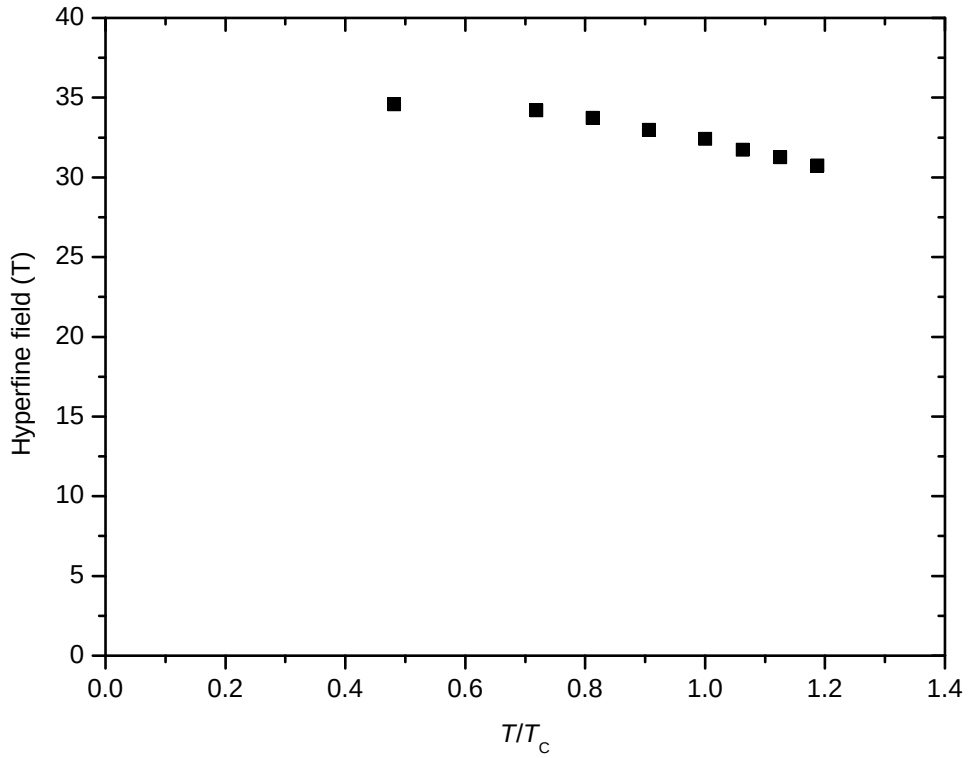

Figure 3.7: Hyperfine field vs. T/T_{C} in $Y_{0.09}La_{0.5}Ca_{0.41}MnO_3$ ($T_{\mathrm{C}} = 160\,\mathrm{K}$).

temperature dependence of the bulk magnetization, at least for temperatures low enough to detect an NMR signal. Therefore, the hyperfine field in these systems follows the conventional temperature behavior of ferromagnetic systems.

3.7.1 Spin dynamics in manganites

Most of the NMR results published on manganites concern the lineshape of the resonance and the temperature dependence of the resonance frequency. Several groups studied the relaxation times of nuclei of non-magnetic ions such as ^{139}La, but only few analyses of the mechanisms leading to the relaxation of ^{55}Mn have been reported. These analyses are potentially of great importance to the understanding of CMR since they give information on the spin fluctuations of the magnetic ion. The studies published by Savosta *et al.* are probably the most complete [75, 83, 86]. In particular, in metallic manganites they have observed a fast increase of the relaxation rates $1/T_1$ and $1/T_2$ with increasing temperature. They suggest that this temperature behavior is the signature of fluctuations in the hyperfine field caused by the "hopping of the e_g electrons of Mn ions" [75]. In their most recent article, in talking about the relaxation processes in the ferromagnetic insulating (FMI) clusters contained in various manganites, they state: "The temperature dependence of ^{139}La and ^{55}Mn relaxation in the FMI clusters is analogous which can be understood as due to the EFG fluctuation on the La nuclei and combined EFG and hyperfine field fluctuation on the Mn nuclei connected to the motion of the Jahn-Teller polarons." [83].

In conclusion, it appears that several of the numerous physical phenomena taking place in manganites might be linked to CMR. It seems to be an intricate task to extract information from NMR results in manganites. Associated with this problem is the fact that the crystal structure of man-

ganites is rather complex. These are clearly the reasons for choosing to study a CMR compound of the europium chalcogenides family, namely europium oxide. As will be shown in this work, even if the structure of EuO is simple (NaCl structure), the physics taking place in these systems is very rich.

Chapter 4

NMR frequency and lineshape

Information on the static properties of the magnetic and electric environment of the nuclei can be obtained through the analysis of NMR lineshapes. In addition, the measurement of the spin-spin and spin-lattice relaxation times provides information on the dynamics of the nuclear environment. In this chapter, we present and discuss our measurements of the lineshape of $Eu_{1-x}Gd_xO$. The relaxation times measurements will be treated in the next chapter, but we will already mention several results of these measurements in this chapter since the two properties, lineshape and relaxation times, are correlated and therefore cannot be treated entirely separately.

The NMR lineshape of ^{153}Eu in single crystals of pure EuO at 4.2 K has already been studied several times. However, the analysis of the broadening mechanisms varies from one author to another. In 1966, Boyd found a single sharp resonance [87] using continuous wave (cw) NMR. Later, Raj *et al.* observed that the zero-field lineshape is composed a sharp central line and two wings but they did not discuss the broadening mechanisms [88]. Then, Fekete *et al.* observed five quadrupolar lines in a saturation field of 2 T [89]. Finally, Arons *et al.* observed a zero-field lineshape that they described as a sharp line on top of a broad line [90–92]. They claimed that the sharp line corresponds to the signal from nuclei located in domain walls and that the broad line corresponds to the signal from nuclei in domains. No measurement of the lineshape above 4.2 K has ever been published. In this work, we reported the first study of the temperature dependence of the ^{153}Eu lineshape. We also reported the first lineshape of the ^{151}Eu resonance in EuO and the first NMR study of Gd doped EuO.

4.1 Preliminary remarks on the NMR signal

Before analyzing the lineshapes of the europium resonance, it is necessary to point out some characteristics of the observed NMR signals, in particular the intensity of the signals. The lineshapes were measured using a spin-echo sequence $t_1 - delay - t_2$ composed of two square pulses separated by a varying delay, as sketched in Fig. 3.2. We used $t_1 = 0.1\,\mu$s, $t_2 = 0.2\,\mu$s and *delay* values of several microseconds. A 16-phase CYCLOPS sequence was used in order to reduce the transients due to the RF pulses [53]. The determination of the amplitude of the RF field $\boldsymbol{H}_1$ needed to flip the nuclear spins by an angle $\pi/2$, the so-called $\pi/2$-pulse, has been made by measuring the echo amplitude as a function of the amplitude $|\boldsymbol{H}_1|$. We always observed a maximum in the spin-echo amplitude, but $|\boldsymbol{H}_{1,max}|$, the value of $|\boldsymbol{H}_1|$ at which the maximum occurs, was usually not precisely determined and

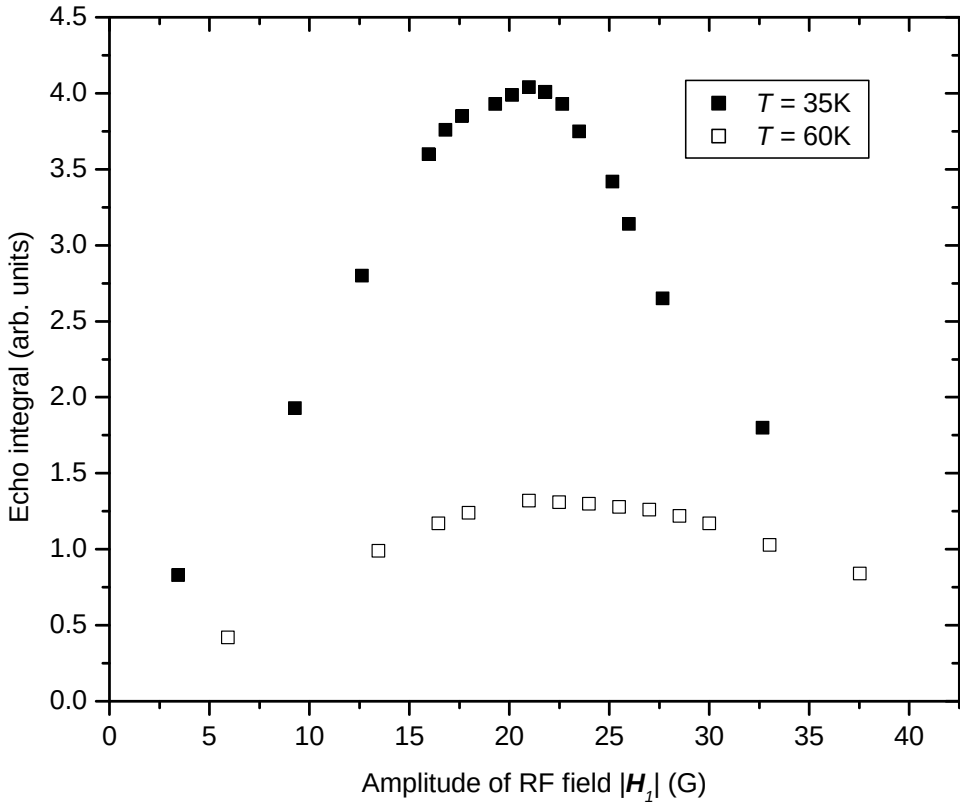

Figure 4.1: Zero-field amplitude of the spin-echo of ^{153}Eu vs. amplitude of the RF field $|\boldsymbol{H}_1|$ in 2% doped EuO. We used $t_1 = 0.1\,\mu$s, $t_2 = 0.2\,\mu$s and $delay = 10.5\,\mu$s.

could be taken over a rather broad range of $|\boldsymbol{H}_1|$, as can be seen in Fig. 4.1. This is most likely due to the fact that the amplification factor is not homogeneous throughout the sample and therefore the value of $|\boldsymbol{H}_1|$ needed to flip the magnetization by an angle $\pi/2$ is not identical for all the nuclear spins. However, we observed that neither the lineshapes nor the relaxation times depended on the chosen value of $|\boldsymbol{H}_1|$, at least for values close to those maximizing the spin-echo amplitude. We also observed that the range of $|\boldsymbol{H}_{1,max}|$ values for which the signal is maximal does not drastically change with the temperature, at least for temperatures sufficiently far below the Curie temperature of the sample.

Note that the value of $|\boldsymbol{H}_{1,max}|$ is calculated from the measurement of the RF power P_{max} needed to maximize the spin-echo amplitude, the quality factor of the tank circuit Q, the frequency ν of the RF signal and the internal volume of the coil V. It is given by

$$|\boldsymbol{H}_{1,max}| = \sqrt{\frac{10 P_{max} Q}{\nu V}}, \tag{4.1}$$

where P is in Watts, ν is in MHz, and V is in cm^3 [43]. We obtained $|\boldsymbol{H}_{1,max}| \cong 21\,$gauss from measurements performed on a 2% Gd doped sample (c.f. Fig. 4.1). Similar values were obtained for samples with different Gd concentration. From this value, the amplification factor defined in Sect. 3.4 can be estimated. The flipping angle θ of the spins are related to $|\boldsymbol{H}_{1,max}|$ through the relation $\theta = \eta\alpha\gamma_n|\boldsymbol{H}_1|t_1$, where the factor η is the amplification factor and the factor $\alpha \cong (I + \frac{1}{2})$ comes from the fact that all the transitions of the spin-$\frac{5}{2}$ multiplet are excited [93, 94]. Assuming that the maximum spin-echo amplitude corresponds to a flipping angle of $\pi/2$, we obtain

$$\eta = \frac{\frac{\pi}{2}}{3\gamma_n |\boldsymbol{H}_{1,max}| t_1} \cong 85. \tag{4.2}$$

This value is of the order of magnitude of the typical amplification factors observed for nuclei located in domains [55].

As we saw in Chap. 2, the conductivity of the samples is strongly dependent on the Gd concentration and on the temperature. Therefore, since not all the samples can be considered insulators, it is necessary to address the problem of the penetration of the RF field in order to estimate the proportion of nuclei participating to the NMR signal. The skin depth δ of a sample of resistivity ρ and permeability μ irradiated by an electromagnetic wave of frequency ω is given by

$$\delta = \sqrt{\frac{2\rho}{\mu\omega}} \tag{4.3}$$

where ρ is in Ω·m, ω in rad/s and μ in H/m [95]. Oliver *et al.*, observed that the resistivity of $Eu_{1-x}Gd_xO$ is within the range $10^{-4}\Omega$·cm$< \rho < 10^{6}\Omega$·cm [27]. Taking $\mu = \mu_0 = 4\pi \cdot 10^{-7}$ and $\omega = 2\pi \cdot 130 \cdot 10^6$ rad/s, we obtained $5 \cdot 10^{-2}$ mm$< \delta <$5 m. The lower value applies to samples with large Gd concentrations at temperatures below 50 K. The thickness of the single crystals we have measured is typically a few millimeters. Therefore, while in the case of pure EuO the RF field will detect all of the nuclei, only a fraction of the nuclei of the Gd doped samples will be detected or irradiated.

To conclude this preliminary Section, let us list the variables affecting the NMR intensity in $Eu_{1-x}Gd_xO$. First, the amplification factor increases the intensity of the observed signal. The amplification factor may vary with temperature as well as with Gd concentration due to a variation of the magnetic anisotropy. Second, the skin depth varies with Gd concentration as well as with temperature. Third, as will be shown later, the spin-spin relaxation times of certain nuclei are too short to be detected by our spectrometer. Also, the spin-spin relaxation times are strongly temperature and frequency dependent in $Eu_{1-x}Gd_xO$. Consequently, the intensity of the signal may be frequency as well as temperature dependent due to short spin-spin relaxation times. These three reasons imply that we will need to be extremely careful when discussing the intensity of the signals. In this work, we will generally not compare NMR intensities from different samples. Let us just underline that at 4.2 K, the signal of ^{153}Eu in $Eu_{1-x}Gd_xO$ is intense and easily detected as a consequence of the amplification mechanism. However, while the intensity of the signal in pure EuO and 0.6% Gd doped EuO is very similar, the intensity in 2% and 4.3% Gd doped EuO is substantially weaker. This is most likely due to the fact that the conductivity is larger for Gd concentrations above $x_c \cong 1.5\%$ and therefore, for $x = 2\%$ and $x = 4.3\%$ we only observe a limited number of nuclei due to small skin depth.

In the following, the intensity of the lines that will be presented has been corrected for the Boltzmann factor ($\hbar\omega/k_BT$) and the factor proportional to ω coming from the e.m.f induced in the coil by the magnetization. Note that since Q is very small, and therefore to a good approximation temperature independent, we did not have to take into account of the extra factor ω linked to Q variations.

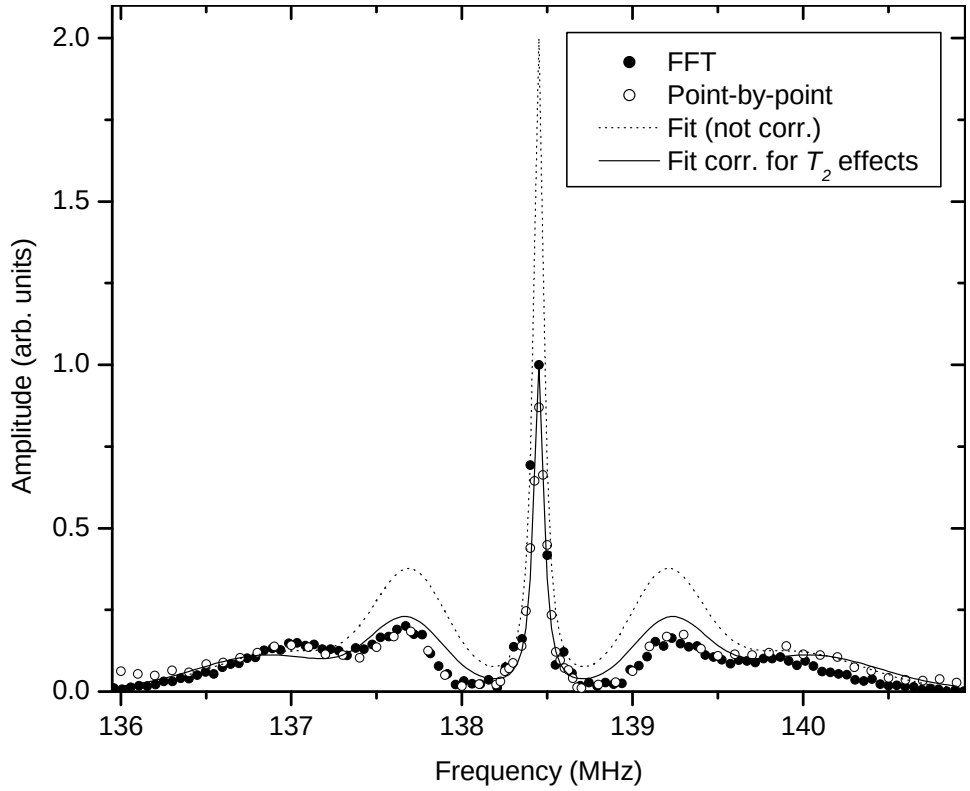

Figure 4.2: Zero-field lineshape of ^{153}Eu in EuO at 4.2 K; measurement and computed lineshape.

4.2 The lineshape of pure EuO

We present in Fig. 4.2 the zero-field lineshape of ^{153}Eu in pure EuO at 4.2 K. We determined the lineshape by two different techniques: on one hand, we measured the echo integral at a certain number of discrete values of frequency (point-by-point measurement). On the other hand, we Fourier transformed the echo measured at the frequency of the central line. As shown in Fig. 4.2, both methods give an almost identical lineshape. This shows that the RF pulses of the spin-echo sequence excited the entire range of frequency and it was appropriate to use the Fourier transform technique. Note that the estimated range in frequency covered by a pulse of duration $t_1 = 0.1\,\mu$s is of the order of $\Delta\nu = 1/(2\pi t_1) \cong 1.6$ MHz.

Since contradictory results and analysis of the lineshape of ^{153}Eu in pure EuO at 4.2 K were published, we present here our own analyze of the lineshape. Since the Eu sites in EuO have a nominal cubic symmetry, we expected to observe a single narrow line. However, as shown in Fig. 4.2, we observed an intense central peak and two wings with a structure suggesting that each wing is composed of two broadened lines. In order to distinguish between the broadening due to EFGs and the broadening due to the magnetic environment of the nuclei, we took advantage of the fact that there are two isotopes of europium with similar natural abundance. The gyromagnetic ratio and the electric quadrupole moment of the two isotopes are shown in Table 4.1. The zero-field lineshape of ^{151}Eu in pure EuO at 4.2 K is shown in Fig. 4.3. By comparing the ^{153}Eu and the ^{151}Eu line at 4.2 K we observed that the lines cannot be described solely by magnetic broadening or quadrupole electrical broadening. We therefore came to the conclusion that the broadening was due to a combination of both effects.

Table 4.1: Spin, natural abundance, gyromagnetic ratio, and electric quadrupole moment of the two europium isotopes (from [96]).

	Spin I	Natural abundance [%]	$\gamma_n/2\pi$ [MHz/T]	Q [barn]
^{153}Eu	5/2	52.19	4.6745	2.41
^{151}Eu	5/2	47.81	10.5856	0.903

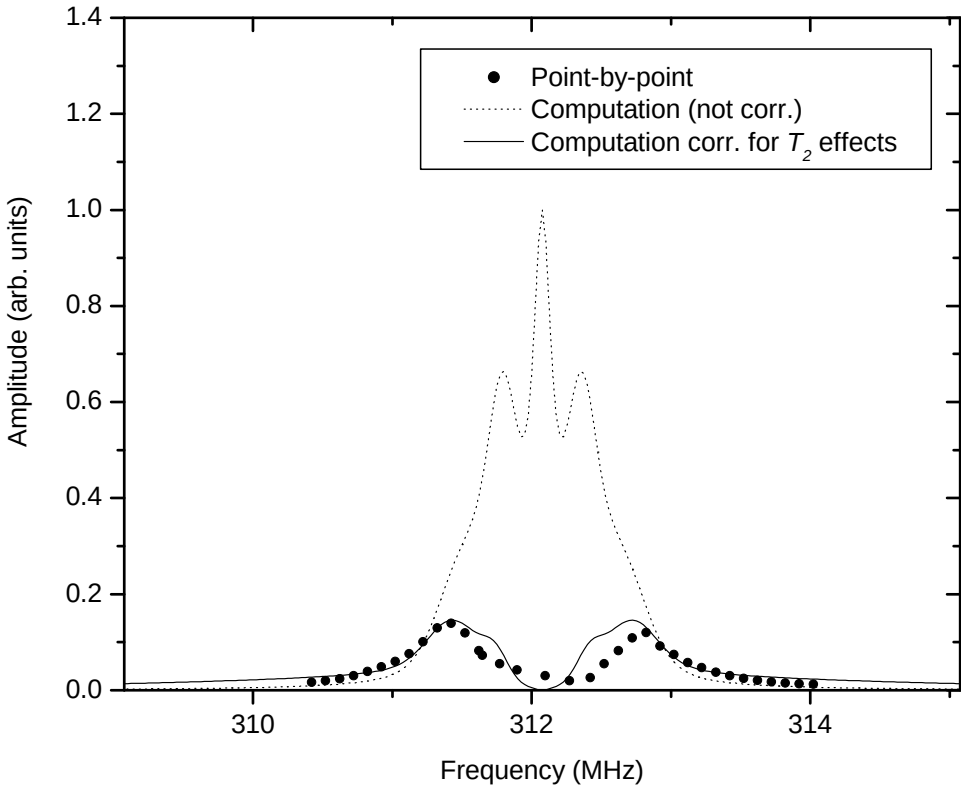

Figure 4.3: Zero-field lineshape of ^{151}Eu in EuO at 4.2 K; measurement and computed lineshape.

Table 4.2: Values of the lineshape fitting parameters for ^{153}Eu along with the deduced parameters for ^{151}Eu.

	Γ [MHz]	$\Delta\nu_Q$ [MHz]	$\delta_{\Delta\nu_Q}$ [MHz]
^{153}Eu	0.072	0.75	0.2
^{151}Eu	0.163	0.281	0.075

In the presence of EFGs, since ^{153}Eu has a spin $I = 5/2$, we expected to observe five lines all separated by the same frequency interval $\Delta\nu_Q$ and with intensity ratios 5:8:9:8:5 [43]. We tried to reproduce the observed lineshape theoretically by assuming a distribution in EFGs and a magnetic broadening. We described the inhomogeneities in the EFGs with a Gaussian distribution leading to a distribution in frequency $G(\nu)$ of second moment $\delta_{\Delta\nu_Q}$ that broadens the five lines. As will be discussed in Chap. 5, a Lorentzian distribution describes correctly the magnetic broadening. The function expressing the overlap of the two broadening mechanisms is a convolution of the two distribution functions. The convolution of a Gaussian and a Lorentzian gives a Voigt function. A Voigt function has the form

$$V(\nu) = \frac{\frac{1}{2}\Gamma}{\pi^{3/2}} \int_{-\infty}^{\infty} \frac{e^{-t^2}}{(\nu - \nu_0 - \sqrt{2}\sigma t)^2 + (\frac{1}{2}\Gamma)^2}\, dt, \tag{4.4}$$

where Γ is the full width at half maximum (FWHM) of the Lorentzian and σ is the second moment of the Gaussian [97]. The resulting lineshape is then given by

$$f(\nu) = \sum_{m=-2}^{m=2} (1 - \frac{m^2}{9}) \frac{\frac{1}{2}\Gamma}{\pi^{3/2}} \int_{-\infty}^{\infty} \frac{e^{-t^2}}{(\nu - (\nu_0 - m\Delta\nu_Q) - \sqrt{2}|m|\delta_{\Delta\nu_Q} t)^2 + (\frac{1}{2}\Gamma)^2}\, dt, \tag{4.5}$$

where Γ represents the FWHM of the magnetic distribution and the factor $(1 - m^2/9)$ accounts for the difference in intensity of the five quadrupolar lines. By fitting the measured ^{153}Eu lineshape with this function, it was possible to determine the parameters Γ, $\Delta\nu_Q$ and $\delta_{\Delta\nu_Q}$. However, there was another characteristic that needed to be taken into account: Raj *et al.* showed that the ^{153}Eu spin-spin relaxation time in pure EuO is short and frequency dependent and, as a consequence, some of the nuclei might not be observed if the delay between the detection pulses is too long [88]. They observed that the intensity of the central part of the line is strongly reduced. We demonstrated this phenomena in Fig. 4.4 where we plotted the FFT of the echo measured at two different values of *delay*.[1] To take into account this effect in the computation of the lineshape, we used the shape of the frequency distribution of T_2 at 4.2 K reported by Raj *et al.* and adapted it to the values of T_2 we measured at several frequencies. The T_2 distribution we deduced is shown in Fig. 4.5 along with our measurements. We will discuss the physical reason for this T_2 distribution in Sect. 5.3.[2] Finally, by multiplying (4.5) by the T_2 distribution shown in Fig. 4.5, we fitted the measured lineshape of ^{153}Eu. The fit is shown in Fig. 4.2 along with the measured lineshape and the deduced values of the fitting parameters are shown in Table 4.2.[3]

To verify if our description of the ^{153}Eu lineshape was correct, we computed the ^{151}Eu lineshape from the fitting parameters we determined for ^{153}Eu and compared the resulting curve with the

[1] Note that since the central peak was sharp, the echo was long and it was not possible to use values of *delay* shorter than about 10 μs to record the entire echo, even with the short recovery time of 0.3 μs of the receiver.

[2] Note that the distribution might be slightly different in the samples we studied, but T_2 was clearly the shortest on the central peak and was increasingly longer as the frequency was shifted away from the central peak.

[3] We used the Mathematica software to compute the lineshape.

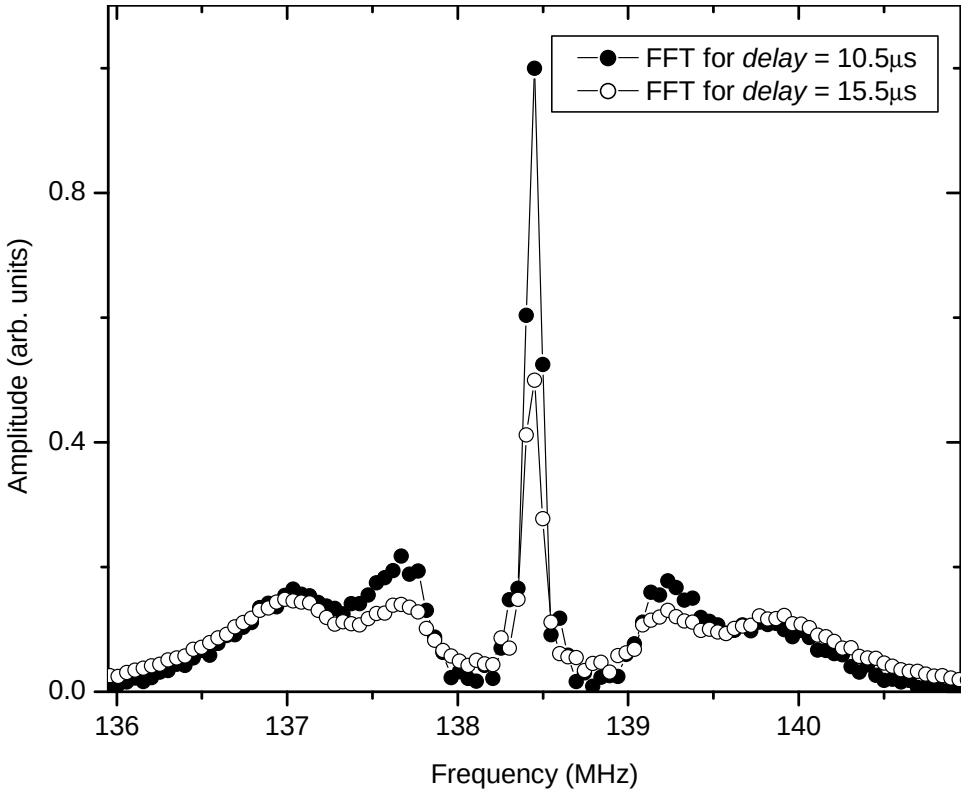

Figure 4.4: Zero-field lineshape of ^{153}Eu in EuO at 4.2 K as a function of *delay* showing the presence of frequency dependent T_2's (the T_2's are shorter near the line center). The lineshapes were obtained by Fourier transform of the spin-echo signal.

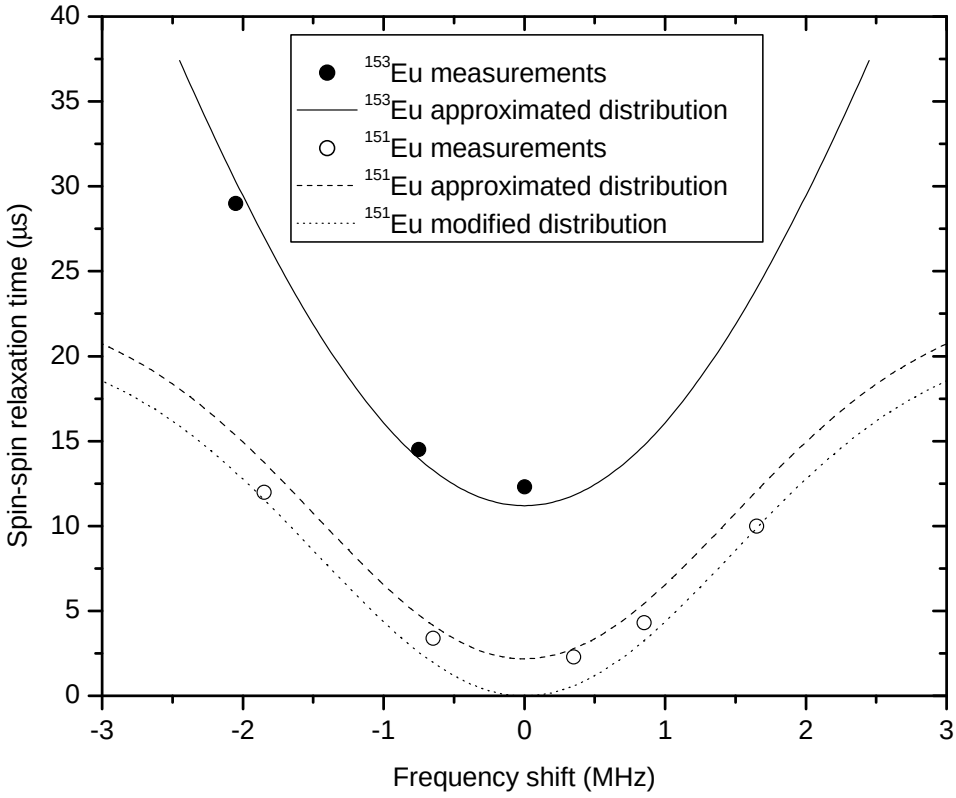

Figure 4.5: Approximated frequency distribution of T_2 at 4.2 K for both Eu isotopes. The zero value on the horizontal scale corresponds to the center of the lineshapes. The shape of the distribution was suggested by the measurements of Raj *et al.* [88].

measured ^{151}Eu lineshape. We first calculated the parameters for ^{151}Eu using the relations

$$\Gamma_{151} = \frac{^{151}\gamma_n}{^{153}\gamma_n}\,\Gamma_{153}, \tag{4.6}$$

$$\Delta\nu_{Q,151} = \frac{^{151}Q}{^{153}Q}\,\Delta\nu_{Q,153}, \tag{4.7}$$

$$\delta_{\Delta\nu_Q,151} = \frac{^{151}Q}{^{153}Q}\,\delta_{\Delta\nu_Q,153}, \tag{4.8}$$

where the indices 151 and 153 refer to ^{151}Eu and ^{153}Eu respectively. We deduced the T_2 distribution of ^{151}Eu from the T_2 distribution of ^{153}Eu using the following process: first, since we observed that T_2 at 4.2 K was proportional to γ_n^2 (c.f. Chap. 5), we divided the amplitude of the distribution by $(^{151}\gamma_n/^{153}\gamma_n)^2$. Second, since T_2 depended on γ_n (and was therefore of magnetic origin), we expected the T_2 distribution to scale with the magnetic distribution. We thus calculated the ^{151}Eu T_2 distribution by multiplying the width of the ^{153}Eu T_2 distribution by $^{151}\gamma_n/^{153}\gamma_n$. The resulting distribution is shown in Fig. 4.5 (dashed line) along with our measurements of T_2. The deduced distribution is in good agreement with our data. In order to take into account the fact that the T_2 of the central peak was too short to be detected, we subtracted the minimum value of T_2 from the computed distribution curve and obtained the distribution shown as a dotted line in Fig. 4.5. Finally, the computed ^{151}Eu lineshape was obtained by multiplying (4.5) by the ^{151}Eu T_2 distribution shown as a dotted line in Fig. 4.5. The result was plotted in Fig. 4.3 along with the measured data. The calculated line was in reasonable agreement with the data and we concluded that our description of the lineshape was correct.

From the above analysis, we deduced a ratio $^{151}\gamma_n/^{153}\gamma_n$ slightly different than the one given in tables. Indeed, by comparing the frequency of the central transition of both isotopes, we obtained

$$\frac{^{151}\gamma_n}{^{153}\gamma_n} = \frac{\omega_{0,151}}{\omega_{0,153}} = \frac{312.075}{138.45} \cong 2.254 \tag{4.9}$$

where $\omega_{0,151}$ and $\omega_{0,153}$ are the frequencies of the center of the ^{151}Eu line and the ^{153}Eu line respectively. The value given in tables is about 2.2645 (from [96]).

4.2.1 Origin of the quadrupolar splitting

There are several mechanisms that can lower the symmetry of cubic sites in ferromagnets. First, the presence of defects or vacancies in the crystal will create a distortion in the lattice. This effect is expected to be small in a sample of good quality. Also associated with lattice distortions is the possibility of magnetostriction. This is an effect that cannot be overlooked and it can be estimated using the microscopic theory formulated by E. R. Callen and H. B. Callen [98]. Finally, even if the lattice has a perfect cubic symmetry, there are some relativistic effects associated with the non-spherical charge distribution of the f-shells in rare-earth ions [99]. This gives rise to a "single-ion" quadrupole hyperfine interaction.

Fekete *et al.* considered two mechanisms to explain the quadrupolar splitting observed in EuO: a single-ion quadrupole interaction in Eu^{2+} and magnetostriction, the latter being dependent on the direction of the applied field whereas the former is not. The single-ion splitting was determined by Baker and Williams in an ENDOR experiment of Eu^{2+} diluted in an CaF_2 matrix to be $\Delta\nu_{Q_{s.i.}} =$

0.305MHz [48].[4] The magnetostriction calculated by Fekete *et al.* leads to $\Delta\nu_{Q_{latt}} = 0.291 \pm 0.03\,\text{MHz}$ for $\boldsymbol{M}$ parallel to the easy axis [111]. The total shift $\Delta\nu_{Q_{tot}} = 0.596\,\text{MHz}$ is therefore comparable to the shift $\Delta\nu_Q = 0.75\,\text{MHz}$ that we measured. The difference is likely due to the fact that the amplitude of the magnetostriction depends on the quality of the sample. It could also come from a difference in defects concentration as discussed by Arons *et al.* [100]. We indeed observed slight differences between the samples. However, the variation in $\Delta\nu_Q$ between the four samples we have measured was less than 15% and we do not think that the splitting was solely due the presence of defects in the samples as argued by Arons *et al.*.

It is important to note that the value of the electric quadrupole splitting we observed in zero-field has a similar value as the splitting observed by Fekete *et al.* in a field saturating the magnetization ($2\,\text{T} < |\boldsymbol{H}_0| < 3\,\text{T}$). In domain walls we expect the magnetostriction to be different than in domains since the deformations leading to the magnetostrictive effects depend on the direction of the magnetization. Therefore, the fact that the quadrupolar splitting we observed is similar to the quadrupolar splitting in high field observed by Fekete *et al.* is an additional suggestion that we observed nuclei located in domains.

4.3 The consequences of doping EuO with Gd on the lineshape

We now turn to the analysis of the lineshapes of ^{153}Eu in Gd doped EuO. In Fig. 4.6, we plotted the lineshape of the three Gd doped EuO samples we studied along with the lineshape of the pure EuO sample previously described. The integral of each curve was normalized to be equal to 1. We observed that the frequency of the central transition of the 0.6% Gd doped EuO lineshape was only slightly shifted towards higher frequency compared to pure EuO, from 138.45 MHz to 138.48 MHz. However, the central line was substantially broader. As discussed in Sect. 4.2, the width of the central transition is determined by magnetic broadening only. Also, as we will see in Sect. 5.3, the spin-spin relaxation rates in 0.6% Gd doped EuO being longer than in pure EuO, the broadening is not due to dynamic effects and it is therefore a static broadening. We think that the observed line is broader in the 0.6% sample than in the pure sample because of the random distribution of Gd atoms in the EuO matrix. Since different Eu atoms have different numbers of nearest and next nearest Gd neighbors, the local field acting on Eu atoms, which is influenced by the presence of Gd (c.f. Sect. 3.1), is not same at each Eu site. The influence of the presence of Gd atoms on the local field might come through an increase in the thermal average value of the electronic magnetization (term $< \hat{S}^z >_T$ in (3.6)), or through the coupling described by the tensors $\mathbf{B}^i$ and $\mathbf{D}^j$ (second and third term (3.6)). We assume that the last term of (3.6) is negligible in the case of 0.6% Gd doped EuO. Another noticeable difference between pure EuO and 0.6% Gd doped EuO is that the quadrupolar structure is not resolvable in 0.6% Gd doped EuO. We think that this is also due to the random distribution of Gd atoms in EuO which leads to a random distribution of EFGs. Finally, it is worth noticing the asymmetry in the wings of the line. We do not presently have an explanation for this asymmetry.

Whereas the addition of 0.6% of Gd in the EuO matrix only slightly shifts the frequency of the center of the NMR line, the center of the 2% and 4.3% Gd doped EuO lines are considerably shifted

[4] CaF_2 is a non-magnetic insulator.

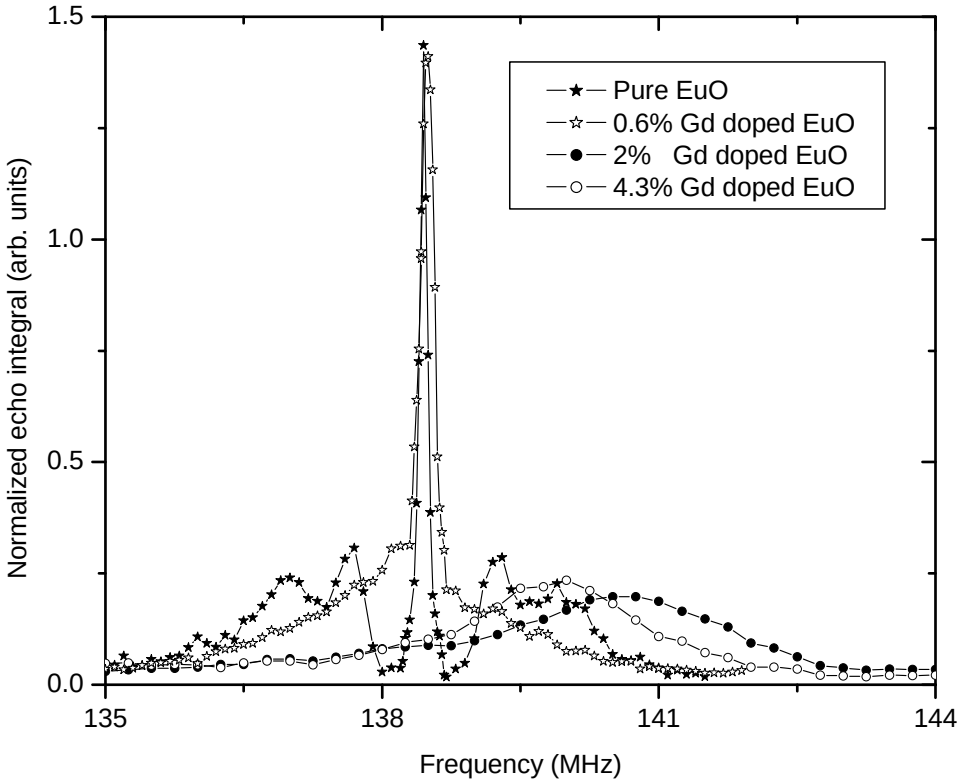

Figure 4.6: Zero-field lineshape of ^{153}Eu in $Eu_{1-x}Gd_xO$ at 4.2 K for $x = 0$, 0.6%, 2%, and 4.3%.

towards higher frequency. We also observed that the shift is smaller for $x = 4.3\%$ than for $x = 2\%$. So, we did not observe a monotonic increase of the shift with the doping. Since we do not know the sign of the coefficients B^i_{zz}, D^j_{zz} and C, appearing in (3.6), we are not able to tell what causes this non-monotonicity, but it is expected that the last term of (3.6) plays an important role for the 2% and 4.3% Gd doped samples since the conductivity in these samples is substantially higher than in 0.6% Gd doped EuO (c.f. Sect. 2.1).

We also observed that increasing the Gd doping strongly influences the shape of the ^{153}Eu line. In particular, we did not observe the central line in the 2% and 4.3% Gd doped samples and the lines were considerably broader than in the case of pure EuO and 0.6% Gd doped EuO. In order to decide whether or not this broadening mechanism was magnetic in origin, we measured the ^{151}Eu lineshape of the 4.3% sample. We did not have the opportunity to measure the lineshape at 4.2 K, but we did compare the ^{153}Eu and ^{151}Eu lineshapes at 20 K. As will be shown in Sect. 4.4, the ^{153}Eu lineshape at 20 K is very similar to the ^{153}Eu lineshape at 4.2 K, and we thought that it was likely that the ^{151}Eu lineshape at 20 K would also be similar to the ^{151}Eu lineshape at 4.2 K. In Fig. 4.7, we plotted the ^{153}Eu and ^{151}Eu lineshapes observed in 4.3% Gd doped at 20 K. The frequency of the ^{151}Eu lineshape was multiplied by the ratio given in (4.9). Since the two curves have a similar shape, we concluded that the broadening mechanism was of magnetic origin. We do not know exactly what interaction causes this large broadening, but we do know from the T_2 measurements (c.f. Sect. 5.3) that the broadening is a static broadening. In conclusion, we observed a remarkable difference between the lineshape of samples belonging to group III and IV and the

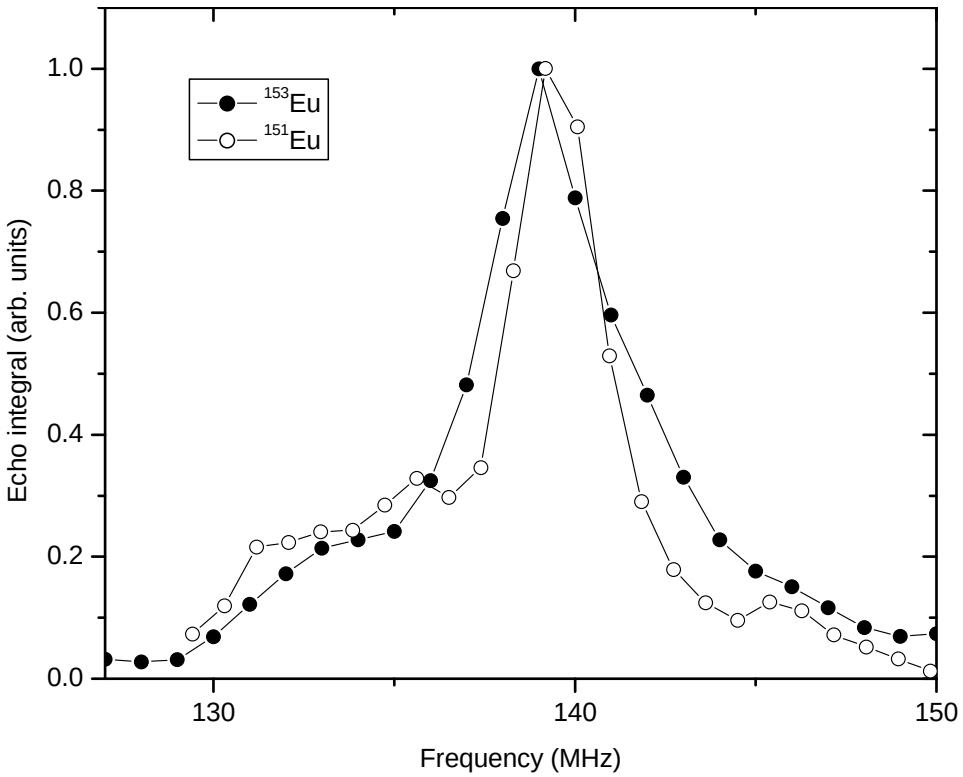

Figure 4.7: Zero-field lineshape of Eu^{153} and Eu^{151} in 4.3% Gd doped EuO at 20 K. The frequency of the Eu^{151} lineshape was multiplied by the ratio $^{153}\gamma_n/^{151}\gamma_n$.

lineshape of samples belonging to group V.[5]

4.4 Temperature dependence of the lineshape

We also analyzed the temperature dependence of the ^{153}Eu lineshape in pure EuO and Gd doped EuO. This analysis is motivated by the conductivity studies we reviewed in Sect. 2.1. The transport properties of $Eu_{1-x}Gd_xO$ change with temperature and several studies show that this change is related to the temperature variation of the magnetic properties of the samples (c.f. references in Chap. 2). We thought that the measurement of the NMR lineshape as a function of temperature could unravel some characteristics of the temperature dependent magnetic properties.

4.4.1 Pure EuO

In Fig. 4.8, we presented the lineshape of pure EuO at 4.2 K and at several temperatures between 4.2 K and 42 K. These lines were obtained by Fourier transforming the spin-echo measured at the frequency of the center of the lines. Since, as shown in Sect. 2.4.1, the NMR frequency varies considerably with the temperature, we shifted the center of the lines presented in the figure to zero frequency in order to compare the lines taken at different temperatures. We also adjusted the amplitude of the lines to superimpose the wings of all the lines. This adjustment allowed us to compare the amplitude and the width of the central peak of the lines.

[5]These groups are defined in Table 2.1.

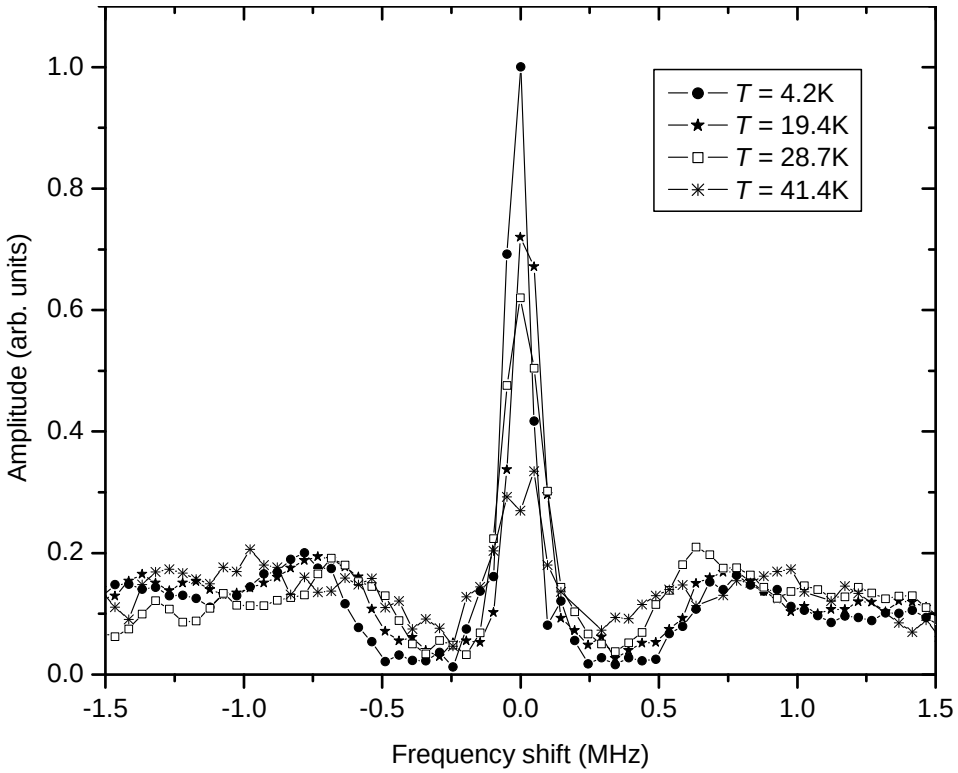

Figure 4.8: Zero-field lineshape of ^{153}Eu in EuO vs. temperature. The lineshapes were obtained by Fourier transform of the spin-echo signal.

We observed that the intensity of the central line was greatly reduced with increasing temperature. As we pointed out in Sect. 4.2, the spin-spin relaxation times are frequency dependent and they are shorter for frequencies close to the central line. Also, as we will see in Chap. 5, we observed that T_2 is strongly temperature dependent, decreasing with increasing temperature. Therefore, we concluded that the intensity of the central peak decreased with increasing temperature as a consequence of the decreasing value of T_2, our spectrometer not being able to detect all the nuclei of the central peak. We also observed that the width of the central line increases almost linearly from about 0.11 MHz at 4.2 K to about 0.23 MHz at 41.4 K. This broadening mechanism did not seem to be linked to T_2 effects since we measured $T_2 \cong 4\,\mu$s at 41.4 K, which corresponds to a Lorentzian width of about 0.08 MHz.

Finally, we observed that the electrical quadrupole splitting decreases with increasing temperature. We estimated the change to be of the order of 25%, from $\Delta\nu_Q \cong 0.75$ MHz at 4.2 K to $\Delta\nu_Q \cong 0.55$ MHz at 41.4 K. We think that this change might be due to a variation of the magnetostriction with temperature. This assumption is supported by the results of F. Levy who observed, by X-ray measurements, that the spontaneous magnetostriction of EuO decreases by about 25% between 4.2 K and 40 K [101]. Note that if the quadrupolar splitting was due to the presence of defects in the crystals, as was proposed by Arons *et al.* [100], we would probably not observe such a temperature dependence.

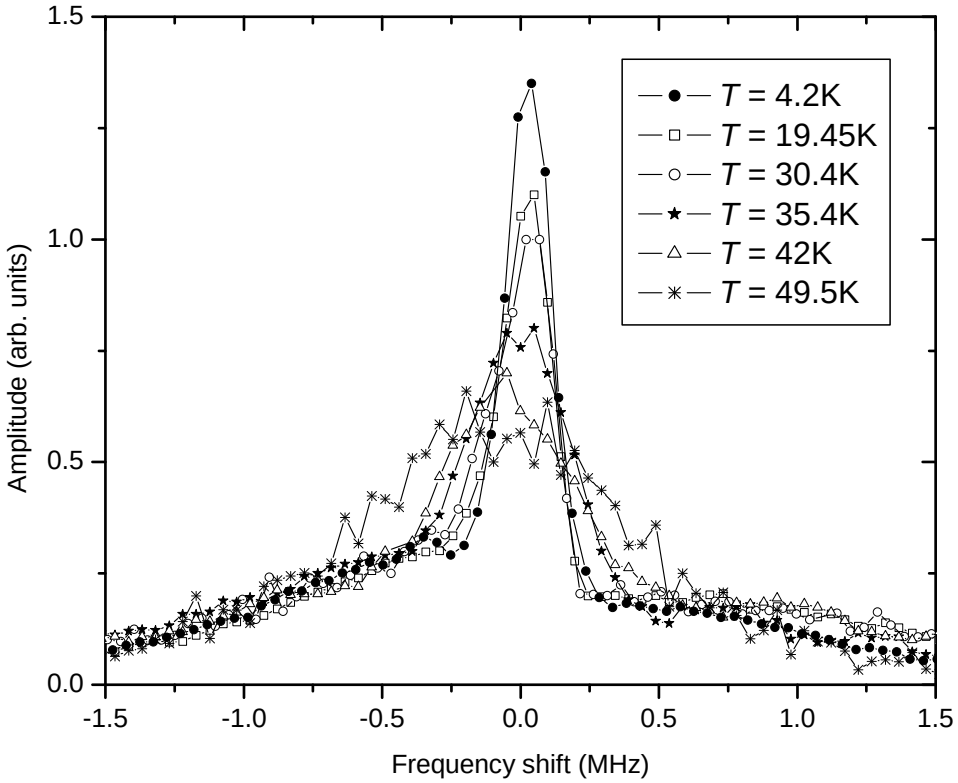

Figure 4.9: Zero-field lineshape of ^{153}Eu in 0.6% Gd doped EuO vs. temperature. The lineshapes were obtained by Fourier transform of the spin-echo signal. Note that while the intensity of the central line in pure EuO was decreasing with increasing temperature due to short T_2's, we observed that the area under the central peak of 0.6% Gd doped EuO was to a good approximation temperature independent. This is most likely because, as will be shown in Chap. 5, the spin-spin relaxation times in 0.6% Gd doped EuO are slower by a factor of about 1.5.

4.4.2 0.6% Gd doped EuO

We measured the lineshape of 0.6% Gd doped EuO as a function of temperature from 4.2 K to 49.5 K. The results are shown in Fig. 4.9. As for pure EuO, the lines were obtained by Fourier transforming the spin-echoes and we plotted the amplitude of the lineshape as a function of the frequency shift from the central line. We adjusted the amplitude of the different lines by superimposing the wings of all the lines.

We observed a temperature dependent broadening of the central line substantially more significant than in pure EuO. We plotted in Fig. 4.10 the Full Width at Half Maximum (FWHM) of the central line as a function of temperature for pure EuO and 0.6% Gd doped EuO.[6] It appears that for temperatures above about 30 K, the FWHM of the 0.6% Gd doped EuO lineshape increases sharply with increasing temperature. We did not observed this phenomena in pure EuO. The measured $1/T_2$ is much less than the observed linewidth. Moreover, we observed that T_2 has the same temperature dependence in 0.6% Gd doped EuO as in pure EuO (c.f. Sect. 5.3). We therefore came to the conclusion that the broadening could not be explained by a variation in T_2 and that the broadening was therefore, a static broadening. This is a key result in this study. It means that the addition

[6]Note that we defined the half maximum of the central line of 0.6% Gd doped EuO from the top of the wings and not from zero intensity. Therefore, we probably underestimated the FWHM of the lineshape of 0.6% Gd doped EuO.

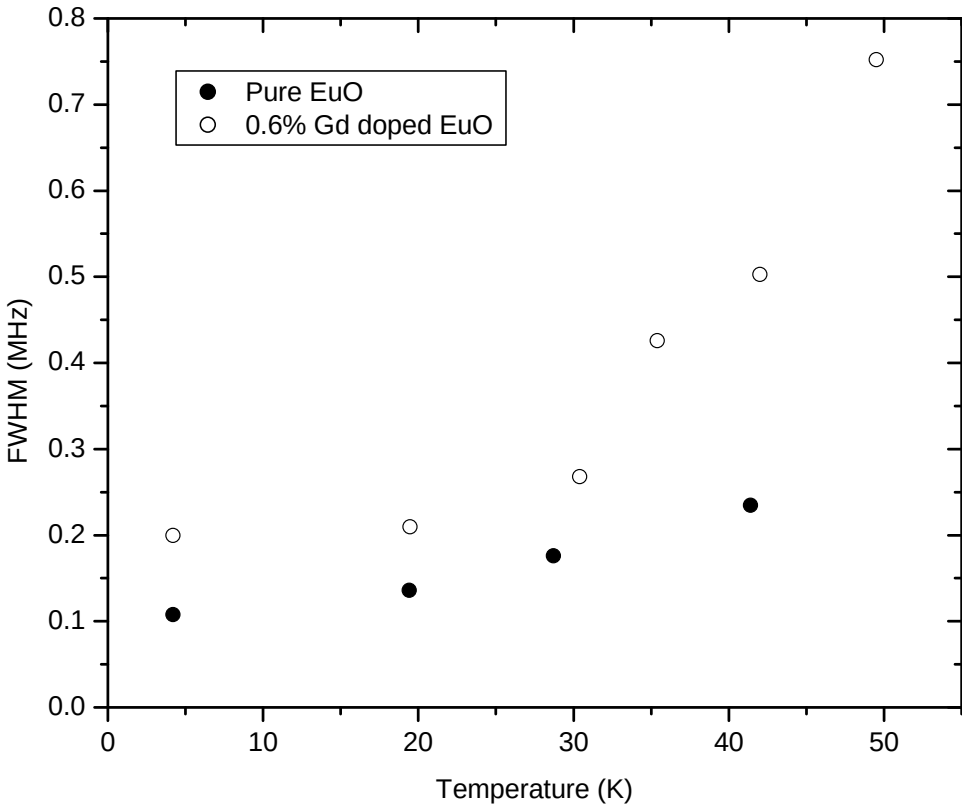

Figure 4.10: FWHM of the zero-field lineshape of Eu^{153} in pure EuO and 0.6% Gd doped EuO vs. temperature. Note that in case of 0.6% Gd doped EuO, the half-maximum is determined from the top of the broad line not from zero intensity.

of 0.6% Gd in the EuO matrix give rise to a temperature dependent phenomena associated with a static magnetic inhomogeneity. The temperature dependent broadening mechanism initiates at about 30 K, the temperature at which the conductivity starts decreasing dramatically according to the results of Godart *et al.* [28] and by Samokhvalov *et al.* [20]. This suggests that the phenomena we observed is likely to be related to the transport properties of the material and in particular to CMR.

The broadening being due to inhomogeneities in the electronic magnetization, a possible explanation for the temperature dependence of the broadening mechanism would be the following: at low temperature, the inhomogeneities are mobile and therefore the line appears narrower due to motional narrowing. At higher temperature, the mobility of the inhomogeneities decreases and when their motion becomes static on the NMR time scale, the line broadens. We found that this explanation is not compatible with our T_2 data. We will give the arguments in Sect. 5.3.2.

We also measured the effect of an external magnetic field of 4T on the temperature dependence of the FWHM of the line. The resulting lineshapes were plotted in Fig. 4.11. A field of 4T was strong enough to saturate the magnetization, and as a consequence a non-negligible demagnetizing field was present in the sample. The demagnetizing field depends on the shape of the sample and it is only homogeneous in ellipsoidal samples (see e.g. [61]).[7] We had to machine the sample to increase the homogeneity of the demagnetizing field. As shown in Fig. 4.11, at 10 K we measured a

[7] The external field needs to be aligned along a principal axis of the ellipsoidal sample.

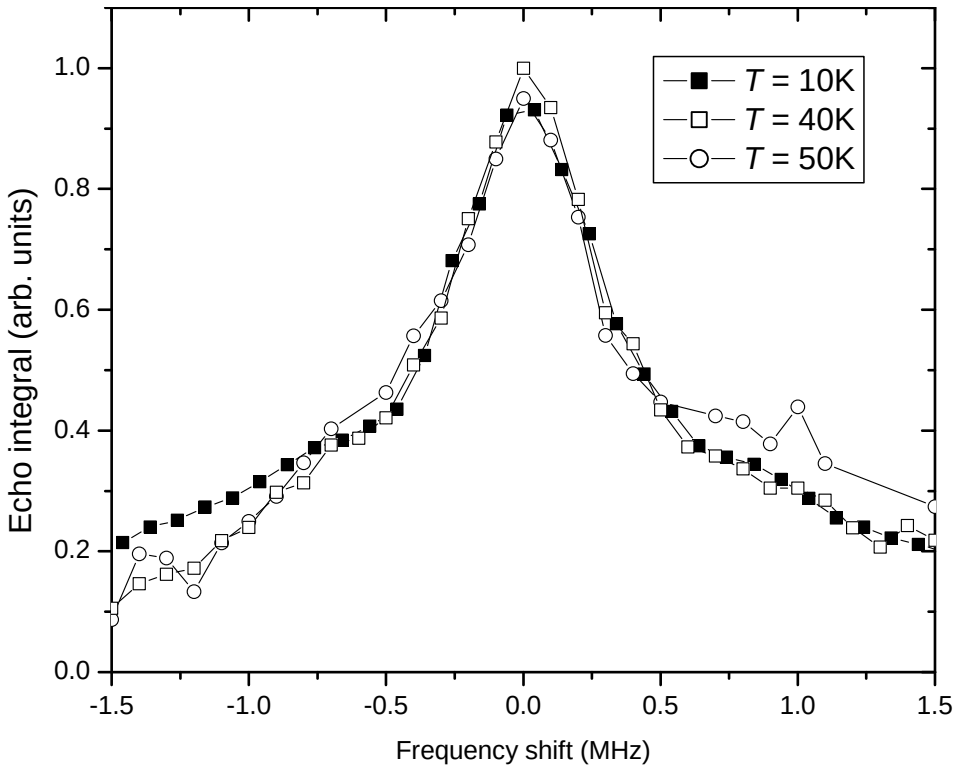

Figure 4.11: Lineshape of ^{153}Eu in 0.6% Gd doped EuO vs. temperature in a field of 4T. The lineshapes were obtained by point-by-point measurement.

FWHM of about 0.5 MHz, which was about 2.5 times broader than the zero-field FWHM at the same temperature. We believe that the fact that the FWHM of the central line at 4T was not as narrow as the zero-field FWHM was due to the inhomogeneity in the demagnetizing field (the sample was not a perfect ellipsoid). However, the FWHM did not increase with increasing temperature, and it was still about 0.5 MHz at 50 K. We concluded that the temperature dependent static inhomogeneities that we measured at zero-field were not present when there was a strong external magnetic field. This observation is an additional suggestion that the broadening might be linked to transport properties of the material. Indeed, since the conductivity of CMR materials is increased by the application of an external magnetic field, applying a field is equivalent to lowering the temperature in terms of transport properties (see, e.g., [5]). Therefore, at a given temperature we can expect the line to be narrower in the presence of an external field than in zero-field. We plan to investigate this phenomena by further studying the broadening as a function of the amplitude of the external field.

4.4.3 2% and 4.3% Gd doped EuO

We also measured the temperature dependence of the ^{153}Eu lineshape in 2% and 4.3% Gd doped EuO. We plotted the measurements for 2% Gd doped EuO in Fig. 4.12. A similar temperature behavior was observed in 4.3% Gd doped EuO. We performed point-by-point measurements to determine the lineshapes. Note that at temperatures higher than about 80 K we could not detect the resonance. This failure was probably due to the fact that the line was too broad and therefore the signal was too weak.

As shown in Fig. 4.12, the lineshape becomes broader with increasing temperature. Also, the

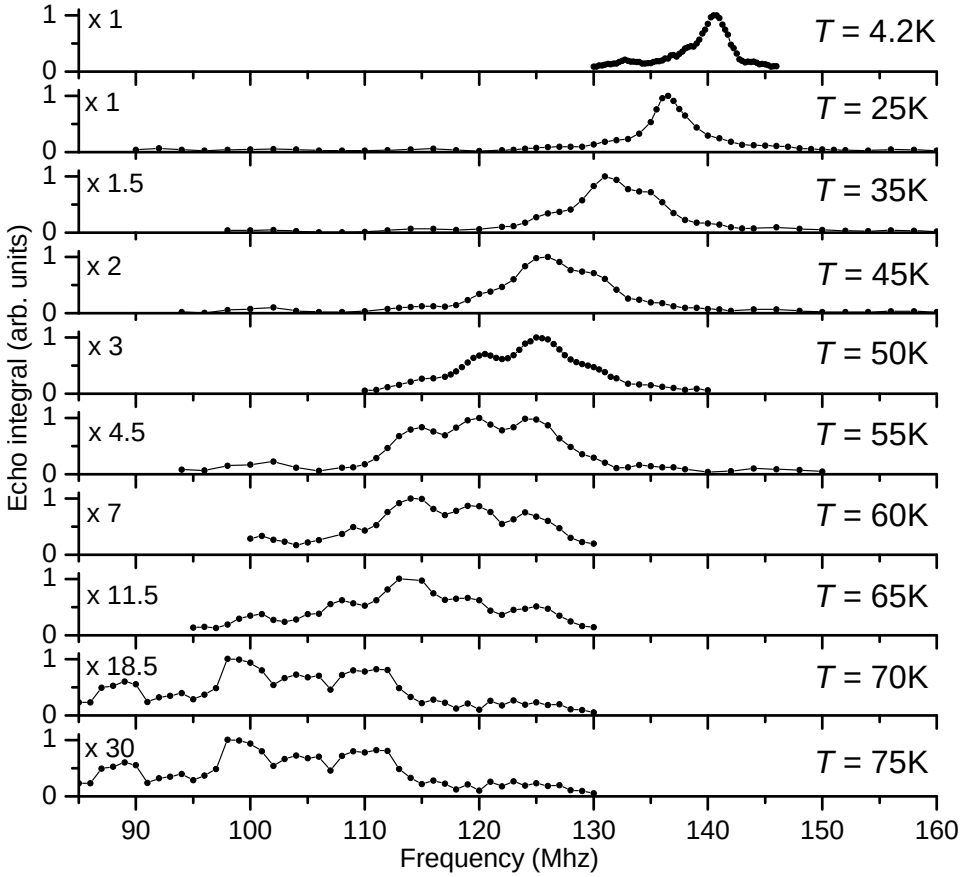

Figure 4.12: Zero-field lineshape of Eu^{153} in 2% Gd doped EuO vs. temperature. The amplitude of the lineshape was multiplied by the coefficient shown on the left side of each curve.

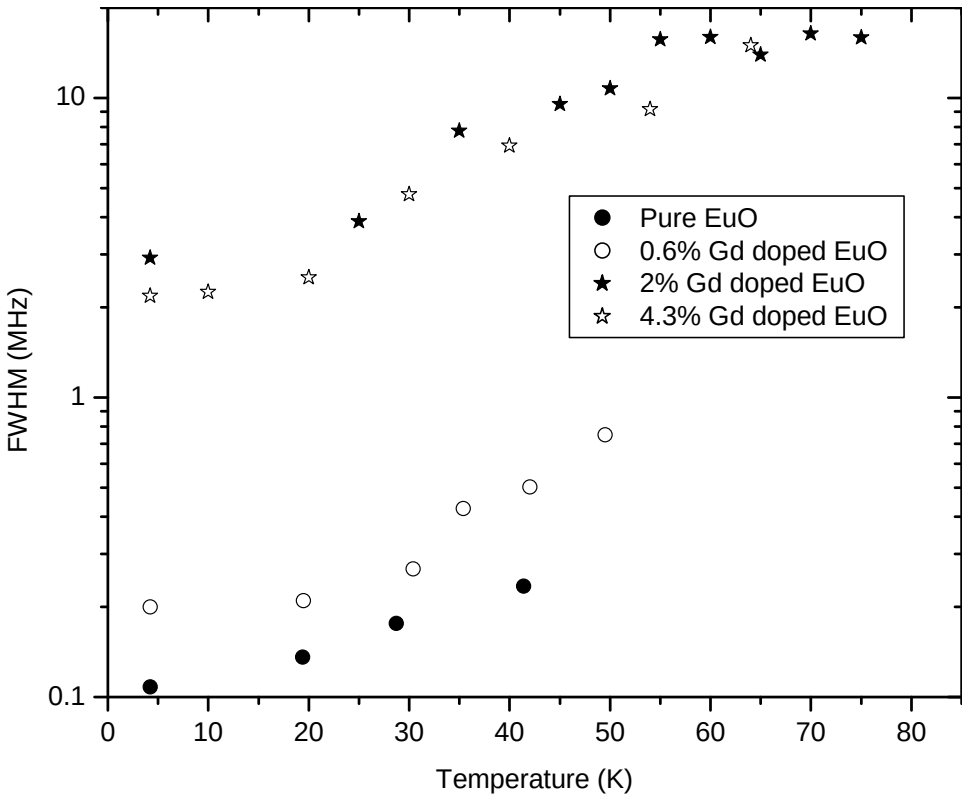

Figure 4.13: FWHM of the zero-field lineshape of Eu^{153} in pure EuO and 0.6%, 2% and 4.3% Gd doped EuO vs. temperature.

structure of the lineshape becomes more and more complex with increasing temperature. In Fig. 4.13 we plotted the FWHM of the lineshape as a function of temperature for 2% and 4.3% Gd doped EuO along with the temperature dependence of the FWHM of the lineshape of pure EuO and 0.6% Gd doped EuO. Note that at temperatures above about 50 K the FWHM of 2% and 4.3% Gd doped EuO is ill-defined since the line has a complex shape. As we showed in Sect. 4.3, the broadening of the 2% and 4.3% Gd doped EuO line at 4.2 K is magnetic in origin. To verify if the temperature dependent broadening was also magnetic, we used the same strategy as used in Sect. 4.3, that is measuring the ^{151}Eu lineshape at a given temperature and comparing it with the ^{153}Eu lineshape at the same temperature. The lineshape of both isotopes measured in 4.3% Gd doped EuO at 40 K are plotted in Fig. 4.14. The frequency of the ^{151}Eu lineshape was multiplied by the ratio given in (4.9). We observed that the two curves have a similar shape, with the same structure, and we therefore concluded that the broadening mechanism was of magnetic origin. Also, as we will see in Sect. 5.3, $1/T_2$ is by far smaller than the linewidth of the lines we measured. Therefore, we concluded that the temperature dependent broadening is a static broadening.

As in 0.6% Gd doped EuO, we also observed that for temperatures above about 30 K, the FWHM of the 2% and 4.3% Gd doped EuO lineshape increases more rapidly with increasing temperature (c.f. Fig. 4.13). However, the amplitude of the broadening is by far larger in 2% and 4.3% Gd doped EuO than in 0.6% Gd doped EuO. As we saw in Sect. 2.1, previous studies showed that the change in transport properties in this type of samples is not as dramatic as in 0.6% Gd doped. Nevertheless, the conductivity still decreases with increasing temperature by a factor of about 10 [28]. This decrease might be linked to the temperature dependent broadening. However, since the

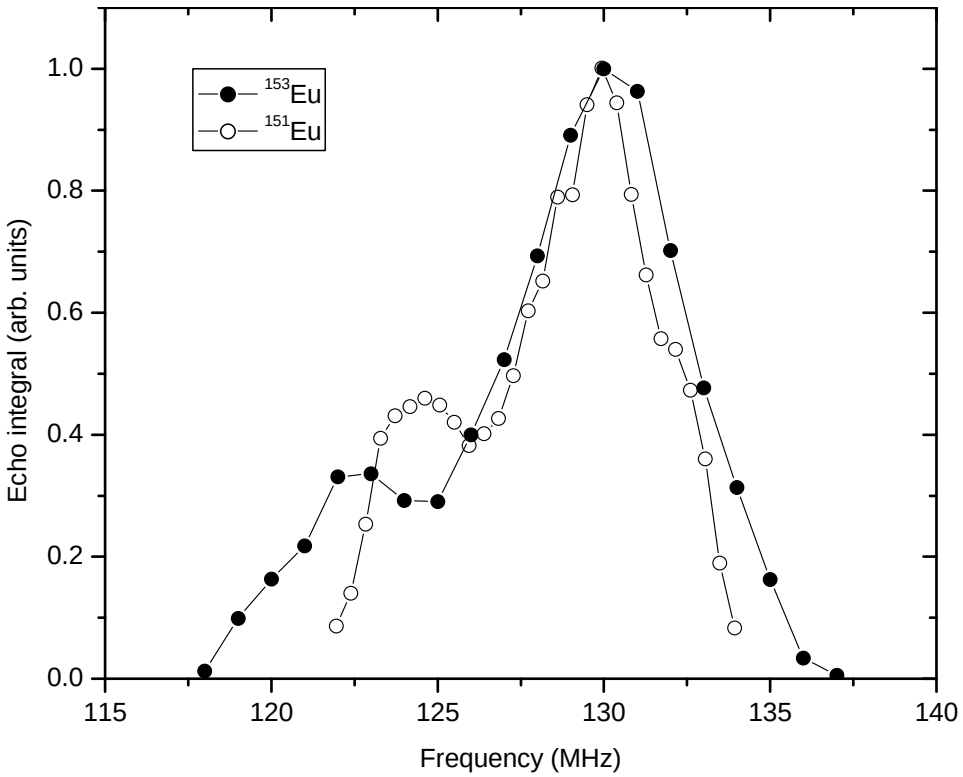

Figure 4.14: Zero-field lineshape of Eu^{153} and Eu^{151} in 4.3% Gd doped EuO at 40 K. The frequency of the Eu^{151} lineshape was multiplied by the ratio ${}^{153}\gamma_n/{}^{151}\gamma_n$.

amplitude of the magnetic inhomogeneity is so large in 2% and 4.3% Gd doped EuO, we suspected that another broadening mechanism could take place in these samples. A possible explanation for the temperature dependent broadening is that the value of the exchange integral is distributed throughout the samples, i.e., different part of the samples have different values of J. The presence of such a distribution could also explain the fact that the magnetization curves do not follow a Brillouin curve (c.f. Sect. 2.2). We show in Fig. 4.15 the temperature dependence of the frequency of the center of the line (dots) along with the temperature dependence of the width of the line (vertical bars). If we assume a distribution of J values corresponding to a distribution of T_C's between 69.55 K (Curie temperature of pure EuO) and 155 K (highest Curie temperature given by the model of Mauger [32]), we can approximatively account for the temperature dependence of the width of the line, as shown in Fig. 4.15. As we will see in Sect. 5.2, the value of J is related to the value of the observed spin-lattice relaxation time T_1 trough the expression given in (3.17). That means that a slight variation in J strongly influences the value of T_1 because $T_1 \propto J^{9/2}$. We did not observe any strong frequency dependence of T_1, i.e. the measured T_1 was, too a good approximation, independent of the position on the line. Therefore, we do not think that a distribution in J causes the temperature dependent broadening.

Finally, let us mention that we tried to measure the influence of an external field of 4T on the lineshape of a 2% Gd doped EuO sample. We observed a signal at 4.2 K but it was weak. We aborted the study since we were not able to detect the signal at temperature higher than about 20 K.

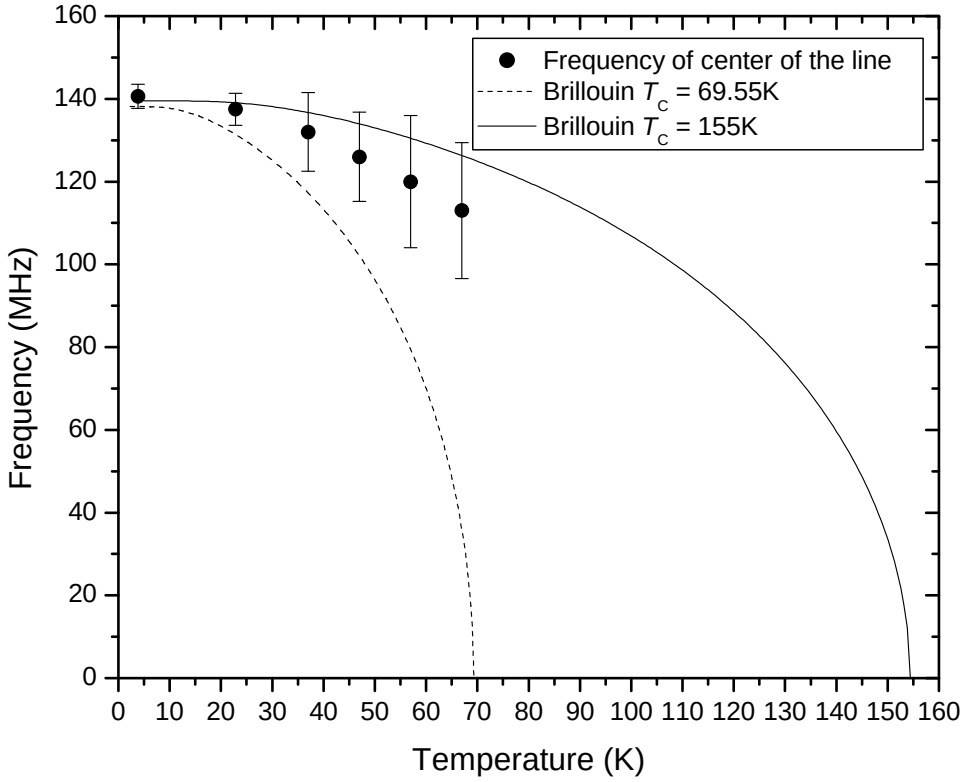

Figure 4.15: Zero-field Eu^{153} frequency of the center of the line and width of the line (shown as vertical bars) in 2% Gd doped EuO vs. temperature. The two Brillouin curves are plot for the maximum the limits of a possible distribution in J

Chapter 5

Relaxation times

The measurement of NMR relaxation times in europium chalcogenides gives some valuable information about the dynamics of their electron spins through the hyperfine coupling. Boyd was the first to report NMR data on EuS [102], and together with Charap, used spin-wave theory to deduce values of J_1 and J_2 from the temperature behavior of the NMR frequency of both ^{151}Eu and ^{153}Eu [103]. The first values of NMR relaxation times in EuO were published in 1965 by Uriano and Streever [104]. They performed zero-field measurements on powdered EuO at two temperatures; at 4.2 K and 20.3 K. They found $T_1 = 9\,\text{ms}$ and $T_2 = 40\,\mu\text{s}$, at 4.2 K and $T_1 = 0.8\,\text{ms}$ and $T_2 = 20\,\mu\text{s}$ at 20.3 K. Following this work, several groups studied NMR relaxation times and compared their data to spin-wave theory as well as to the Suhl-Nakamura theory in order to explain their results and to obtain information on the magnetic properties of the system.

In this chapter, we present our measurements of the relaxation times. We extended the study of relaxation times in EuO to much higher temperature than in previous studies and we measured the relaxation times in Gd doped EuO. We will compare the relaxation times in EuO to the relaxation times in Gd doped EuO and determine the influence of doping on the dynamic properties of the electronic magnetization.

5.1 Measuring T_1

As mentioned in Sect. 4.1, the definition of a $\pi/2$- or a π-pulse in a ferromagnetic system is somewhat arbitrary. Therefore, it makes sense to use a saturation recovery (SR) sequence instead of an inversion recovery (IR) sequence to perform T_1 measurements in a ferromagnetic system. In an IR sequence, a π-pulse is applied to invert the longitudinal component of the nuclear magnetization before measuring the recovery time constant T_1. It is thus necessary to have a well-defined π-pulse. For the SR sequence, an exact π-pulse is not required since the sequence consists in destroying the nuclear magnetization by applying a series of pulses before measuring the signal.

Various pulse sequences can be used to destroy the magnetization in a SR scheme. In Fig. 5.1 we present the sequence we used to measure T_1 in the $Eu_{1-x}Gd_xO$ systems. Sometimes called a RF comb, it consists of a series of 8 pulses all separated by a time τ. The idea is to apply a $\pi/2$-pulse along a given direction in the plane perpendicular to the effective static field and to wait a time τ of the order of T_2 so the nuclear spins that were flipped lose their coherence. Then another $\pi/2$-pulse along the same direction is applied to erase the magnetization left in the perpendicular plane. The

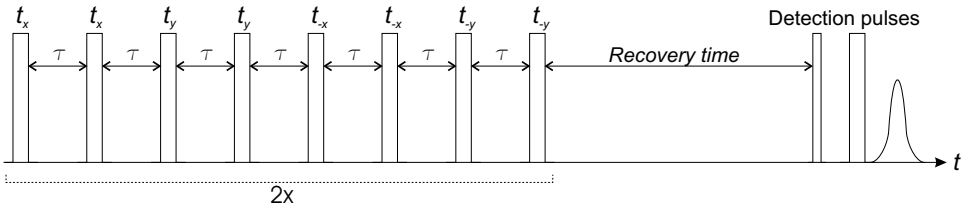

Figure 5.1: Saturation recovery (SR) pulse sequence. The sequence is composed of a RF comb that erases the nuclear magnetization and a spin-echo detection sequence.

process is applied in each of the 4 directions of the perpendicular plane, x, y , -x and -y. We applied the series twice in a row to increase the efficacy of the erasing procedure.

After waiting for a time denoted *Recovery time*, a standard spin-echo sequence $t_1 - delay - t_2$ is applied to detect the amplitude of the magnetization that has recovered equilibrium (c.f. Sect. 4.1 for more details on the spin-echo sequence). For all the measurements performed, we used $t_x = t_y = t_{-x} = t_{-y} = 0.2\mu s$ and $\tau \cong T_2$. We therefore always started by determining T_2. This sequence is well adapted to measurements at low temperatures since the pulses of the RF comb are short and therefore the amount of heat transferred from the coil to the measured sample is small.

We saw in the previous chapter that although the crystal structure of $Eu_{1-x}Gd_xO$ is nominally cubic, there are EFGs acting on the Eu nuclei. That means that even at zero-field the spin degeneracy is lifted and, since ^{153}Eu and ^{151}Eu nuclei are spin $I = 5/2$, there are five possible transitions between the spin levels. Therefore, assuming relaxation of magnetic origin, we expected the relaxation processes to be described by 5 relaxation rates $W_{m\leftrightarrow m+1}$ associated with the 5 allowed transitions $m \leftrightarrow m+1$, $m = -\frac{5}{2}, -\frac{3}{2}, -\frac{1}{2}, \frac{1}{2}, \frac{3}{2}, \frac{5}{2}$.[1] The relaxation rates can be calculated using Fermi's Golden Rule

$$W_{m\leftrightarrow m+1} = \frac{2\pi}{\hbar} | < m|\hat{\mathcal{H}}_{int}|m+1 > |^2 \delta(E_m - E_{m+1}). \tag{5.1}$$

where E_m and E_{m+1} are the energy of the levels m and $m+1$ respectively, and $\hat{\mathcal{H}}_{int}$ is the Hamiltonian describing the interactions causing the relaxation processes. In an SR scheme, the evolution of the longitudinal nuclear magnetization just after the RF comb (t=0) can be written as

$$m_z(t) = m_z(t=\infty)\,(1 - \varepsilon w(t)), \tag{5.2}$$

where ε is the fraction of spins that have been flipped by the RF comb and $w(t)$ is given by

$$w(t) = \sum_{m\ states} c_m e^{-\alpha_m W_{m\leftrightarrow m+1} t}, \tag{5.3}$$

where the c_m coefficients are determined by the initial conditions and the α_m coefficients are determined by the so-called normal modes problem [105]. When all the transitions $m \leftrightarrow m+1$ are excited and detected, the solution of the normal modes problem gives a single-exponential function for $w(t)$.

A typical magnetization recovery curve, obtained by applying the sequence described above to a $Eu_{1-x}Gd_xO$ sample for a series of values of *Recovery time*, is plotted in Fig. 5.2. The fitting curve was a single exponential. Consequently, all the transitions were excited and detected. This confirms the assumption that we made in the previous chapter. This could also be verified by comparing the

[1] Note that quadrupolar relaxation also gives $m \leftrightarrow m \pm 2$ transitions

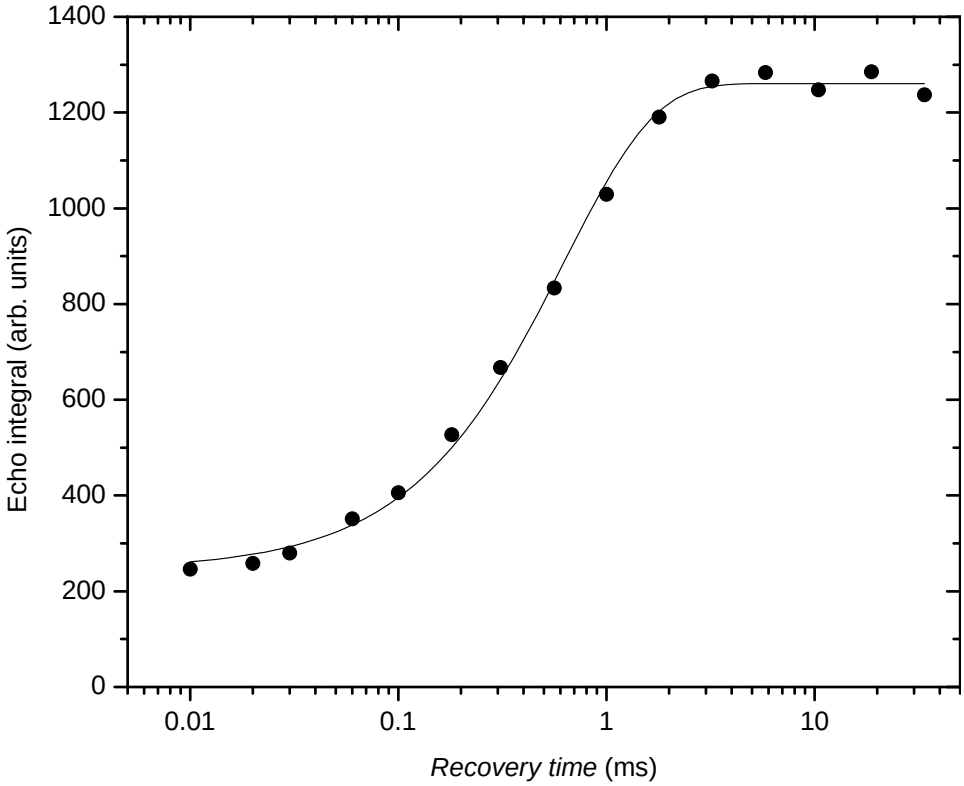

Figure 5.2: Spin-echo integral as a function of *Recovery time* values in pure EuO at 20 K. The fitting curve is defined in (5.2) and (5.3) with all the coefficients c_m but one taken to be zero.

Fourier transform of echoes recorded at different values of *Recovery time*. The FFT of two echoes is shown in Fig. 5.3, where the amplitude of the curve corresponding to the short value of *Recovery time* was multiplied by a factor of 3. The similar shape of the two curves suggested that all the spins that were detected by the spin-echo sequence were excited by the RF comb. It also meant that the relaxation processes were the same for all the nuclear spins (i.e. at all parts of the NMR line) This is because by destroying all the magnetization, the system recovers in a single normal mode (the uniform mode) where all population differences are the same.

It was important to note that the values of T_1 we measured were independent of the amplitude of the RF field H_1. This fact further suggests that we observed the nuclei located in domains and not those located in domain walls, as noted in Sect. 3.4.1.

5.2 Spin-lattice relaxation times vs. temperature

Barak, Gabai and Kaplan determined that the spin-lattice relaxation in powdered EuO at temperatures below 14 K are dominated by two-magnon processes [106]. Also, between 14 K and 20 K, they observed that three-magnon process surpasses the two-magnon process. However, to explain the short values of T_1 they observed, they had to take into account the second-order three-magnon process that enhances the first-order process (c.f. Sect. 3.5). The enhancement factor when an external field is applied has been calculated to be 4 [106].

The results we obtained confirmed that, for temperatures above about 14 K, the three-magnon process is the dominant spin-lattice relaxation process in EuO. Indeed, as shown in Fig 5.4, the

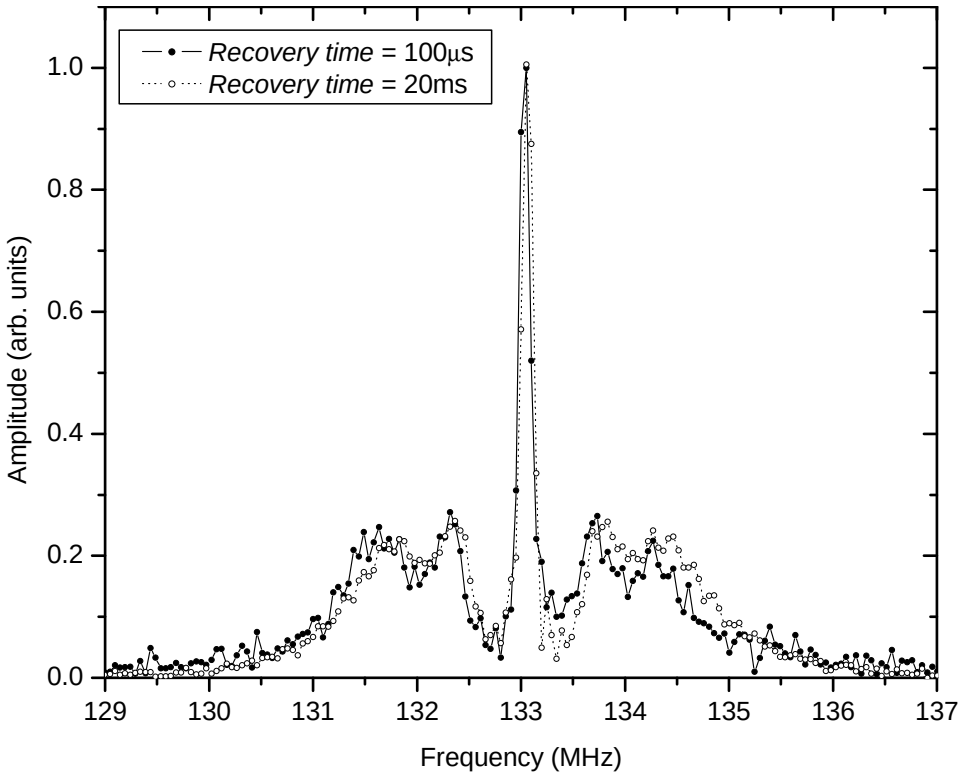

Figure 5.3: FFT of two echoes recorded at two different values of *Recovery time* at 20 K. The amplitude of the curve corresponding to a value of *Recovery time* of 100 μs was multiplied by a factor of 3.

Table 5.1: Values of J as a function of Gd doping.

Doping level x (%)	Exchange integral J/k_B (K)
0	0.754 ± 0.01
0.6	0.750 ± 0.01
2	1.203 ± 0.01
4.3	1.211 ± 0.01

temperature dependence of T_1 for EuO was proportional to $T^{7/2}$. To fit the data, we used (3.17) multiplied by the exchange scattering enhancement factor that we determined to be $\xi \cong 8$, in agreement with the calculation of Beeman and Pincus [68] (c.f. Appendix A). Taking $S = 7/2$ and determining the hyperfine constant from the zero-field resonance frequency extrapolated to $T = 0\,\mathrm{K}$, $A = -\hbar\omega/S \cong -2.6 \cdot 10^{-26}\,\mathrm{J}$, we deduce from the fit a value of the exchange integral of $J/k_B = 0.754 \pm 0.01\,\mathrm{K}$. As noted in Sect. 3.5, $J = J_1 + J_2$.

Let us discuss the accuracy of the determination of J: first, even if the enhancement factor is not precisely known, the fact that $1/T_1$, and therefore ξ/T_1, is proportional to $J^{-9/2}$ (c.f. (3.17)) means that a large change in ξ corresponds to a small change in J. For example, if we take $\xi = 7.9$ instead of $\xi = 8$, which corresponds to a ratio of $k_1/k_2 = 3/4$ between the amplitude of the magnon wave vectors $\boldsymbol{k_1}$ and $\boldsymbol{k_2}$ of the two scattered magnons (c.f. Appendix A), we obtain $J/k_B = 0.752\,\mathrm{K}$ instead of $J/k_B = 0.754\,\mathrm{K}$. The other causes of uncertainty are the uncertainty of the T_1 value and the uncertainty of the temperature. An evaluation of the total error gives $\Delta J/k_B = 0.01\,\mathrm{K}$.

As mentioned in Sect. 2.2, previous measurements on powdered EuO by neutron scattering experiments [31] and specific heat measurements [107] led respectively to $(J_1 + J_2)/k_B = 0.725 \pm 0.006\,\mathrm{K}$ and $(J_1 + J_2)/k_B = 0.714 \pm 0.007\,\mathrm{K}$. More recently, Mook measured single crystals of EuO by neutron scattering methods and he obtained the following values [108]: $J_1/k_B = 0.625 \pm 0.007\,\mathrm{K}$ and $J_2/k_B = 0.125 \pm 0.01\,\mathrm{K}$. These values lead to a value of the exchange integral $J = 0.750 \pm 0.017\,\mathrm{K}$ which in very good agreement with our measurement. It is however important to remember that if the samples are not stoichiometric, their magnetic properties can vary substantially.

In 1966 E. L. Boyd deduced J_1 and J_2 by measuring the temperature dependence of the NMR frequency of ^{153}Eu [87]. He found a value of $J_1/k_B = 0.750 \pm 0.0025\,\mathrm{K}$ that is very close to the value of J that we determined. However, he found a negative value of J_2.

After we showed that the data led to a value of J for pure EuO that was in very good agreement with the values determined by other measurement techniques, we examined the case of Gd doped EuO. As shown in Fig 5.4, the temperature dependence of the spin-lattice relaxation times for the three doped samples we studied were proportional to $T^{7/2}$. As for pure EuO, the three-magnon process was the dominant relaxation process. Using expression (3.17) and the enhancement factor $\xi = 8$, we deduce the values of J shown in Table 5.1 for the doped samples. As evident in Fig. 5.4, the samples can be separated in two categories according to their value of J. To show that this separation is indeed due to a variation in the amplitude of the exchange integral, let us evaluate the difference between the T_1 of the two categories: from the mean-field theory for Heisenberg ferromagnets, keeping the nearest neighbor coupling only, we have the relation between T_C and J_1

$$T_\mathrm{C} = z_1 J_1 \frac{2S(S+1)}{3k_B} \cong z_1 J_1 \frac{2S^2}{3k_B} \propto J_1 S^2, \tag{5.4}$$

where z_1 is the number of nearest neighbours of a Eu atom (c.f. e.g. [109]). With this approximation

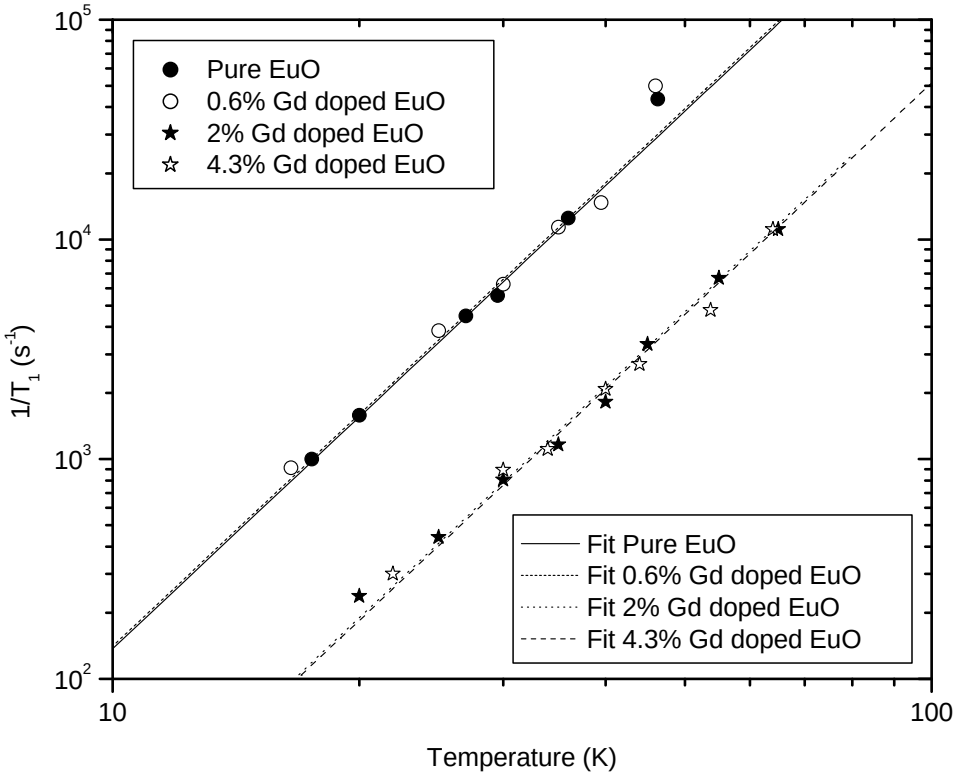

Figure 5.4: Zero-field spin-lattice relaxation rates of ^{153}Eu in $Eu_{1-x}Gd_xO$ as a function of temperature. The expression used to fit the curves is defined in (3.17).

and assuming $J \cong J_1$, we can rewrite (3.17) as

$$\frac{1}{T_1} \propto \frac{A^2}{\hbar T_{\mathrm{C}}} \left(\frac{S k_B T}{T_{\mathrm{C}}} \right)^{7/2}. \tag{5.5}$$

Then, S can be related to the NMR resonance frequency by noting that

$$\omega_0 = \gamma |\boldsymbol{H_{eff}}| \propto \gamma |\boldsymbol{M}| \propto S. \tag{5.6}$$

This leads to

$$\frac{1}{T_1} \propto \frac{A^2}{\hbar T_{\mathrm{C}}} \left(\frac{\omega_0 k_B T}{T_{\mathrm{C}}} \right)^{7/2} \propto \frac{(\omega_0 T)^{7/2}}{T_{\mathrm{C}}^{9/2}}. \tag{5.7}$$

From (5.7) we can approximate the ratio between the spin-lattice relaxation time of pure EuO, $T_{1,pure}$, and the spin-lattice relaxation of $Eu_{0.98}Gd_{0.02}O$, $T_{1,2\%}$.[2] Taking an approximate value of 120 K for the Curie temperature of the doped sample and $T_{\mathrm{C}} = 69.55$ K for pure EuO (c.f. Sect. 2.4), we obtain

$$\frac{T_{1,2\%}}{T_{1,pure}} = \left(\frac{\omega_{0,pure}}{\omega_{0,4.3\%}} \right)^{7/2} \left(\frac{T_{C,4.3\%}}{T_{C,pure}} \right)^{9/2} \cong 11. \tag{5.8}$$

[2]The result is approximatively the same if the 2% sample is replace by the 4.3% since their Curie temperature is approximatively the same.

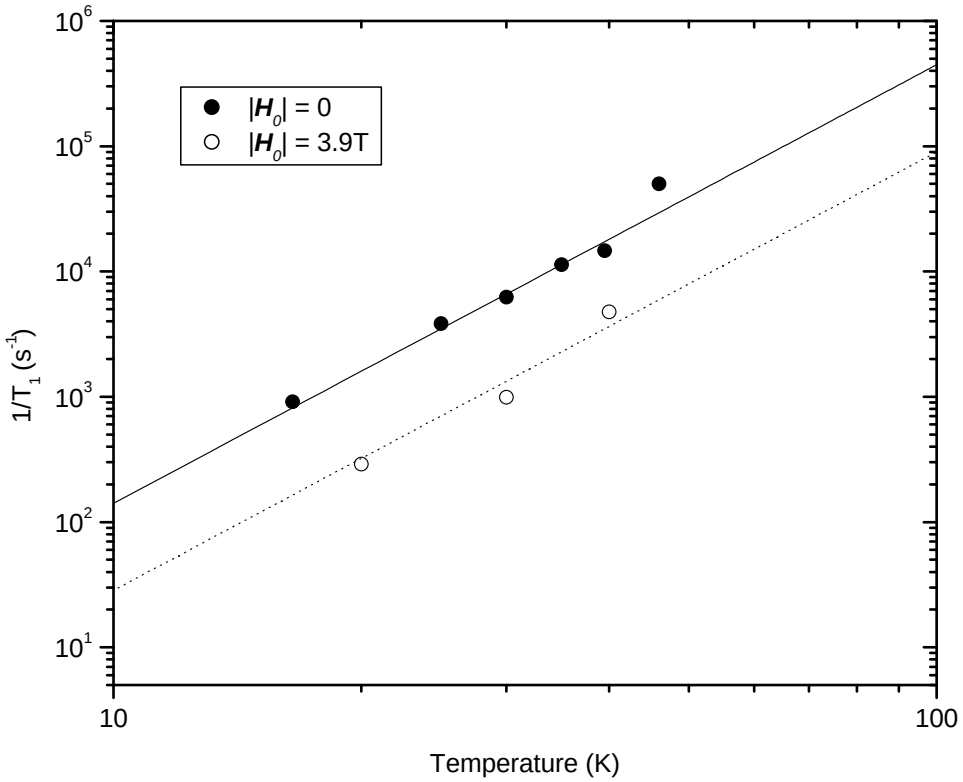

Figure 5.5: Spin-lattice relaxation rates of ^{153}Eu in 0.6% Gd doped EuO as a function of temperature for zero external field and $|\boldsymbol{H}_0| = 3.9\,\mathrm{T}$. The expression used to fit the curves is defined in (3.17).

This ratio is close to the value of about 8.7 that we determined experimentally as revealed in Fig. 5.4. We can therefore have confidence in the J values we determined in the above analysis.

In order to observe the influence of a field on the relaxation rates, we also measured the temperature dependence of T_1 of ^{153}Eu in 0.6% Gd doped EuO in a strong external field. The results obtained in a field of 4 T are shown in Fig. 5.5. We also observed a temperature behavior proportional to $T^{7/2}$ as expected from the results of Barak *et al.* [106]. Also, we observed that T_1 was larger than at zero-field due to the fact that there were fewer magnons when a strong external field was applied.

The fact that the temperature dependence of the spin-lattice relaxation time is the same for a strong external field as for zero-field validates the assumption that the nuclei we measured at zero-field are the nuclei located in domains and not in domain walls where other relaxation mechanisms such as thermal fluctuations of the domain walls are expected to take place [110]. Note that Guenther *et al.* observed that the temperature dependence of T_1 is field dependent (the measurements were done between 1.2 K and 4.2 K), which might be explained by the fact that they were measuring nuclei in domain walls for low values of field [111].

5.3 Spin-spin relaxation times vs. temperature

Except for the value of T_2 at 20.3 K determined by Uriano and Streever [104] and the decay curve at 13.8 K published by Barak *et al.* [112], there are no spin-spin relaxation time data for EuO above

4.2 K in the literature. However, there were several studies of T_2 at 4.2 K and lower temperatures, following the work of Barak *et al.* [112, 113]: Raj *et al.* [88], Fekete *et al.* [73] and numerous articles by a German group [91, 92, 100, 114–116]. The main reason for this interest is that the decay curve is not a single exponential. As Lütgemeier *et al.*[91] first noted, this is because there are two relaxation mechanisms: a fast one due to the Suhl-Nakamura indirect interaction, and a slow one due to direct dipolar coupling. However, the original Suhl-Nakamura theory fails to explain the amplitude of the observed spin-spin relaxation time and its frequency dependence that was first reported by Raj *et al.* [88]. Barak *et al.* used the HJNP theory (c.f. Sect. 3.6) to explain why the value of T_2 they observed in a powdered EuO sample at 4.2 K is longer than the one predicted by the Suhl-Nakamura theory [112]. The HPNJ theory assumes the existence of an inhomogeneous line broadening and predicts a frequency dependent T_2. Also, whereas the Suhl-Nakamura theory predicts a Gaussian line shape and therefore a Gaussian echo decay, the HPNJ theory predicts a Lorentzian line shape and therefore an exponential decay.

In 1976, Fekete *et al.* successfully described the decay curves of the five transitions they had observed by assuming an inhomogeneous Suhl-Nakamura relaxation process (deduced from HPJN model) and a dipolar coupling [73]. They were the only ones to take into account all the elements necessary to describe the lineshape and its variation with delay as shown in Fig. 4.4. However, they did not discuss the implication of their results on the lineshape. Arons *et al.* published in 1975 the zero-field lineshape vs. delay and observed, as we did, the reduction of the amplitude of the central peak with increasing delay [92]. However, Arons *et al.* claimed that the T_2 of the central line was shorter because the signal was coming from nuclei located in domain walls, which is, in the light of our results, an incorrect interpretation.

We have performed spin-spin relaxation measurements in pure EuO and in Gd doped EuO using a standard spin-echo sequence $t_1 - delay - t_2$ composed of two pulses separated by a varying delay.[3] Typical values were $t_1 = 0.1\,\mu$s and $t_2 = 0.2\,\mu$s. As shown in Chap. 4, the width of the lineshape increases with increasing Gd doping and consequently the duration of the echo decreases with increasing x. The values of *delay* were adapted to the duration of the echo: for long echo, it was necessary to use long delays and conversely, for short echoes it was possible to use very short delays.

Since T_2 was strongly frequency dependent, it was necessary to specify at what frequency it was measured. In the following, T_2 always corresponds to the spin-spin relaxation time measured at the frequency corresponding to the center of the central line or the center of gravity of the line in cases the central line is not well defined. Also, as for T_1 measurements, we always excited all the transitions.

Let us start by looking at the decay curve of the spin-echo of ^{153}Eu in EuO at 4.2 K (c.f. Fig. 5.6). In agreement with previous measurements, the decay consists of a sum of two decays, one fast, caused by Suhl-Nakamura interactions, and one slow, due to dipolar coupling. The time variation of the echo amplitude $A(t)$ can be fit with the function

$$A(t) = A_{S-N} \exp(-t/T_2^{S-N}) + A_{dip} \exp(-t/T_2^{dip}) \tag{5.9}$$

where T_2^{S-N} is the spin-spin relaxation time associated with the Suhl-Nakamura process, T_2^{dip} is the spin-spin relaxation time associated with the dipolar process, A_{S-N} and A_{dip} are coefficients

[3] As for lineshape and T_1 measurements, we used a 16-phase CYCLOPS sequence to reduce the transients due to the RF pulses.

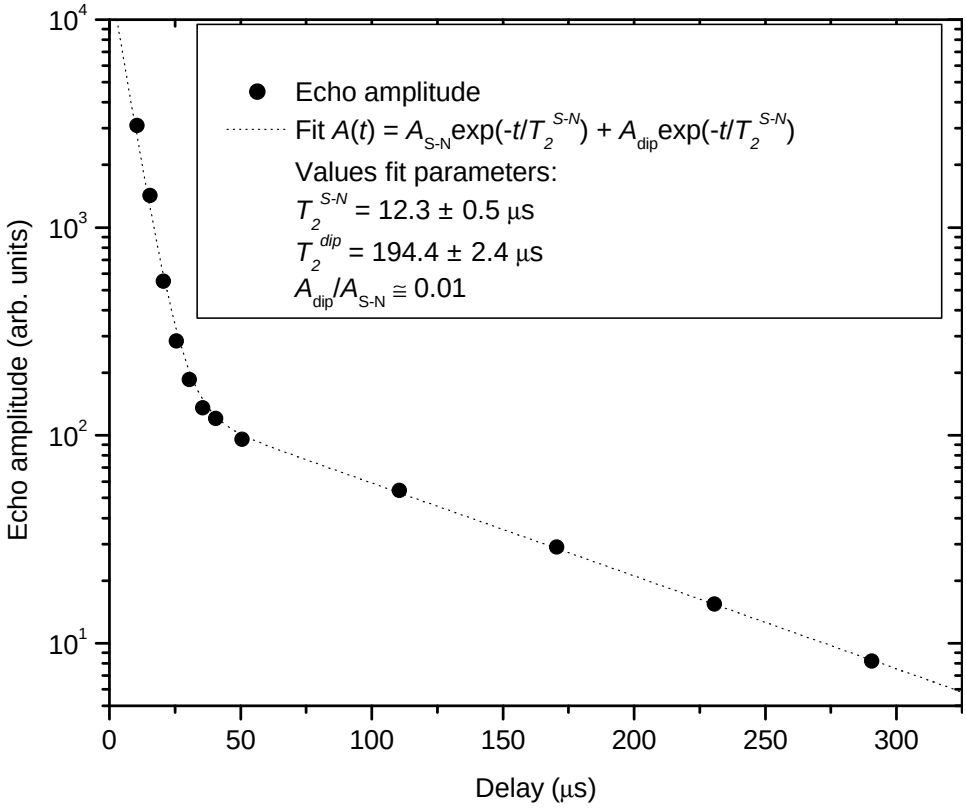

Figure 5.6: Zero-field echo decay curve of the central transition of ^{153}Eu in EuO at 4.2 K.

independent of time. The ratio A_{dip}/A_{S-N} is equal to the ratio number of spin relaxing through the dipolar relaxation divided by number of spin relaxing through the Suhl-Nakamura relaxation. We observed that $T_2^{S-N} = 12.3 \pm 0.5\,\mu$s, $T_2^{dip} = 194.4 \pm 2.4\,\mu$s and $A_{dip}/A_{S-N} \cong 0.01$ (c.f. Fig. 5.6). Let us state the main difference between the Suhl-Nakamura coupling and the dipolar coupling. The Suhl-Nakamura (or the HJNP) Hamiltonian describes an interaction involving terms of the form $\hat{I}_i^+ \hat{I}_j^-$ (c.f. (3.18)). This means that a nuclear spin in state m can relax in state $m+1$ only if at least one of its neighbors is in the state $m' = m+1$ (mutual spin-flip). In addition to terms of the form $\hat{I}_i^+ \hat{I}_j^-$, the dipolar hamiltonian has terms of the form $\hat{I}_i^z \hat{I}_j^z$ and therefore a spin in state m can also relax if at least one of its neighbors is in the same state m. However, as long as one of the neighbors is in a state allowing mutual spin-flip, we expect the Suhl-Nakamura to participate in the relaxation of a larger number of spins since in EuO the amplitude of the Suhl-Nakamura coupling is much larger than the dipolar coupling (Barak *et al.* calculated that the second moment of the Suhl-Nakamura is about 10^3 times larger than the dipolar second moment [112]).

The probability that a given nucleus relaxes by the dipolar mechanism is therefore given by the probability that it cannot relax by mutual spin flips using the Suhl-Nakamura coupling. Thus, the dipolar relaxation arises from those nuclei whose neighbors cannot undergo mutual spin-flips. The probability that each neighbor is in the wrong m state is 5/6. If there were only one Eu isotope, the probability that no first neighbor can have a spin-flip is thus $(5/6)^{12} \cong 0.11$. However, the first neighbors might change states by coupling to the second neighbors, so 0.11 is an overestimate. In this way, we can see why dipolar relaxation only is an unlikely process, in agreement with Fig. 5.6.

Let us mention that the fast decay shown in Fig. 5.6 is well fitted by an exponential, in agreement

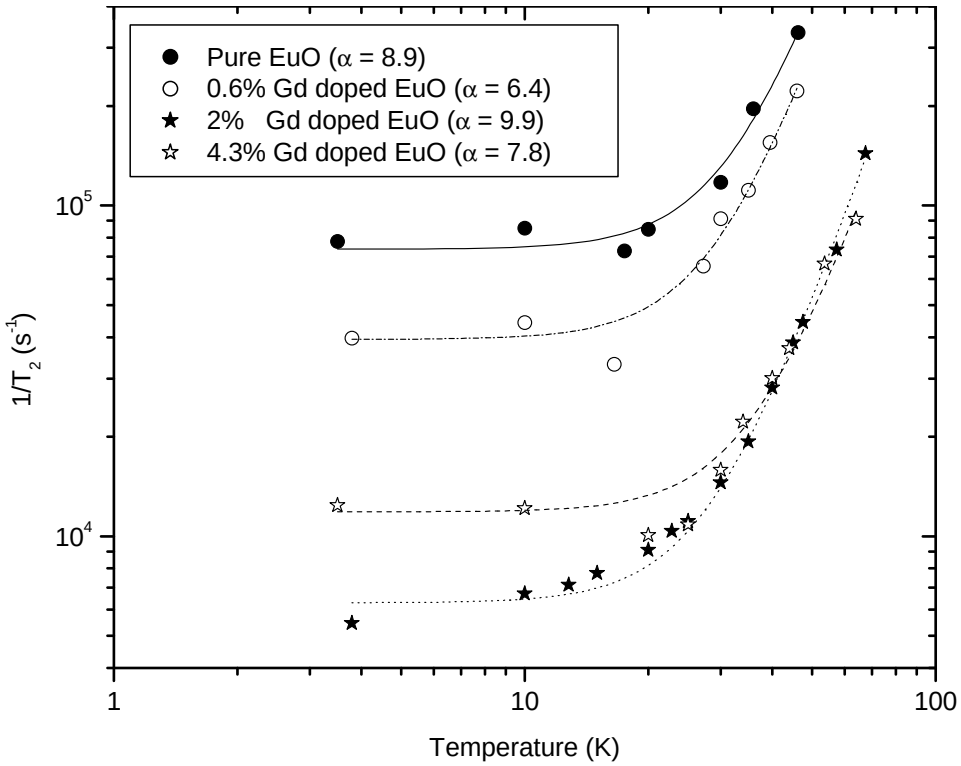

Figure 5.7: Zero-field spin-spin relaxation rates of ^{153}Eu in $Eu_{1-x}Gd_xO$ as a function of temperature. The parameter α and the fitting curve are defined in (5.11).

with previous measurements and consistently with the HJNP theory (c.f. e.g. [73]). Note that this was the reason for using a Lorentzian as magnetic distribution function to fit the lineshapes in Chap. 4.

Let us calculate the spin-spin relaxation time of the central line given by the original (homogeneous) Suhl-Nakamura theory. Using $|\boldsymbol{H}| = |\boldsymbol{H}_{an}(T = 4.2\,\mathrm{K})| = 247.5 \pm 2.5\,\mathrm{Oe}$ [59], calculating $|\boldsymbol{H}_{ex}|$ from $J_1/k_B = 0.625 \pm 0.007\,\mathrm{K}$ [108], and $\nu_0 = 138.5\,\mathrm{MHz}$ the frequency of the central line we have measured at 4.2 K, we obtain $T_2 = \sqrt{2}/\sigma \cong 2.9\,\mu\mathrm{s}$ from (3.21) (Note that we replaced the factor $\frac{1}{3}I(I+1)$ of (3.21) by $F(\frac{5}{2}, -\frac{1}{2}\ )$ given in (3.23)). This value is about 4 times shorter than the fast T_2 observed on the central transition (c.f. 5.6). Therefore, as shown in previous studies, the line is indeed inhomogeneously broadened and it is necessary to use the HPJN theory to calculate T_2^{S-N}.

All the relaxation times that will be presented in the following correspond to measurements done with short delays. Therefore, the discussion and the analysis will focus on the fast decay times unless specified otherwise.

The temperature dependence of the spin-spin relaxation times is presented in Fig. 5.7. For pure EuO as well as for all the Gd doped samples, T_2 seems to be temperature independent at temperatures below about 15 K. For higher temperatures, we observed a rapid increase of the relaxation rates with increasing temperature. We analyze these two regimes below.

5.3.1 Electron spin fluctuations

We saw in Sect. 5.3 that the spin-lattice relaxation processes are dominated by the scattering of magnons by nuclear spins, in particular by processes involving three magnons. Another way to describe these processes is to consider the fluctuations of the hyperfine field. From (3.16), we can write the perturbation Hamiltonian as

$$\hat{\mathcal{H}}'_{hf}(t) = -\gamma_n \hbar [H_x(t)\hat{I}_x + H_y(t)\hat{I}_y + H_z(t)\hat{I}_z], \tag{5.10}$$

where $H_x(t)$, $H_y(t)$ and $H_z(t)$ are the fluctuating fields at the nuclear site due to fluctuations of $\hat{\boldsymbol{S}}$ in the x, y and z directions respectively.[4] The relaxation rates deriving from these interactions can be calculated using the Redfield theory (c.f. e.g. [43]). The calculation for the particular case of a spin $I = \frac{5}{2}$ is presented in Appendix B. The result for the spin-spin relaxation time is expressed as

$$\frac{1}{T_2} = \gamma_n^2 \overline{H_z^2} \tau_0 + \alpha \frac{1}{T_1}, \tag{5.11}$$

where $\overline{H_z^2}$ is amplitude of the correlation function between $H_z(t)$ and $H_z(t+\Delta t)$, τ_0 is the correlation time (or lifetime) of the scattering process between the magnons and the nuclear spins, and

$$\alpha = I(I+1) - m(m+1) = \begin{cases} 5 & \text{for the } -5/2 \leftrightarrow -3/2 \text{ and } 3/2 \leftrightarrow 5/2 \text{ transitions} \\ 8 & \text{for the } -3/2 \leftrightarrow -1/2 \text{ and } 1/2 \leftrightarrow 3/2 \text{ transitions} \\ 9 & \text{for the } -1/2 \leftrightarrow 1/2 \text{ transition.} \end{cases} \tag{5.12}$$

We have assumed that the fluctuations of the three components of field x, y, and z are independent and that the correlation functions are simple exponential (c.f. Appendix B). Since we excited all the transitions, we expect to have a mixture of these rates. As shown in Fig. 5.7, the factor α obtained from fitting the curves with the function $1/T_2 = \alpha/T_1 + \beta$ is between 6.3 and 9.9. This is in good agreement with the theoretical values calculated above. Therefore, according to the Redfield theory, the temperature dependence of the spin-spin relaxation in $Eu_{1-x}Gd_xO$ is entirely determined by transverse fluctuating fields. Our results showed that these fluctuations were due to fluctuations of the electronic spins well described by spin-wave theory.

5.3.2 More on the line broadening mechanism

Magnetic entities such as magnetic polarons are thought to play a crucial role in these materials. In particular, they are thought to be the main cause of CMR. We discuss their existence as a possible explanation of the linewidth and T_2 data for the 0.6% sample. We present below a quantitative model based on the hypothetical presence of magnetic entities and we test this model by trying to explain the temperature dependent magnetic inhomogeneity we observed in Gd doped EuO (c.f. Sect. 4.4).

Let us assume that magnetic entities are present in the material. We assume that they give rise to the static NMR line broadening which we observe at higher temperatures. To explain the narrow lines at low temperatures, we assume they diffuse rapidly at low temperatures, giving rise

[4] Note that we do not need to make any assumption on the anisotropy of the hyperfine coupling. This expression is valid even if the hyperfine coupling needs to be describe by a tensor $\mathbf{A}$ as in (3.4).

to motional narrowing. Thus they create a fluctuating field at the nuclear site with correlation time τ. The relaxation time deriving from the presence of this fluctuating field can be written

$$\frac{1}{T_2} = \frac{\delta\omega^2\tau}{1+(\delta\omega\tau)^2} \tag{5.13}$$

where $\delta\omega$ is the distribution in NMR frequency caused by the fluctuating magnetic field [43]. Since we observed that the line is broadened at high temperature, we assume that at high temperature the correlation time is long, i.e. $T_2 \cong \tau$. This is consistent with the model of magnetic polarons, since magnetic polarons are thought to be trapped at high temperature (leading to a decrease in conductivity). At low temperature we assume that the entities are moving, which means that τ is short. In this case, $1/T_2 \cong \delta\omega^2\tau$ and the line is motionaly narrowed. In between the high temperature regime and the low temperature regime, we expect that $\delta\omega\tau = 1$ at a given temperature. At that temperature, $1/T_2$ is maximum and $T_2 = 2\tau = 2/\delta\omega$. Assuming that $\delta\omega$ is temperature independent, that means that the relaxation rate is about equal to the static linewidth at high temperatures. But in fact, at all temperatures $1/T_2$ is much less than the observed line width. Thus we cannot explain the data consistently with this model. Rather we believe that at low temperatures, the material is spatially uniform, but as the temperature rises, spatial non uniformity sets in.

5.3.3 Temperature independent relaxation mechanisms

Let us now analyze the temperature independent part of the spin-spin relaxation times. For temperatures far below the magnetic transition temperature, the Suhl-Nakamura interaction is expected to be temperature independent, since its temperature dependence comes mostly from the hyperfine constant (c.f. (3.18) and (3.19)). The nuclear dipole-dipole interaction is also independent of temperature. Therefore, two processes compete and may be the source of the observed temperature independent T_2's.

In the case of pure EuO, as we mentioned earlier, the relaxation time due to the dipole-dipole interaction is considerably slower and we saw in Fig. 5.6 that the Suhl-Nukamura processes dominate the dipole-dipole processes for short delays. However, as shown in Fig. 5.7, the relaxation time of Gd doped EuO is substantially slower than for pure EuO. The slowest T_2 we have measured corresponds to $T_2 = 183\,\mu$s, for $Eu_{0.98}Gd_{0.02}O$ at 3.8 K (c.f. Fig. 5.7). This value is only slightly larger than the dipolar $T_2 = 194 \pm 2.4\,\mu$s we measured in pure EuO (c.f. Fig. 5.6). Therefore, in that case, it is likely that a substantial part of the relaxation is due to dipole-dipole interactions even for short delays. Note that the dipole-dipole relaxation time in Gd doped EuO is expected to be slightly longer than in pure EuO due to the fact that interactions between Eu nuclear spins and Gd nuclear spins (unlike spins) lead to less effective relaxation processes (c.f. e.g. [43]).

Let us examine why the spin-spin relaxation rates in Gd doped EuO are smaller than in pure EuO. As we have seen in Chap. 4, adding Gd in the EuO matrix leads to magnetic broadening which increases with doping. Therefore the distribution function $g(\omega)$ introduced in the HJPN theory (c.f. Sect. 3.6) becomes broader with increasing doping and the Suhl-Nakamura relaxation rate (3.26), which is proportional to the distribution function $g(\omega)$, decreases with doping since $g(\omega)$ is a normalized function.[5] In other words, the replacement of Eu atoms by Gd atoms in the

[5] Note that we should write $g_{m=\frac{1}{2}}(\omega)$ instead of $g(\omega)$ since, as we have noted in Sect. 3.6 the distribution function depends on the observed transition.

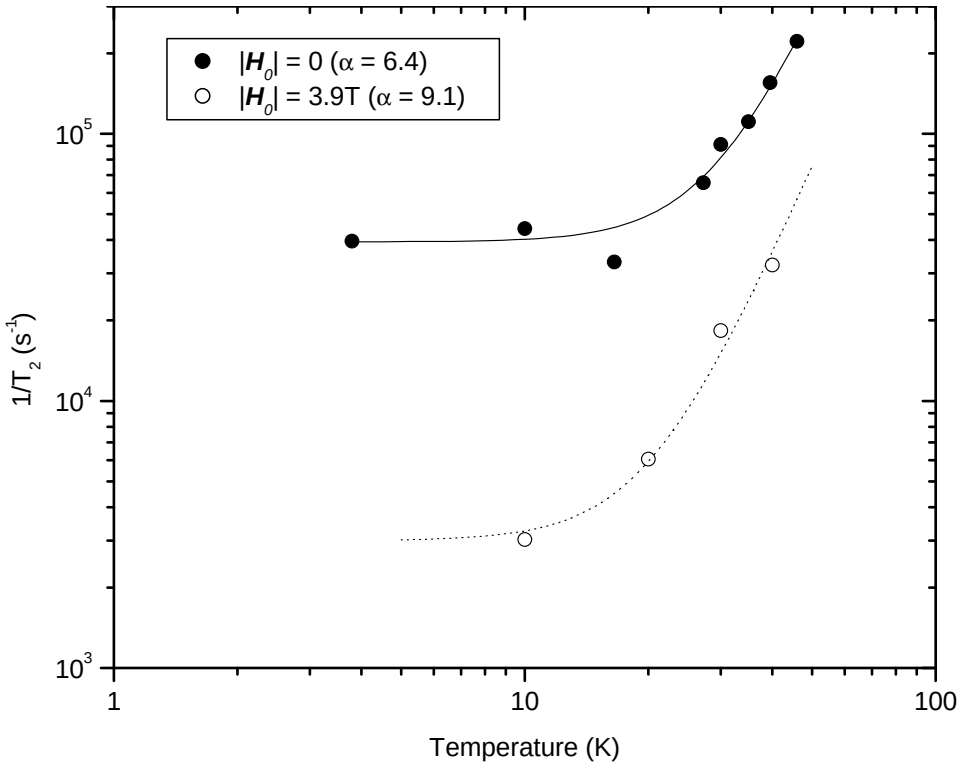

Figure 5.8: Spin-spin relaxation rate vs. temperature of 0.6% Gd doped EuO for zero external field and $|\boldsymbol{H}_0| = 3.9\,\mathrm{T}$. The parameter α and the fitting curve are defined in (5.11)

EuO matrix further reduces the allowed mutual spin-flips between Eu nuclei and consequently the relaxation rates are smaller.

However, as shown in Fig. 5.7, the temperature independent relaxation rate is larger for $x = 2\%$ than for $x = 4.3\%$. As we discussed in Chap. 2, the conduction band starts being populated when x becomes larger than $x_c \cong 1.5\%$. Therefore, above this critical concentration we expect the nuclei to interact through a RKKY indirect interaction. The RKKY interaction depends on the density of states at the Fermi energy (the RKKY Hamiltonian is proportional to the second power of the density of states at the Fermi energy [43]). Since the Fermi energy and therefore the density of states at the Fermi energy increases with doping, we expect the RKKY interaction to be larger in 4.3% Gd doped EuO than in 2% Gd doped EuO, and therefore the relaxation processes deriving from this interaction are expected to be more effective in 4.3% Gd doped EuO. This might explain why the temperature independent relaxation rate of the $x = 2\%$ sample is larger than the temperature independent relaxation rate of the $x = 4.3\%$.

Finally, we show in Fig. 5.8 the spin-spin relaxation time of 0.6% Gd doped EuO as a function of temperature when a external field $|\boldsymbol{H}_0| = 4\,\mathrm{T}$ is applied. As expected from the T_1 values shown in Fig. 5.5, the spin-spin relaxation rates in the region above 15 K are smaller in a strong external magnetic field. When the curve is fitted with the function the function $1/T_2 = \alpha/T_1 + \beta$, we obtain a value $\alpha = 9.1$, which is in good agreement with the values calculated in (5.12). This clearly shows that the relaxation processes are similar at zero-field and in high field.

Chapter 6

Discussion and conclusion

The study of $Eu_{1-x}Gd_xO$ was motivated by the unconventional electrical and magnetic properties observed in this system. Our NMR measurements led to results giving new information on the microscopic magnetic properties of $Eu_{1-x}Gd_xO$. We observed a dramatic difference between pure (x=0) or nearly pure (x=0.6%) samples, and samples with higher Gd concentration in both static and the dynamic magnetic properties and correlate these with other properties of these materials. Let us examine and discuss the main outcomes of our study.

Exchange integral J vs. doping

Spin-wave theory is applicable to the low temperature regime in ferromagnets and it is expected to describe the electron magnetization correctly only for temperature $T \ll T_C$. Nevertheless, we observed that the relaxation times in $Eu_{1-x}Gd_xO$ were in good agreement with a law derived from spin-wave theory for temperatures as high as $T = 0.6\,T_C$. From this law, we inferred the value of the exchange integral J as a function of Gd doping. We observed that $J = 0.754 \pm 0.01$ and $J = 0.750 \pm 0.01$ for pure EuO and 0.6% Gd doped EuO respectively, and $J = 1.203 \pm 0.01$ and $J = 1.211 \pm 0.01$ for 2% Gd doped EuO and 4.3% Gd doped EuO respectively. Therefore, we observed a non-linear increase of the amplitude of the exchange interaction with doping. These results are consistent with the dependence on Gd concentration of the Curie temperature and they were explained by Mauger using a model based on the RKKY interaction [32, 33]. However, while several neutron scattering studies of EuO led to the determination of J in pure EuO, no direct measurement of the exchange integral in Gd doped EuO was ever published. Our results provided therefore the first measurement of J in $Eu_{1-x}Gd_xO$ for $x > 0$.

Variation of static magnetic broadening with temperature

We discovered that the lineshape of the Eu resonance in Gd doped EuO was broader than in pure EuO and we showed by comparing the two isotopes of Eu that the broadening was due to static inhomogeneities in the local magnetic field acting on the Eu nuclei. Our measurements showed that the inhomogeneity increased non-linearly with Gd concentration. We confirmed that this increase was not due to temperature dependent fluctuations of the electron spins since $1/T_2$, which was shown to be completely determined by these fluctuations, was considerably smaller than the width of the broadening showing that the magnetic inhomogeneities were static, at least at the time scale of NMR, which is of the order of several microseconds.

In 0.6% Gd doped EuO, we observed that above about 30 K the magnetic inhomogeneity increased rapidly with increasing temperature. According to previous transport measurements, the conductivity of samples containing a similar Gd concentration increases dramatically above about 30 K (CMR) [20, 28]. This suggests that the broadening mechanism is linked to the change in transport properties of the sample. Numerous theories explain this change in transport properties by the formation of bound magnetic polarons.

As a possible explanation, we considered localized magnetic entities, which were static at high temperatures, giving static line broadening, but highly mobile at low temperatures, giving motionally narrowed lines and high conductivity. We showed that the existence of moving magnetic entities required that $1/T_2$ would be equal to the static linebreadth at some temperature. However, since the relaxation rates we observed were considerably smaller than the linewidth, we could rule out this model.

We think that at low temperatures the sample is homogeneous, but static inhomogeneities in the lattice are formed when the temperature is increased. We propose a quantitative model to link the presence of these inhomogeneities to the transport properties of Gd doped EuO. We use the idea that at temperatures below the Curie temperature, the conduction band is split into two spin-up and spin-down subbands (see, e.g., the theory developed by Mauger [33]). At temperature below about 30 K, the localized spins are aligned with respect to each other and the s-f interaction forces all the conduction electron spins to be in a spin-up state. Therefore, since all the conduction electrons are in the same state, they form a band (the spin-up band) and they can tunnel from one location to another since they do not experience spin-dependent scattering processes. The magnetic inhomogeneity due to the conduction electron spins is low. When the temperature is increased, the magnetization of the localized spins decreases and therefore not all localized spins are in the same state. Therefore, due to the s-f interaction, the conduction electrons are not all in the same state anymore. They cannot tunnel between different location and they cannot form a band. Consequently the conduction is now through hopping and the conductivity decreases. The electrons are more localized and in different states and from the point of view of the nuclear spins, the hyperfine field is now more inhomogeneous. This model fits with the temperature dependence of the transport properties and it can explain the temperature dependent inhomogeneity that we observed in our NMR data. This picture is different from the model of Mauger in which it is assumed that the electron magnetization is uniform over the sample.

In samples with higher Gd concentration ($x = 2\%$ and $x = 4.3\%$), the observed static broadening was much larger than in 0.6% Gd doped EuO. We also observed that the inhomogeneity increased with increasing temperature and that the structure of the lineshape varied considerably with temperature, becoming more and more complex. We showed that the broadening was probably not due to a distribution in the value of the exchange integral J throughout the material.

S.L. Cooper *et al.*, who measured Gd doped EuO by Raman spectroscopy, also observed magnetic inhomogeneities in Gd doped EuO [13, 38, 39]. Since the time scale in Raman spectroscopy is of the order of a femtosecond, they could not distinguish between static and dynamic inhomogeneity. Therefore it was not possible to verify if the inhomogeneity we observed had the same origin as the inhomogeneity they measured.

Related experiments

We tried to performed NMR measurements on EuO at temperature above T_C, in the paramagnetic state, but we did not observe any signal. We concluded that it was because the T_2 was too short to be measured with our spectrometer. We also tried to observe the NMR signal of the oxygen nuclei. We did not detect the resonance, either in the ferromagnetic phase or in the paramagnetic phase. It was probably due to the low natural abundance of the isotope ^{17}O (about 0.04%) that can be detected by NMR (the nuclear spin of ^{16}O is zero).

Previous studies showed that EuB_6 is also a compound exhibiting CMR [117, 118]. We performed Eu NMR measurements on this system and observed that T_2 was strongly temperature dependent, becoming increasingly short with increasing temperature. However, we did not further study this material since we focused on $Eu_{1-x}Gd_xO$. Finally, we looked for the Eu resonance in EuO thin films that were grown by M. Albrecht (Swiss Federal Institute of Lausanne in collaboration with the University of Wisconsin), was motivated by the possibility of driving a current through the films to observe the effect of the current on the NMR resonance. Unfortunately, we did not detect the Eu resonance in these samples.

Suggestions for future experiments

To analyze the dynamics of the electronic spins in $Eu_{1-x}Gd_xO$ further, it would probably be helpful to grow crystals with a large abundance of the ^{17}O isotope. The relaxation times of the oxygen spins might be substantially shorter than those of Eu spins since O^{2-} is not a magnetic ion. Therefore, it might be possible to perform NMR measurements at temperatures closer to the magnetic transition temperature, and thus closer to the region in which more dramatic transport effects take place. For the same reason, EuO doped with La as well as EuB_6 doped with La would certainly be good candidates to study CMR related properties. We would also encourage an NMR study of Eu-rich EuO since previous studies showed that the CMR is larger in this system than in $Eu_{1-x}Gd_xO$ and that the CMR peak appears at lower temperature. Finally, we think that it would be valuable to seek further to detect the Eu or oxygen NMR resonance in EuO thin films. Steeneken *et al.* showed that the conduction electrons in Eu-rich EuO thin films are close to being 100% spin polarized [12]. Performing NMR measurements while driving a current through the films could give information, through the hyperfine interaction, on the interaction between a spin-polarized current and localized ferromagnetic spins.

Appendix A

Three-magnon relaxation process

The purpose of this Appendix was to recalculate formula (2.22) from the article published by Beeman and Pincus, i.e. the formula giving the relaxation rate due to three-magnon process [68]. Following the derivation of Beeman and Pincus, we started from the hyperfine Hamiltonian (3.16) and kept only the first term. This term can be developed in boson creation and annihilation operators using the Holstein-Primakoff transformations [65]. Assuming that the spin $\hat{\boldsymbol{S}}$ is located at the origin, we obtained

$$\frac{1}{2}\, A\hat{I}^{+}\hat{S}^{-} = \frac{1}{2}\, A\hat{I}^{+}\sqrt{\frac{2S}{N}}\left\{\sum_{\boldsymbol{k}_1} b^{\dagger}_{\boldsymbol{k}_1} - \frac{1}{4SN}\sum_{\boldsymbol{k}_1,\boldsymbol{k}_2,\boldsymbol{k}_3} b^{\dagger}_{\boldsymbol{k}_1} b^{\dagger}_{\boldsymbol{k}_2} b_{\boldsymbol{k}_3} + ...\right\}, \tag{A.1}$$

where N is the number of spins in the sample, and $b^{\dagger}_{\boldsymbol{k}_i}$ and $b_{\boldsymbol{k}_i}$ are the creation and annihilation operators of a spin wave of wave vector $\boldsymbol{k}_i$. The first term in the right hand side of (A.1) corresponds to the one-magnon interaction and it is usually not allowed since the minimum energy of a spin wave, $g\mu_B|\boldsymbol{H}|$, is substantially greater than the energy of a nuclear spin flip AS.[1] The hyperfine interaction therefore reduced to

$$\hat{\mathcal{H}}'_{hf} = -\frac{A}{8SN}\sqrt{\frac{2S}{N}}\,\hat{I}^{+}\sum_{\boldsymbol{k}_1,\boldsymbol{k}_2,\boldsymbol{k}_3} b^{\dagger}_{\boldsymbol{k}_1} b^{\dagger}_{\boldsymbol{k}_2} b_{\boldsymbol{k}_3}. \tag{A.2}$$

This interaction is diagrammatically represented in Fig. A.1.

Then, using the Fermi's Golden rule (given in (5.1)), we determined the transition rate $W_{m\leftrightarrow m+1}$ induced by this interaction and computed the spin-lattice relaxation using

$$T_1 = \frac{(I-m)(I+m+1)}{2W_{m\leftrightarrow m+1}}, \tag{A.3}$$

[1] Note that the field $\boldsymbol{H}$ is defined as in Sect. 3.6, that is $\boldsymbol{H} = \boldsymbol{H}_{an} + \boldsymbol{H}_0 + \boldsymbol{H}_{dm}$, where $\boldsymbol{H}_{an}$ is the anisotropy field, $\boldsymbol{H}_0$ is the applied external field, and $\boldsymbol{H}_{dm}$ is the demagnetization field.

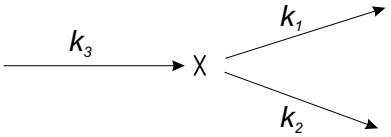

Figure A.1: Diagrammatic representation of the three-magnon interaction leading to nuclear spin-lattice relaxation in a ferromagnet. The cross represents the nuclear spin-flip.

taken from [119]. The calculation led to

$$\frac{1}{T_1} = \frac{\pi A^2}{8\hbar S N^3} \sum_{\boldsymbol{k}_1,\boldsymbol{k}_2,\boldsymbol{k}_3} (1+\overline{n}_{\boldsymbol{k}_1})(1+\overline{n}_{\boldsymbol{k}_2})\overline{n}_{\boldsymbol{k}_3}\delta(E_{\boldsymbol{k}_3} - E_{\boldsymbol{k}_1} - E_{\boldsymbol{k}_2} - AS), \tag{A.4}$$

where

$$\overline{n}_{\boldsymbol{k}_i} = < b^\dagger_{\boldsymbol{k}_i} b_{\boldsymbol{k}_i} > = \frac{1}{\exp(E_{\boldsymbol{k}_i}/k_BT) - 1} \tag{A.5}$$

is the mean number of magnons in the state $\boldsymbol{k}_i$. Beeman and Pincus neglected AS, the energy of the nuclear flip, because it is small in comparison with the spin-wave energy $E_{\boldsymbol{k}}$. Therefore, the relaxation rate could be written

$$\begin{aligned}\frac{1}{T_1} = \frac{\pi A^2}{8\hbar S N^3} \sum_{\boldsymbol{k}_1,\boldsymbol{k}_2,\boldsymbol{k}_3} & \frac{\exp(E_{\boldsymbol{k}_1}/k_BT)}{\exp(E_{\boldsymbol{k}_1}/k_BT) - 1} \\ \times & \frac{\exp(E_{\boldsymbol{k}_2}/k_BT)}{\exp(E_{\boldsymbol{k}_2}/k_BT) - 1} \, \frac{1}{\exp(E_{\boldsymbol{k}_3}/k_BT) - 1} \, \delta(E_{\boldsymbol{k}_3} - E_{\boldsymbol{k}_1} - E_{\boldsymbol{k}_2}).\end{aligned} \tag{A.6}$$

The sums can be replaced by integrals using the transformation

$$\lim_{V\to\infty} \frac{1}{V} \sum_{\boldsymbol{k}} F(E_{\boldsymbol{k}}) = \int F(E_{\boldsymbol{k}}) g(E_{\boldsymbol{k}}) dE_{\boldsymbol{k}}, \tag{A.7}$$

where V is the volume of the sample, $F(E_{\boldsymbol{k}})$ is a smooth function of $E_{\boldsymbol{k}}$, and $g(E_{\boldsymbol{k}})$ is the density of states of the spin waves [120]. In the case of a cubic crystal, e.g., in the case of $Eu_{1-x}Gd_xO$, $V = Na^3$, where a is the lattice constant of the crystal. Taking into account the conservation of energy, $E_{\boldsymbol{k}_3} = E_{\boldsymbol{k}_1} + E_{\boldsymbol{k}_2}$, we obtained

$$\begin{aligned}\frac{1}{T_1} = \frac{\pi A^2 a^9}{8\hbar S} \int_{E_{min}}^{E_{max}} \int_{E_{min}}^{E_{max}} & \frac{\exp(E_{\boldsymbol{k}_1}/k_BT)}{\exp(E_{\boldsymbol{k}_1}/k_BT) - 1} \\ \times & \frac{\exp(E_{\boldsymbol{k}_2}/k_BT)}{\exp(E_{\boldsymbol{k}_2}/k_BT) - 1} \, \frac{g(E_{\boldsymbol{k}_1}) g(E_{\boldsymbol{k}_1}) g(E_{\boldsymbol{k}_2} + E_{\boldsymbol{k}_2})}{\exp((E_{\boldsymbol{k}_1} + E_{\boldsymbol{k}_2})/k_BT) - 1} \, dE_{\boldsymbol{k}_1} dE_{\boldsymbol{k}_2}.\end{aligned} \tag{A.8}$$

Pincus and Beeman made the assumption that the $\boldsymbol{k}_i$ are small, so the dispersion relation of magnons has the form

$$E_{\boldsymbol{k}} = 2JS|\boldsymbol{k}|^2 a^2 + g\mu_B|\boldsymbol{H}| \equiv \epsilon_{\boldsymbol{k}} + g\mu_B|\boldsymbol{H}|, \tag{A.9}$$

where $J = J_1 + J_2$ is the exchange integral, and we defined $\epsilon_{\boldsymbol{k}}$ as the magnon energy for $|\boldsymbol{H}| = 0$. They also made the assumption that $k_BT \ll 2JS$, which means that $\overline{n}_{\boldsymbol{k}}$ are small for large $\boldsymbol{k}$ and therefore the upper limit of the integrals could be replaced by infinity. Equation (A.8) could therefore be rewritten

$$\begin{aligned}\frac{1}{T_1} = \frac{\pi A^2 a^9}{8\hbar S} \int_0^\infty \int_0^\infty & \frac{\exp((\epsilon_{\boldsymbol{k}_1} + g\mu_B|\boldsymbol{H}|)/k_BT)}{\exp((\epsilon_{\boldsymbol{k}_1} + g\mu_B|\boldsymbol{H}|)/k_BT) - 1} \\ \times & \frac{\exp((\epsilon_{\boldsymbol{k}_2} + g\mu_B|\boldsymbol{H}|)/k_BT)}{\exp((\epsilon_{\boldsymbol{k}_2}/k_BT + g\mu_B|\boldsymbol{H}|)) - 1} \, \frac{g(\epsilon_{\boldsymbol{k}_1}) g(\epsilon_{\boldsymbol{k}_1}) g(\epsilon_{\boldsymbol{k}_2} + \epsilon_{\boldsymbol{k}_2})}{\exp((\epsilon_{\boldsymbol{k}_1} + \epsilon_{\boldsymbol{k}_2} + 2g\mu_B|\boldsymbol{H}|)/k_BT) - 1} \, d\epsilon_{\boldsymbol{k}_1} d\epsilon_{\boldsymbol{k}_2}.\end{aligned} \tag{A.10}$$

Finally, we calculated the density of state of the magnons from

$$g(\epsilon_{\boldsymbol{k}}) = \int\limits_{S(\epsilon_k)} \frac{1}{8\pi^3} \frac{d\boldsymbol{S}}{|\boldsymbol{\nabla}\epsilon_{\boldsymbol{k}}|}, \tag{A.11}$$

where $S(\epsilon_k)$ is a sphere of constant energy [120]. We obtained

$$g(\epsilon_{\boldsymbol{k}}) = \frac{1}{8\pi^3} \int\limits_0^{\pi} \int\limits_0^{2\pi} \frac{|\boldsymbol{k}|^2 \sin\theta}{4JSa^2|\boldsymbol{k}|} d\theta d\varphi = \frac{1}{(2\pi)^2} \sqrt{\frac{\epsilon_{\boldsymbol{k}}}{(2JSa^2)^3}}. \tag{A.12}$$

Replacing (A.12) in (A.10), we obtained

$$\begin{aligned} \frac{1}{T_1} = \frac{1}{16(2\pi)^5} \frac{A^2}{2JS \cdot \hbar S} \frac{1}{(2JS)^{7/2}} \int\limits_0^{\infty} \int\limits_0^{\infty} \frac{\exp((\epsilon_{\boldsymbol{k}_1} + g\mu_B|\boldsymbol{H}|)/k_BT)}{\exp((\epsilon_{\boldsymbol{k}_1} + g\mu_B|\boldsymbol{H}|)/k_BT) - 1} \\ \times \frac{\exp((\epsilon_{\boldsymbol{k}_2} + g\mu_B|\boldsymbol{H}|)/k_BT)}{\exp((\epsilon_{\boldsymbol{k}_2}/k_BT + g\mu_B|\boldsymbol{H}|)) - 1} \frac{\sqrt{\epsilon_{\boldsymbol{k}_1}^2 \epsilon_{\boldsymbol{k}_2} + \epsilon_{\boldsymbol{k}_2}^2 \epsilon_{\boldsymbol{k}_1}}}{\exp((\epsilon_{\boldsymbol{k}_1} + \epsilon_{\boldsymbol{k}_2} + 2g\mu_B|\boldsymbol{H}|)/k_BT) - 1} \, d\epsilon_{\boldsymbol{k}_1} d\epsilon_{\boldsymbol{k}_2}. \end{aligned} \tag{A.13}$$

Pincus and Beeman used the fact that $k_BT \gg g\mu_B|\boldsymbol{H}|$ to compute the double integral. They found the integral to be equal to $7.6\,(k_BT)^{7/2}$. This corresponds to the result (2.22) in [68].[2] It was not clear to us what value of $g\mu_B|\boldsymbol{H}|/k_BT$ they used to obtain this result and we therefore decided to recompute the integral in order to obtain a value adapted to our experimental conditions.

In the case of our zero-field measurements of the Eu resonance in EuO we had $|\boldsymbol{H}| = |\boldsymbol{H}_{an}|$ and at 4.2 K the ratio $g\mu_B|\boldsymbol{H}_{an}|/k_BT$ was equal to approximately $8 \cdot 10^{-3}$. Since we observed that the three-magnon process was the main relaxation process for temperatures between about 15 K and 40 K, we had to take a substantially smaller value of $g\mu_B|\boldsymbol{H}|/k_BT$. With $T = 30\,\mathrm{K}$ and (c.f. [59]) $|\boldsymbol{H}_{an}(T = 30\,\mathrm{K})|/|\boldsymbol{H}_{an}(T = 4.2\,\mathrm{K})| \cong 2.5$, we had $g\mu_B|\boldsymbol{H}|/k_BT \cong 4 \cdot 10^{-4}$. With this value, we evaluated the double integral using Mathematica and we obtained approximatively $10.5\,(k_BT)^{7/2}$. This value was very close to the value obtained with $|\boldsymbol{H}| = 0$, and since there was no apparent reason to compute the integral with $T = 30\,\mathrm{K}$ instead of with another temperature, we decided to use the result for $|\boldsymbol{H}| = 0$ that is

$$\int\limits_0^{\infty} \int\limits_0^{\infty} \frac{\exp(x/k_BT)\exp(y/k_BT)\sqrt{x^2y + y^2x}}{(\exp(x/k_BT) - 1)(\exp(y/k_BT) - 1)(\exp((x+y)/k_BT) - 1)} dxdy \cong 11.29(k_BT)^{7/2}, \tag{A.14}$$

where we have replaced $\epsilon_{\boldsymbol{k}_1}$ and $\epsilon_{\boldsymbol{k}_2}$ by x and y to simplify the notation. Equation (A.13) with the value of the integral given in (A.14) corresponds to (3.17) in our text.

Since we were interested in evaluating J using (A.13), we had to determine the influence of a variation in the value of the integral on J. We calculated that if the factor 11.29 were replaced by the factor 10.5, obtained for $T = 30\,\mathrm{K}$, the value of J changed by about 1%. Therefore we decided that (A.14) could be used to determine a fairly accurate value of J from our data.

Let us turn now to the evaluation of the exchange-scattering enhancement factor

$$\{M\}^2 = \left\{1 - \frac{2[\boldsymbol{k}_1 \cdot \boldsymbol{k}_2 + \boldsymbol{k}_3 \cdot (\boldsymbol{k}_1 + \boldsymbol{k}_2 - \boldsymbol{k}_3)]}{(\boldsymbol{k}_1 + \boldsymbol{k}_2 - \boldsymbol{k}_3) \cdot (\boldsymbol{k}_1 + \boldsymbol{k}_2 - \boldsymbol{k}_3)}\right\}^2, \tag{A.15}$$

[2] Note that there is a mistake in equation (2.22) of [68] and $h^{7/2}$ should be replaced by $\hbar^{7/2}$.

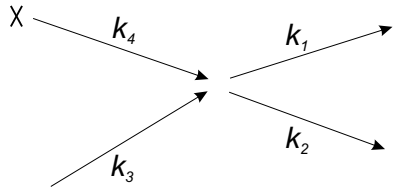

Figure A.2: Diagrammatic representation of the second order three-magnon interaction leading to nuclear spin-lattice relaxation in a ferromagnet.

defined in equation (3.4) of the article of Beeman and Pincus [68]. A diagrammatic representation of the exchange-scattering-enhanced three magnon process is shown in Fig. A.2. A virtual magnon of wave vector $\boldsymbol{k}_4$ is created by a nuclear spin-flip. This virtual magnon scatters a thermal magnon of wave vector $\boldsymbol{k}_3$ and two magnons of wave vector $\boldsymbol{k}_1$ and $\boldsymbol{k}_2$ result from this interaction. We defined the angles

$$\alpha = \measuredangle(\boldsymbol{k}_1, \boldsymbol{k}_2), \tag{A.16}$$

$$\theta = \measuredangle(\boldsymbol{k}_2, \boldsymbol{k}_3), \tag{A.17}$$

$$\varphi = \measuredangle(\boldsymbol{k}_1, \boldsymbol{k}_3), \tag{A.18}$$

where $\measuredangle(\boldsymbol{k}_i, \boldsymbol{k}_j)$ represents the angle between the directions of $\boldsymbol{k}_i$ and $\boldsymbol{k}_j$, and we obtained, using $|\boldsymbol{k}_1|^2 + |\boldsymbol{k}_2|^2 = |\boldsymbol{k}_3|^2$ (energy conservation),

$$\{M\}^2 = \frac{1}{4}\left\{\frac{|\boldsymbol{k}_3|^2 - 3|\boldsymbol{k}_1||\boldsymbol{k}_3|\cos\varphi - 3|\boldsymbol{k}_2||\boldsymbol{k}_3|\cos\theta}{|\boldsymbol{k}_3|^2 + |\boldsymbol{k}_1||\boldsymbol{k}_2|\cos\alpha - |\boldsymbol{k}_1||\boldsymbol{k}_3|\cos\varphi - |\boldsymbol{k}_2||\boldsymbol{k}_3|\cos\theta}\right\}^2. \tag{A.19}$$

Pincus and Beeman evaluated the angular average of this expression to be about 8. We computed the angular average using the assumption that α is in the range $[0, \pi]$, and θ and φ are in the range $[\pi/2, \pi]$. The integral that needed to be evaluate was therefore

$$\xi = \int_0^\pi \int_{\pi/2}^\pi \int_{\pi/2}^\pi \frac{1}{4}\left\{\frac{|\boldsymbol{k}_3|^2 - 3|\boldsymbol{k}_1||\boldsymbol{k}_3|\cos\varphi - 3|\boldsymbol{k}_2||\boldsymbol{k}_3|\cos\theta}{|\boldsymbol{k}_3|^2 + |\boldsymbol{k}_1||\boldsymbol{k}_2|\cos\alpha - |\boldsymbol{k}_1||\boldsymbol{k}_3|\cos\varphi - |\boldsymbol{k}_2||\boldsymbol{k}_3|\cos\theta}\right\}^2 d\alpha d\theta d\varphi, \tag{A.20}$$

with the constraint $|\boldsymbol{k}_1|^2 + |\boldsymbol{k}_2|^2 = |\boldsymbol{k}_3|^2$.

From (A.9), the energy of a magnon of wave vector $|\boldsymbol{k}|$ is approximately

$$\hbar\omega = 2JS|\boldsymbol{k}|^2 a^2. \tag{A.21}$$

From (A.5), we obtained that the highest energy level occupied at temperature T is approximatively given by $\hbar\omega_{max} \cong k_B T$. Thus,

$$|\boldsymbol{k}|_{max} = \sqrt{\frac{k_B T}{2JS}}\frac{1}{a}, \tag{A.22}$$

is approximately the maximum amplitude of the wave vector for a magnon at temperature T. In the case of EuO, $S = 7/2$, $J/k_B \cong 0.725\,\mathrm{K}$ (c.f. [31]), and $a = 5.14\,\text{Å}$[15], and we obtained the plot $|\boldsymbol{k}|_{max}$ vs. temperature shown in Fig. A.3.

We then plotted the value of the enhancement factor ξ given in (A.20) as a function of $|\boldsymbol{k}_1|$ and $|\boldsymbol{k}_2|$ in the range determined in Fig. A.3. We obtained the surface shown in Fig. A.4. We observed

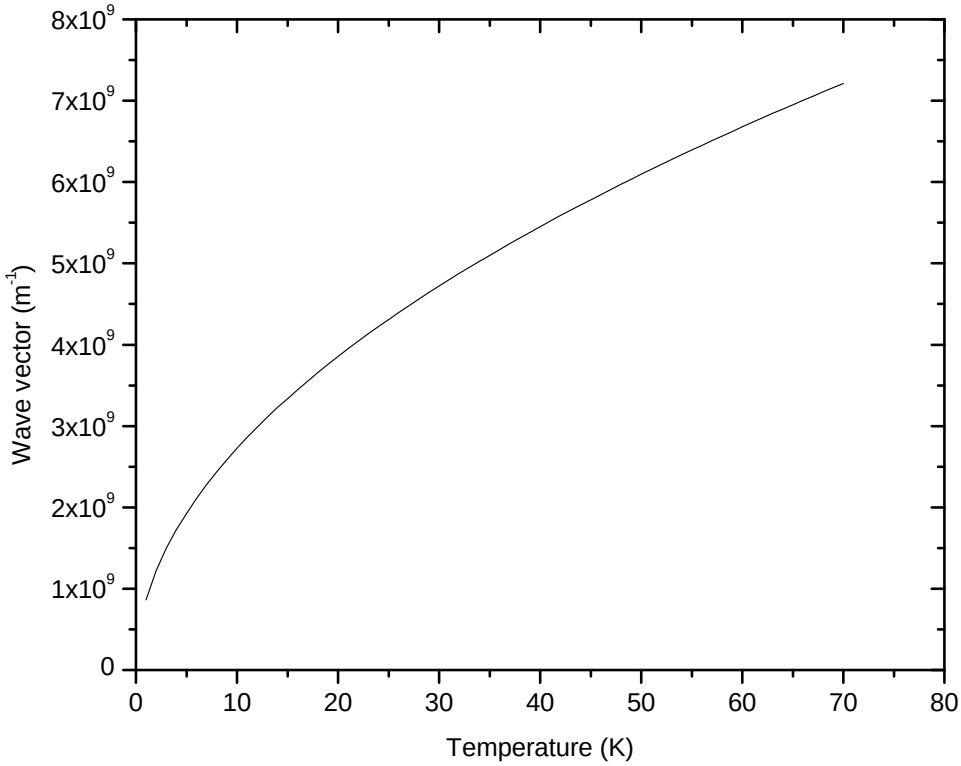

Figure A.3: Maximum magnon wave vector amplitude in EuO as a function of temperature.

that if $|\boldsymbol{k}_2| = |\boldsymbol{k}_1|$, the enhancement factor is about 8.03. If $|\boldsymbol{k}_2| \neq |\boldsymbol{k}_1|$, ξ is smaller. However, the value of ξ stays close to 8, and even if $|\boldsymbol{k}_2| = 2|\boldsymbol{k}_1|$, which is not very likely, $\xi = 7.5$. The influence of a variation in ξ on the determination of J is therefore limited, and we evaluated the error to be less than 1%.

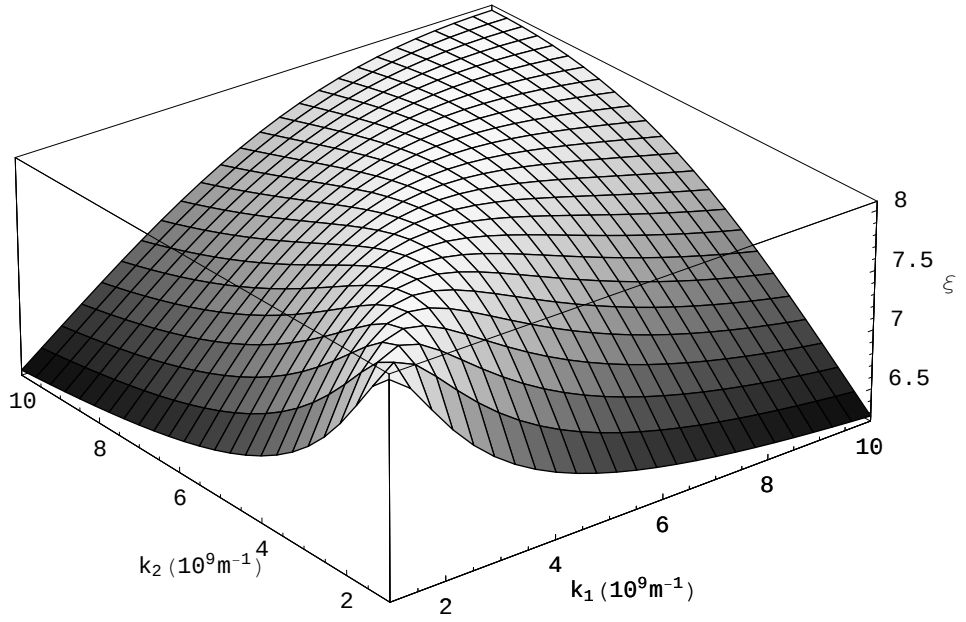

Figure A.4: Enhancement factor ξ as a function of the amplitude of the created magnon wave vectors $k_1 = |\boldsymbol{k_1}|$ and $k_2 = |\boldsymbol{k_2}|$.

Appendix B

Applying Redfield Theory to calculate the relaxation times due to fluctuating fields

The derivation we presented in this Appendix was based on the calculation of C.P. Slichter of the relaxation times using the Redfield Theory (c.f. Chapter 5 in [43]). We extended the calculation of Slichter to the case of a spin $I > \frac{1}{2}$. We started from the Redfield equation that corresponds to equation (5.304) of [43], i.e.

$$\frac{d}{dt} < m|\hat{\rho}^*|m' >= \sum_{l,l'} R_{mm',ll'} < l|\hat{\rho}^*|l' >, \tag{B.1}$$

where $\hat{\rho}^*$ is the operator density matrix of the studied system expressed in the interaction representation, and the $R_{mm',ll'}$ are coefficients that are constant in time. The expression for these coefficients is given in (5.330) of [43], that is

$$\begin{aligned} R_{mm',ll'} = \frac{1}{2\hbar^2}[&J_{mlm'l'}(m'-l') + J_{mlm'l'}(m-l) \\ &-\delta_{m'l'}\sum_k J_{klkm}(k-l) - \delta_{ml}\sum_k J_{km'kl'}(k-l')], \end{aligned} \tag{B.2}$$

where the spectral densities $J_{mlm'l'}(\omega)$ are defined as

$$J_{mlm'l'}(\omega) = \int_{-\infty}^{\infty} \overline{< m|\hat{\mathcal{H}}_1(t)|l >< l'|\hat{\mathcal{H}}_1(t+\tau)|m' >} \exp(-i\omega\tau)d\tau, \tag{B.3}$$

where $\hat{\mathcal{H}}_1(t)$ is the time-dependent Hamiltonian representing the interaction causing the spin system to relax. The sum in (B.1) is restricted to the terms for which $m - m' = l - l'$. We took for $\hat{\mathcal{H}}_1(t)$ the hyperfine Hamiltonian defined in (5.10), i.e.

$$\hat{\mathcal{H}}_1(t) = \hat{\mathcal{H}}'_{hf}(t) = -\gamma_n\hbar \sum_{q=x,y,z} H_q(t)\hat{I}_q, \tag{B.4}$$

where $H_x(t)$, $H_y(t)$ and $H_z(t)$ were the fluctuating fields at the nuclear site due to fluctuations of $\hat{\boldsymbol{S}}$ in the x, y and z directions respectively. Equation (B.3) can then be written

$$\frac{1}{2\hbar^2}J_{mlm'l'}(\omega) = \frac{\gamma_n^2}{2}\sum_{q,q'} < m|\hat{I}_q|l >< l'|\hat{I}_{q'}|m' > \int_{-\infty}^{\infty} \overline{H_q(t)H_{q'}(t+\tau)}\exp(-i\omega\tau)d\tau. \tag{B.5}$$

In order to simplify the notation, the quantities

$$k_{qq'}(\omega) = \frac{1}{2}\int_{-\infty}^{\infty} \overline{H_q(t)H_{q'}(t+\tau)}\exp(-i\omega\tau)d\tau, \tag{B.6}$$

are defined. We made the same assumption about the fluctuations as Slichter, that is the three components $H_q(t)$ of the fluctuating field are independent, i.e.

$$\overline{H_q(t)H_{q'}(t+\tau)} = 0 \quad \text{if} \quad q \neq q'. \tag{B.7}$$

Equation (B.5) can then be rewritten as

$$\frac{1}{2\hbar^2}J_{mlm'l'}(\omega) = \gamma_n^2\sum_{q} < m|\hat{I}_q|l >< l'|\hat{I}_q|m' > k_{qq}(\omega) \tag{B.8}$$

Slichter [43] showed that for a given transition $m \leftrightarrow m+1$,

$$W_{m\leftrightarrow m+1} = R_{mm,m+1m+1}, \tag{B.9}$$

$$\left(\frac{1}{T_2}\right)_{m\leftrightarrow m+1} = R_{mm+1,mm+1}, \tag{B.10}$$

where $W_{m\leftrightarrow m+1}$ was defined in Sect. 5.1 of this text. From (B.2) and (B.8), taking into account that $\hat{I}_z$ is diagonal in the base $|m>$ and that $\hat{I}_x = \frac{1}{2}\,[\hat{I}^+ + \hat{I}^-]$ and $\hat{I}_y = \frac{1}{2i}[\hat{I}^+ - \hat{I}^-]$ couple only to states such as $\Delta m = \pm 1$, we obtained for the above relaxation rates,

$$\frac{1}{T_1} = \gamma_n^2[k_{xx}(\omega_0) + k_{yy}(\omega_0)], \tag{B.11}$$

$$\left(\frac{1}{T_2}\right)_{m\leftrightarrow m+1} = \gamma_n^2 k_{zz}(0) + \gamma_n^2(I(I+1) - m(m+1))[k_{xx}(\omega_0) + k_y y(\omega_0)] \tag{B.12}$$

where we used (A.3) and we assumed that all the transitions where excited (spin-lattice relaxation is described by a single rate). The spin-spin relaxation rate can therefore be rewritten as

$$\left(\frac{1}{T_2}\right)_{m\leftrightarrow m+1} = \gamma_n^2 k_{zz}(0) + \frac{I(I+1) - m(m+1)}{T_1}. \tag{B.13}$$

We calculated $k_{zz}(0)$ using the hypothesis of Slichter that the correlation function is a simple exponential with the same correlation time τ_0 for the three components $q = x, y, z$, so that

$$\overline{H_q(t)H_q(t+\tau)} = \overline{H_q^2}\exp(-|\tau|/\tau_0). \tag{B.14}$$

We obtained from (B.6), that

$$k_{zz}(0) = \frac{1}{2}\int_{-\infty}^{\infty} \overline{H_z^2}\exp(-|\tau|/\tau_0)d\tau = \overline{H_z^2}\tau_0. \tag{B.15}$$

We finally obtained the result given in (5.11), that is

$$\left(\frac{1}{T_2}\right)_{m\leftrightarrow m+1} = \gamma_n^2 \overline{H_z^2}\tau_0 + \frac{I(I+1) - m(m+1)}{T_1}. \tag{B.16}$$

.

References

[1] E. L. Nagaev. *Physics of Magnetic Semiconductors* (Mir Publishers, Moscow, 1983).

[2] C. Kapusta, P. C. Riedi, W. Kocemba, G. J. Tomka, M. R. Ibarra, J. M. D. Teresa, M. Viret, and J. M. D. Coey. *J. Phys.: Condens. Matter* **11** 4079 (1999).

[3] T. Wu, S. B. Ogale, J. E. Garrison, B. Nagaraj, A. Biswas, Z. Chen, R. L. Greene, R. Ramesh, T. Venkatesan, and A. J. Millis. *Phys. Rev. Lett.* **86** 5998 (2001).

[4] P. Novák, M. Maryško, M. M. Savosta, and A. N. Ulyanov. *Phys. Rev. B* **60** 6655 (1999).

[5] Y. Shapira, S. Foner, and T. B. Reed. *Phys. Rev. B* **8** 2299 (1973).

[6] M. R. Oliver, J. A. Kafalas, J. O. Dimmock, and T. B. Reed. *Phys. Rev. Lett.* **24** 1064 (1970).

[7] G. Petrich, S. von Molnár, and T. Penney. *Phys. Rev. Lett.* **26** 885 (1971).

[8] P. Ball. *Nature* **404** 918 (2000).

[9] R. Schiller and W. Nolting. *Phys. Rev. Lett.* **86** 3847 (2001).

[10] C. Santos and W. Nolting. *Phys. Rev. B* **65** 144419 (2002).

[11] P. Boeni, B. Roessli, D. Goerlitz, and J. Koetzler. *Phys. Rev. B* **65** 144434 (2002).

[12] P. G. Steeneken, L. H. Tjeng, I. Elfimov, G. A. Sawatzky, G. Ghiringhelli, N. B. Brookes, and D.-J. Huang. *Phys. Rev. Lett.* **88** 047201 (2002).

[13] H. Rho, C. S. Snow, S. L. Cooper, Z. Fisk, A. Comment, and J.-P. Ansermet. *Phys. Rev. Lett.* **88** 127401 (2002).

[14] B. T. Matthias, R. M. Bozorth, and J. H. V. Vleck. *Phys. Rev. Lett.* **7** 160 (1961).

[15] D. B. McWhan, P. C. Souers, and G. Jura. *Phys. Rev.* **143** 385 (1966).

[16] S. J. Cho. *Phys. Rev. B* **1** 4589 (1970).

[17] G. Guentherodt, P. Wachter, and D. M. Imboden. *Phys. Kondens. Mater.* **12** 292 (1971).

[18] M. W. Shafer, J. B. Torrance, and T. Penney. *J. Phys. Chem. Solids* **33** 2251 (1972).

[19] M. W. Shafer and T. R. McGuire. *J. Appl. Phys.* **39** 588 (1968).

[20] A. A. Samokhvalov, N. A. Viglin, B. A. Gizhevskii, T. I. Arbuzova, and N. M. Chebotaev. *Phys. Status Solidi B* **148** 361 (1988).

[21] A. Mauger and C. Godart. *Phys. Rep.* **141** 51 (1986).

[22] N. F. Mott. *Metal-Insulator Transitions* (Taylor & Francis Ltd, London, 1974).

[23] N. F. Mott. *Phil. Mag.* **6** 287 (1961).

[24] P. P. Edwards and M. J. Sienko. *Phys. Rev. B* **17** 2575 (1978).

[25] J. D. Axe. *J. Phys. Chem. Solids* **30** 1403 (1969).

[26] P. Leroux-Hugon. *Phys. Rev. Lett.* **29** 939 (1972).

[27] M. R. Oliver, J. O. Dimmock, A. L. McWhorter, and T. B. Reed. *Phys. Rev. B* **5** 1078 (1972).

[28] C. Godart, A. Mauger, J. P. Desfours, and J. C. Achard. *J. Phys.* **41, C5** 205 (1980).

[29] J. Schoenes and P. Wachter. *Phys. Rev. B* **9** 3097 (1974).

[30] T. Kasuya. *IBM J. Res. Develop.* **14** 426 (1970).

[31] L. Passell, O. W. Dietrich, and J. Als-Nielsen. *Phys. Rev. B* **14** 4897 (1976).

[32] A. Mauger. *Phys. Status Solidi B* **84** 761 (1977).

[33] A. Mauger, C. Godart, M. Escorne, J. C. Achard, and J. P. Desfours. *J. Phys.* **39** 1125 (1978).

[34] F. Holtzberg, T. R. McGuire, S. Methfessel, and J. C. Suits. *Phys. Rev. Lett.* **13** 18 (1964).

[35] W. Nolting and A. M. Oleś. *Z. Phys. B* **43** 37 (1981).

[36] J. B. Torrance, M. W. Shafer, and T. R. McGuire. *Phys. Rev. Lett.* **29** 1168 (1972).

[37] P. A. Wolff. *Semiconductors and Semimetals.* Edited by J. K. Furdyna and J. Kossut (Academic Press, 1988).

[38] C. S. Snow, S. L. Cooper, D. P. Young, Z. Fisk, A. Comment, and J.-P. Ansermet. *Phys. Rev. B* **64** 174412 (2001).

[39] H. Rho, C. S. Snow, S. L. Cooper, Z. Fisk, A. Comment, and J.-P. Ansermet. *Physica B* **312-313** 775 (2002).

[40] A. A. Samokhvalov, V. G. Bamburov, N. V. Volkenshteyn, T. D. Zotov, A. Ivakin, Y. N. Morozov, and M. I. Simonova. *Fiz. Metal. i. Metalloved* **20** 308 (1964).

[41] A. A. Samokhvalov, T. I. Arbuzova, M. I. Simonova, and L. D. Fal'kovskaya. *Fizika Tv. Tela* **15** 3690 (1973).

[42] E. L. Nagaev. *Colossal Magnetoresistance and Phase Separation in Magnetic Semiconductors* (Imperial College Press, London, 2002).

[43] C. P. Slichter. *Principles of Magnetic Resonance*, 3rd edition (Springer-Verlag, 1990).

[44] P. Heller and G. Benedek. *Phys. Rev. Lett.* **14** 71 (1965).

[45] K. Ueno, A. Yanase, and T. Kasuya. *J. Mag Mag. Mat.* **31-34** 427 (1983).

[46] T. Moriya. *Progr. Theor. Phys.* **16** 641 (1956).

[47] H. Yasuoka, T. Ngwe, V. Jaccarino, and H. J. Guggenheim. *Phys. Rev.* **177** 667 (1969).

[48] J. M. Baker and F. I. B. Williams. *Proc. R. Soc. A* **267** 283 (1962).

[49] S. Huefner and J. H. Wernick. *Phys. Rev.* **173** 448 (1968).

[50] I. Nowik, B. D. Dunlap, and J. H. Wernick. *Phys. Rev. B* **8** 238 (1973).

[51] W. Marshall. *Phys. Rev.* **110** 1280 (1958).

[52] M. A. Ruderman and C. Kittel. *Phys. Rev.* **96** 99 (1954).

[53] D. I. Hoult and R. E. Richards. *Proc. R. Soc. A* **344** 311 (1975).

[54] E. Fukushima and S. B. W. Roeder. *Experimental Pulse NMR. A Nuts and Bolts Approach* (Addison-Wesley, 1981).

[55] E. A. Turov and M. P. Petrov. *Nuclear Magnetic Resonance in Ferro- and Antiferromagnets* (John Wiley & Sons, New York, 1972).

[56] A. C. Gossard and A. M. Portis. *Phys. Rev. Lett.* **3** 164 (1959).

[57] A. M. Portis and A. C. Gossard. *J. Appl. Phys.* **31** 205S (1960).

[58] A. Flossdorff, D. Görlitz, and J. Köstler. *J. Appl. Phys.* **79** 6054 (1996).

[59] R. S. Hughes, G. E. Everett, and A. W. Lawson. *Phys. Rev. B* **9** 2394 (1974).

[60] D. S. Rodbell. *J. Phys. Soc. Japan* **17** 313 (1962).

[61] A. Herpin. *Théorie du magnétisme* (Presses universitaires de France, Paris, 1968).

[62] A. Kasuya and M. Tachiki. *Phys. Rev. B* **8** 5298 (1973).

[63] P. Panissod. *Hyperfine Interactions* **24-26** 607 (1985).

[64] M. Weger. *Phys. Rev.* **128** 1505 (1962).

[65] T. Holstein and H. Primakoff. *Phys. Rev.* **58** 1098 (1940).

[66] T. Oguchi and F. Keffer. *J. Phys. Chem. Solids* **25** 405 (1964).

[67] P. Pincus. *Phys. Rev. Lett.* **16** 398 (1966).

[68] D. Beeman and P. Pincus. *Phys. Rev.* **166** 359 (1968).

[69] A. H. Mitchell. *J. Chem. Phys.* **27** 17 (1957).

[70] H. Suhl. *Phys. Rev.* **109** 606 (1958).

[71] T. Nakamura. *Progr. Theor. Phys.* **20** 542 (1958).

[72] D. Hone, V. Jaccarino, T. Ngwe, and P. Pincus. *Phys. Rev.* **186** 291 (1969).

[73] D. Fekete, N. Kaplan, and T. B. Reed. *Phys. Lett.* **55A** 356 (1976).

[74] G. Allodi, R. D. Renzi, and G. Guidi. *Phys. Rev. B* **57** 1024 (1998).

[75] M. M. Savosta, V. A. Borodin, and P. Novák. *Phys. Rev. B* **59** 8778 (1999).

[76] Y. Yoshinari, P. C. Hammel, J. D. Thompson, and S.-W. Cheong. *Phys. Rev. B* **60** 9275 (1999).

[77] C. Kapusta, P. C. Riedi, M. Sikora, and M. R. Ibarra. *Phys. Rev. Lett.* **84** 4216 (2000).

[78] G. Allodi, M. C. Guidi, R. D. Renzi, A. Caneiro, and L. Pinsard. *Phys. Rev. Lett.* **87** 127206 (2001).

[79] K. E. Sakaie, C. P. Slichter, P. Lin, M. Jaime, and M. B. Salamon. *Phys. Rev. B* **59** 9382 (1999).

[80] G. Matsumoto. *J. Phys. Soc. Japan* **29** 615 (1970).

[81] G. Allodi, R. D. Renzi, G. Guidi, F. Licci, and M. W. Pieper. *Phys. Rev. B* **56** 6036 (1997).

[82] M. Pattabiraman, P. Murugaraj, G. Rangarajan, C. Dimitropoulos, J.-P. Ansermet, G. Papavassiliou, G. Balakrishnan, D. M. Paul, and M. R. Lees. *Phys. Rev. B* **66** 224415 (2002).

[83] M. M. Savosta, V. I. Kamenev, V. A. Borodin, P. Novák, M. Maryško, J. Hejtmánek, K. Doerr, and M. Sahana. *Phys. Rev. B* **67** 094403 (2003).

[84] C. Kapusta, P. C. Riedi, W. Kocemba, M. R. Ibarra, and J. M. D. Coey. *J. Appl. Phys.* **87** 7121 (2000).

[85] M. M. Savosta, V. A. Borodin, P. Novák, Z. Jirák, J. Hejtmánek, and M. Maryško. *Phys. Rev. B* **57** 13379 (1998).

[86] M. M. Savosta, P. Novák, Z. Jirák, J. Hejtmánek, and M. Maryško. *Phys. Rev. Lett.* **79** 4278 (1997).

[87] E. L. Boyd. *Phys. Rev.* **145** 174 (1966).

[88] K. Raj, T. J. Burch, and J. I. Budnick. *Int. J. Magnetism* **3** 355 (1972).

[89] D. Fekete, N. Kaplan, and T. B. Reed. *Solid State Comm.* **15** 1827 (1974).

[90] H. G. Bohn, R. R. Arons, and H. Luetgemeier. *Proceedings of XVIIIth Ampere Congress* (Nottingham, 1974).

[91] H. Luetgemeier, R. R. Arons, and H. G. Bohn. *Proceedings of XVIIIth Ampere Congress* (Nottingham, 1974).

[92] R. R. Arons, H. G. Bohn, and H. Luetgemeier. *Physica B* **80** 12 (1975).

[93] V. Scarani, H. D. Riedmatten, and J.-P. Ansermet. *Appl. Phys. Lett.* **76** 903 (2000).

[94] A. Abragam. *The Principles of Nuclear Magnetism* (Oxford University Press, 1961).

[95] J. D. Jackson. *Classical Electrodynamics*, 3rd edition (John Wiley & Sons, New York, 1999).

[96] *CRC Handbook of Chemistry and Physics*, 84th edition (CRC Press, 2003).

[97] W. J. Thompson. *Computers in Physics* **7** 627 (1993).

[98] E. R. Callen and H. B. Callen. *Phys. Rev.* **129** 578 (1963).

[99] L. Evans, P. G. H. Sandars, and G. K. Woodgate. *Proc. R. Soc. A* **289** 114 (1966).

[100] R. R. Arons, H. G. Bohn, K. J. Fischer, and H. Luetgemeier. *Solid State Comm.* **26** 625 (1978).

[101] F. Levy. *Phys. Kond. Mater.* **10** 71 (1969).

[102] E. L. Boyd. *Bull. Am. Phys. Soc.* **8** 439 (1963).

[103] S. H. Charap and E. L. Boyd. *Phys. Rev.* **133** A811 (1964).

[104] G. A. Uriano and R. L. Streever. *Phys. Lett.* **17** 205 (1965).

[105] E. R. Andrew and D. P. Tunstall. *Proc. Phys. Soc.* **78** 1 (1961).

[106] J. Barak, A. Gabai, and N. Kaplan. *Phys. Rev. B* **9** 4914 (1974).

[107] O. W. Dietrich, J. A. J. Henderson, and H. Meyer. *Phys. Rev. B* **12** 2844 (1975).

[108] H. A. Mook. *Phys. Rev. Lett.* **46** 508 (1981).

[109] C. Kittel. *Introduction to Solid State Physics*, 6th edition (John Wiley & Sons, New York, 1986).

[110] R. L. Streever. *Phys. Rev.* **134** A1612 (1964).

[111] B. D. Guenther, C. R. Christensen, A. C. Daniel, and D. T. Teaney. *J. Appl. Phys.* **40** 1404 (1969).

[112] J. Barak, I. Siegelstein, A. Gabai, and N. Kaplan. *Phys. Rev. B* **8** 5282 (1973).

[113] J. Barak, I. Siegelstein, A. Gabai, and N. Kaplan. *Phys. Rev. Lett.* **27** 817 (1971).

[114] H. G. B. R. R. Arons, H. Luetgemeier, and K. J. Fischer. *J. Mag Mag. Mat.* **2** 67 (1976).

[115] R. R. Arons, H. G. Bohn, and H. Luetgemeier. *Physica B* **86-88** 1303 (1977).

[116] M. W. Pieper, D. Baetjer, and K. Fischer. *Z. Phys. B* **98** 1 (1995).

[117] Z. Fisk, D. C. Johnston, B. Cornut, S. von Molnar, S. Oseroff, and R. Calvo. *J. Appl. Phys.* **50** 1911 (1979).

[118] S. Suellow, I. Prasad, M. C. Aronson, S. Bogdanovich, J. L. Sarrao, and Z. Fisk. *Phys. Rev. B* **62** 11626 (2000).

[119] N. Bloembergen, E. M. Purcell, and R. V. Pound. *Phys. Rev.* **73** 679 (1948).

[120] N. W. Ashcroft and N. D. Mermin. *Solid State Physics* (Saunders College Publishing, 1976).

Curriculum Vitæ

Arnaud Comment was born September 20, 1973. He grew up in the French-speaking Swiss canton of Jura. In 1993 he received his science-based baccalaurat from the Cantonal Secondary School of La Chaux-de-Fonds, Switzerland. Following high school, Arnaud attended the Swiss Federal Institute of Technology Lausanne (EPFL) where he specialized in experimental physics and received his physics diploma entitled *Spin dependent electronic transport in cobalt nanostructures.* In December of 1999 Arnaud began graduate school under EPFL thesis advisor Professor Jean-Philippe Ansermet. Arnaud conducted his graduate studies at the University of Illinois at Urbana-Champaign in the laboratory of Professor Charles P. Slichter.

Publications

J.-E. Wegrowe, A. Comment, Y. Jaccard, J.-Ph. Ansermet, N. M. Dempsey, and J.-P. Nozières, "*Spin-dependent scattering of a domain wall of controlled size*", Phys. Rev. B **61**, 12216 (2000)

C.S. Snow, S.L. Cooper, D.P. Young, Z. Fisk, A. Comment, and J.-Ph. Ansermet, "*Magnetic polarons and the metal-semiconductor transitions in (Eu,La)B_6 and EuO: Raman scattering studies*", Phys. Rev. B **64**, 174412 (2001)

J.-E. Wegrowe, A. Sallin, A. Fábián, A. Comment, J.-M. Bonard, and J.-Ph. Ansermet, "*Magnetoresistance properties of granular nanowires composed of carbon nanoparticles embedded in a Co matrix*", Phys. Rev. B **65**, 012407 (2002)

H. Rho, C.S. Snow, S.L. Cooper, Z. Fisk, A. Comment, and J.-Ph. Ansermet, "*The evolution of magnetic polarons in $Eu_{1-x}Gd_xO$: A light scattering study*", Physica B **312-313**, 775 (2002)

H. Rho, C.S. Snow, S.L. Cooper, Z. Fisk, A. Comment, and J.-Ph. Ansermet, "*Evolution of Magnetic*

Polarons and Spin-Carrier Interactions through the Metal-Insulator Transition in $Eu_{1-x}Gd_xO$", Phys. Rev. Lett. **88**, 127401 (2002)

Presentations

Talk at the March Meeting 2000 of the American Physical Society, "*Spin dependent scattering of a domain-wall of controlled size*"

Poster at the Gordon conference on Magnetic Resonance 2003, "*Europium NMR study of EuO and Gadolinium doped EuO*"